Title	Round robin findings and recommendations.
Authors	Judge, Frances M.;Gueydon, Sebastien;Salvatore, Francesco;Johnstone, Cameron;Ohana, Jérémy;Thiebaut, Florent;Bouscasse, Benjamin;Davey, Thomas;Hann, Martyn;Le Boulluec, Marc;Khalid, Faryal;Finnegan, William;Davies, Peter;Goggins, Jamie
Publication date	2021-12
Original Citation	Judge, F., Gueydon, S., Salvatore, F., Johnstone, C., Ohana, J., Thiebaut, F., Bouscasse, B., Davey, T., Hann, M., Le Boulluec, M., Khalid, F., Finnegan, W., Davies, P., Goggins, J. (2021)Round robin findings and recommendations, MaRINET2, D2.5 (117pp).
Type of publication	Report
Rights	© 2021, the Authors. The content of this publication reflects the views of the Authors and not necessarily those of the European Union. No warranty of any kind is made in regard to this material.
Download date	2025-07-03 23:43:04
Item downloaded from	https://hdl.handle.net/10468/15162

WP2 Standardisation of Offshore Energy System Testing

D2.5 Round robin findings and recommendations

Project Reports

Status: Final

Version: 1

Date: December 2021

MaRINET2

Deliverable 2.5: Round robin findings and recommendations

This project has received funding from the European Union's Horizon 2020 research and innovation programme under grant agreement number 731084.

Document Details	
Grant Agreement Number	731084
Project Acronym	MaRINET2
Work Package	2
Task(s)	2.3
Deliverable	2.5
Title	Round robin findings and recommendations
Authors	Frances Judge (UCC), Sebastien Gueydon (UCC), Francesco Salvatore (CNR), Cameron Johnstone (UoS), Jérémy Ohana (ECN), Florent Thiebaut (ECN), Benjamin Bouscasse (ECN), Thomas Davey (UoE), Martyn Hann (UoP), Marc Le Boulluec (Ifremer), Faryal Khalid (UNEXE), William Finnegan (NUIG), Peter Davies (NUIG), Jamie Goggins (NUIG)
File name	D2.5 Round robin findings and recommendations FINAL
Delivery date	22/12/21
Dissemination level	Public
Keywords	Round robin; research; offshore renewable energy; laboratory testing; wave; tidal, floating wind; cross-cutting;

Document Approval Record		
	Name	**Date**
Prepared by	Frances Judge	17/12/21
Checked by	Michael O'Shea	22/12/21
Approved by	Michael O'Shea	22/12/21

Document Changes Record			
Revision Number	**Date**	**Sections Changed**	**Reason for Change**

Disclaimer

Table of Contents

List of Acronyms

Acronym	Description
ADV	Acoustic Doppler Velocimeter
CoG	Centre of Gravity
CWR	Capture Width Ratio
DoF	Degree of Freedom
FAIR	Findable Accessible Interoperable Reusable
FE	Finite Element
FEA	Finite Element Analysis
FOWT	Floating Offshore Wind Turbine
GM	Metacentric Height
IEC	International Electrotechnical Commission
IICC	Integrated Infrastructure Correlation Coefficient
IP	Intellectual Property
ITTC	International Towing Tank Conference
NREL	National Renewable Energy Laboratory
ORE	Offshore Renewable Energy
OWC	Oscillating Water Column
PIV	Paricle Image Velocimetry
PTO	Power Take-Off
RAO	Response Amplitude Operator
RRT	Round Robin Test
TRL	Technology Readiness Level
TSR	Tip Speed Ratio
WEC	Wave Energy Converter

1 Introduction

EU H2020 MaRINET2 project aims to improve the quality, robustness and accuracy of physical modelling and testing practices implemented by test infrastructures. A key element of the project is a round robin testing program where generic wave, floating wind, and tidal devices are tested in different infrastructures in order to assess the impact the facility itself has on the experimental results. Innovative laboratory testing was also conducted for cross-cutting applications through this research initiative.

MaRINET2 builds on the EU FP7 MaRINET project which concluded in 2015. A tidal round robin campaign was conducted in the MaRINET project [1] but efforts to conduct a meaningful wave round robin were unsuccessful. Therefore, in MaRINET2, four round robin testing campaigns were conducted involving tidal, wave, floating wind and cross-cutting devices. The tidal round robin used the same device as in the MARINET project, whereas the wave campaign involved the design and build of new generic devices. In the wind round robin, the device was chosen based on an open-access model previously designed as part of the INNWIND.EU project. The cross-cutting campaign involved several different activities, including mooring line testing, tidal blade testing, and subsea umbilical testing.

All round robin devices were successfully tested in several facilities around Europe. This report summarises each test campaign. The objectives of each test programme are explained, the models are described, and the results are presented and analysed. Learnings from each campaign and recommendations for future round robin activities are discussed.

Data from the round robin campaigns is open-access and available through the MaRINET2 e-infrastructure. The e-infrastructure is accessible via the link on the MaRINET2 website, or through the OpenAIRE Explore database (https://explore.openaire.eu).

2 Tidal round robin

2.1 Tidal round robin summary

The MaRINET2 tidal Round Robin Test (RRT) campaign was organized with two objectives, the first objective set out to analyse the impact of different testing environments on the characterization of model turbine operation within combined wave-current operations; and the second objective compared laboratory and sea testing operations to establish consistency in operations. For the laboratory testing campaign, a horizontal-axis layout was chosen, and a 3-bladed model device with diameter D = 724 mm was provided by IFREMER. Four partners took part in the activity: IFREMER, University of Strathclyde (UoS), CNR-INM, and Flowave. In comparison of laboratory with sea testing, a 3-blades, horizontal axis turbine was selected with a Diameter of 1.05m. Two partners took part in this testing program, Queen's University of Belfast (QUB) and University of Strathclyde (UoS). To evaluate and address both the objectives, testing was performed in five different infrastructures, as described below. The activity represents an extension of the preliminary Tidal Round Robin test carried out in the EU-FP7 MaRINET Project (2011-2015) and limited to current flow only water conditions [2]. In the following, this former Round Robin test is referred to as the "2015 RRT".

2.1.1 Campaign objectives

The characterisation of the effects of surface waves on tidal turbine operation is a problem of primary interest for device developers. The vast literature on the subject identifies a number of aspects that affect the performance and reliability of turbine operation in waves. In particular, velocity fluctuations associated to orbital motions induced by surface waves are responsible for transient loads on turbine blades with risk of fatigue. The capability of power control strategies to compensate the variability of onset flow velocity in waves is another area of research and technology development.

Wave-induced effects are significant for floating turbines operating in proximity of the free surface, whereas sea bottom installations can be affected depending on site depth and sea state conditions.

The MaRINET-2 Tidal Round Robin test represents the first experimental campaign specifically designed to investigate the influence of the testing environment when the performance of a tidal turbine in representative wave-current and sea conditions is measured. Specific attention was devoted to analysing the quality of turbine operating conditions, flow and waves, that were established in each of the considered testing environment.

2.1.2 Round robin model choice

The MaRINET2 tidal round robin laboratory tests were conducted by using a generic 3-bladed horizontal-axis model turbine developed by IFREMER. The model has a diameter D = 0.724 m and can be considered as representative of a 14.5 m diameter turbine at full scale, corresponding to a scale ratio of approximately 1: 20. The nacelle has a diameter D_H = 110 mm (D_H /D = 0.15). Compared with the model turbine used for the 2015 RRT, blade design used a NACA 63-418 profile, and the dimensions are the same, while the nacelle diameter is 24 mm larger.

The nacelle is equipped with a flange to adjust a supporting stanchion or tower according to installation requirements. Specifically, the stanchion is mounted from the top and fixed to carriage frames in a towing tank installation, whereas the tower fits into a supporting base for bottom-based installations in a flume tank or wave/current basin, see Figure 1.

The model is instrumented with load cells to measure thrust and mechanical torque at the rotor shaft and encoder to measure the rotor rotational speed. Single blade loads are measured by dedicated load cells positioned at the root of each blade. Electrical signals coming from all sensors are acquired using National Instruments hardware and electronics in-house developed by IFREMER.

The nacelle hosts a generator converting mechanical power into electricity that is dissipated by a remote resistors rack. The rotor shaft is connected to the generator shaft through a gearbox with 1:26 speed ratio.

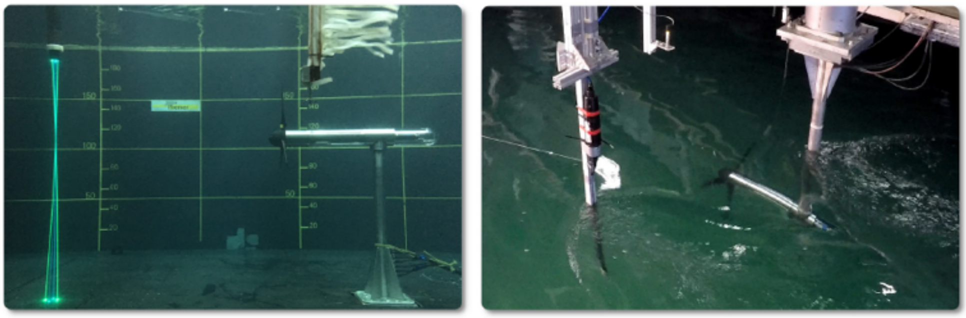

Figure 1 The tidal Round Robin test model turbine installed in the IFREMER flume tank (left) and in the CNR-INM towing tank (right).

2.1.3 Laboratory to Sea Transition Testing Model Choice

The laboratory to sea transition tests were conducted using a generic 3-bladed horizontal-axis model turbine developed by Queens University Belfast. The model has a diameter D = 1.04 m and can be considered as representative of a 20.8 m diameter turbine at full scale, corresponding to a scale ratio of approximately 1: 20. The blade design used is a Wortmann FX63-137.

The nacelle is equipped with a fixed structural flange transitioning into the structural supporting stanchion. Specifically, the stanchion is mounted from the top of a cantilever supporting structure fixed to carriage frames in a towing tank installation, whereas the cantilever structure protrudes from the bow of the testing vessel, see Figure 1.

The model is instrumented with load cells to measure thrust and mechanical torque at the rotor shaft and encoder to measure the rotor rotational speed. Electrical signals coming from all sensors are acquired using an in-house SCADA system developed by Queens University Belfast.

The nacelle hosts a generator converting mechanical power into electricity that is dissipated by a remote resistors rack. The rotor shaft is connected to the generator shaft through a gearbox.

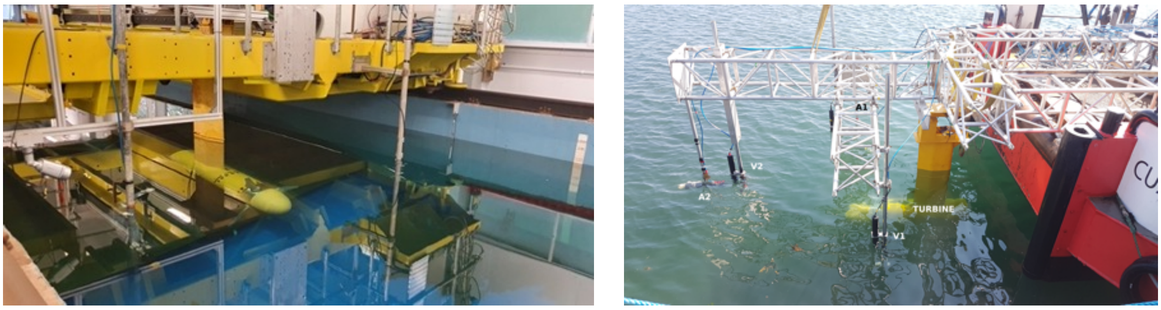

Figure 2 Laboratory to sea transition testing model turbine installed in th eUniversity of Strathclyde towing tank (left) and on the bow of the Queen's University Belfast 'pushing' vessel (right).

2.1.4 Round robin laboratory test campaign description

Four different testing environments were initially proposed: flume tank (IFREMER), towing tank (CNR-INM and UoS), wave/current basin (FloWave), marine field site (QUB). Due to facility access limitations resulting from COVID 19 restrictions, the final test program included three facilities as summarised in Table 1, where main facility facts are given.

Table 1 Main characteristics of the facilities involved in the tidal Round Robin test.

Laboratory Name	IFREMER	CNR-INM	FLOWAVE
Type of tank	flume	towing	flume
Length [m]	18	220	15
Width × Depth [m]	4 × 2	9 × 3.5	15 × 2
Blockage ratio [%]	5.1	1.3	1.4
Speed range [m/s]	0.1 to 2.2	0.1 to 10	0.1 to 1.6
Turbulence int. [%]	1.5 to 15	NA	5 to 11
Wave freq. [Hz]	0.5 to 2	0.4 to 1.25	0.2 to 1.2
Wave max. amp. [mm]	150	450	450

The selection of common test conditions was made by taking into account operational limitations in each of the facilities involved in the round robin activity.

As a result, the following conditions were selected:

- flow velocities of 0.8 and 1.0 m/s
- uni-directional regular waves with amplitude of 35, 55, and 75 mm and encountering frequency of 0.5, 0.6, 0.7 Hz.
- uni-directional irregular waves (JONSWAP spectrum) with significant height of 100 mm and encountering frequency of 0.6 Hz.

Seven combinations of the above conditions were selected for comparative tests, as summarized in Table 2 below. Note that some conditions were considered in only two facilities out of three.

Table 2 The MaRINET-2 tidal round robin test matrix.

Case	Type	Flow speed [m/s]	Wave freq. [Hz]	Wave ampl. [mm]
1	current	0.8	-	-
2	regular	0.8	0.6	75
3	regular	0.8	0.5	35
4	current	1.0	-	-
5	regular	1.0	0.7	75
6	regular	1.0	0.6	55
7	irregular	0.8	$T_P = 1.67$ s	$H_S = 100$ mm

For each condition, turbine rotational speed was varied to test 11 different TSR values, from 0 to freewheeling. In all tests, the turbine depth was kept constant at 1.0 m (1.38 D). The common test set-up realized in all the facilities is sketched in Figure 3 taken from [3].

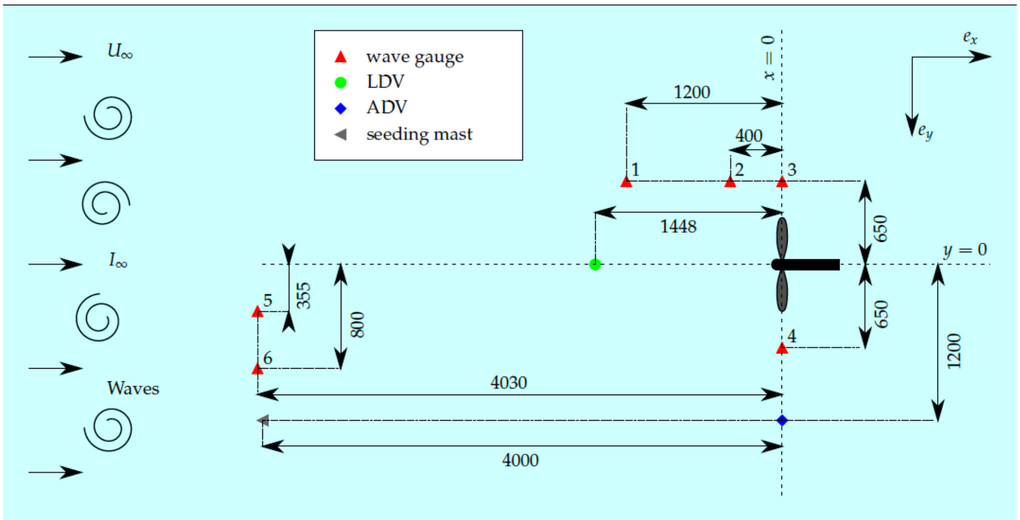

Figure 3 Test set-up realized for the Tidal Round Robin test campaign (from [3]).

The onset flow speed was measured using an Acoustic Doppler Velocimeter (ADV) placed in line with the rotor plane at a distance of 1.2 m (1.6 D) aside of it. In flume tank installations, the ADV was mounted by a support frame independent from the turbine. In towing tank installations, the device was mounted from the carriage. In towing tank tests, the flow speed was also given by the imposed carriage speed. In order to characterize the variation of wave-induced velocity with depth, bare-basin measurements (*i.e.*, without turbine) of flow speed were taken at 3 or 5 positions spanning vertically across the rotor plane.

Wave gauges of different types were used to measure wave elevation and period and verify the accuracy of the established patterns with respect to imposed nominal conditions. A resistive wave probe in line with the rotor plane at a distance of 650 mm (0.9 D) aside of it was common to all installations (wave probe no. 3 in Figure 3). In addition to that, ultrasound and dynamic wave probes were also used in towing tank tests at CNR-INM (wave probes no. 4-6 in Figure 3).

All signals from the model turbine are sampled at a frequency of 128 Hz. Flow measurements and water surface elevation were synchronised with the turbine instrumentations by means of a short impulse trigger signal.

Tests were performed by following the guidelines given in the EquiMar protocol [4] adapted from the ITTC Procedure 7.5-02-07-03.9 [5].

2.1.5 Laboratory to sea transition testing campaign description

The sea testing setup consisted of the turbine being mounted forward facing below an aluminium truss protruding midships from the bow of the vessel with a hub height of 1.26m below the water level, Figure 4.

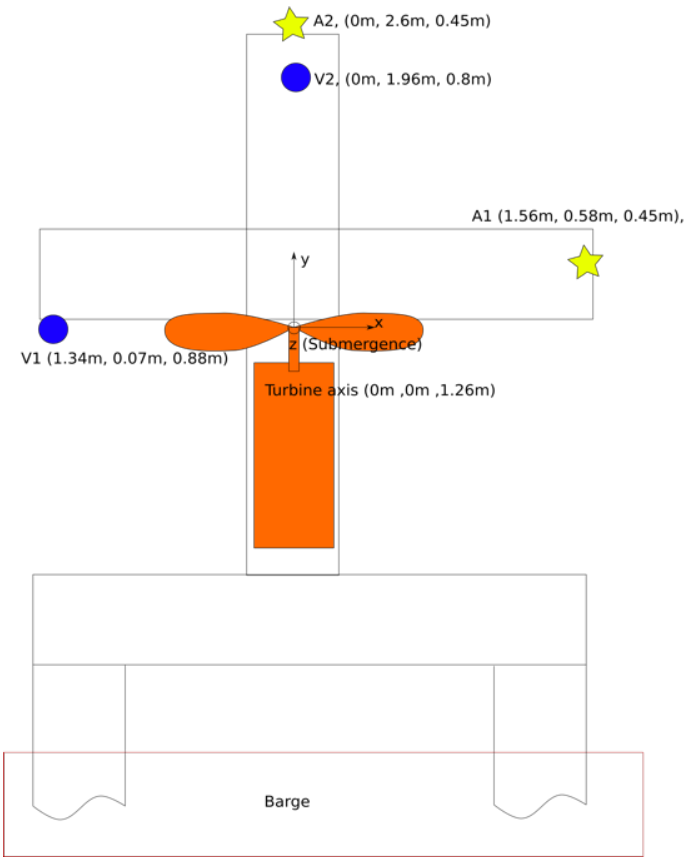

Figure 4 Instrumentation configuration and location of turbine in front of the bow of the 'pushing barge'

Flow measurements were performed using two Aquadopp Profilers (2MHz) and two Nortek Vector probes. One Aquadopp (A2) was mounted midships 2.6m in front of the turbine plane with the sensor head submerged 0.45m. A Vector probe (V2) was installed downstream, 1.96m from the turbine plane and at 0.8m depth. The second Vector (V1) measured flow 1.34m to the portside of the turbine axis and 0.07m upstream in 0.88m water depth. The second Aquadopp (A1) was mounted 1.24m starboard and 0.58m upstream at a depth of 0.45m. A1 and A2 sampled with 1Hz resolution, whereas Vectors recorded with 16Hz. The turbine was equipped with a TorqSense RWT411 torque and rotation sensor and also recorded electrical power with 10Hz temporal resolution. A sensor at the top of the stanchion recorded turbine thrust with 16Hz resolution. The Supervisory Control and Data Acquisition (SCADA) system was operated in constant speed mode, attempting to maintain a set-point RPM. The SCADA uses a National Instruments CompactRIO, allowing real time monitoring of the inflow and turbine metrics. The vessel used was an Easy Worker 1460 anchor handling barge. Overall length, beam and depth at sides were 14m, 6m and 1.8m respectively. Maximum draught aft was 1.2m. The barge can achieve 8 knots maximum speed and 4t maximum thrust under bollard pull conditions. The crane is rated for loads up to 8t. For testing the barge was driven at different locations, covering highly turbulent flow in the tidal channel and virtually stagnant water in Strangford Lough. Water depth was always higher than 20m to ensure no disturbance by blockage effects. Test runs and data recordings typically lasted 128s.

Laboratory testing set up was undertaken at the Kelvin Hydrodynamic laboratory at Strathclyde University, Glasgow, UK. The turbine can be seen in Figure 2. Table 3 shows the characteristics of the facility and the settings used for the laboratory tests. To ensure Reynold's independence, the Reynolds number for the testing was calculated based on [1]. Data from tank tests relied on carriage 159 speed for turbine inflow velocity.

Table 3 Kelvin Hydrodynamic Laboratory testing specifications

Kelvin Hydrodynamic Laboratory Details	
length × width × depth	76m × 4.6m × 2.5m
Flow velocity Maximum speed	5 m/s
Blockage ratio	6.97%
Flow velocities tested	1.7m/s, 1.8m/s and 2.0m/s
Repeated tests per flow speed	2, 2 and 3
Number of data sets per flow speed	24, 32 and 54
Reynolds number at 70% of the blade length at TSR=4 per flow speed	5.16E5, 5.46E5 and 6.07E5

The turbine was installed to the carriage using steel frames mounted to the carriage 161 structure, as can be observed in Figure 4. The flow velocities tested at the tow carriage were based on the initial real-site trials. The laboratory campaign primarily focused on the evaluation of the three velocities listed in Table 3 for which repeated tests were carried out. As listed in the table, the blockage ratio within the tow tank facility was 6.97%. Blockage correction was applied to the experimental data to facilitate comparison of sea and laboratory data, using methodologies presented by [6], [7]. The resulting thrust forces acting on the turbine was available from turbine sensors.

2.2 Tidal testing results

2.2.1 Laboratory round robin results

The main findings from the tidal Round Robin test are summarized here, whereas a fully detailed description can be found in published papers [8][9].

The instruments available to measure turbine performance and flow conditions, current and waves, made possible to collect data for the comparative analysis of the following aspects:

- Quality of onset flow intensity across the vertical profile – w/ and w/o waves
- Quality of established wave patterns
- Sensitivity of turbine performance to flow conditions – w/ and w/o waves

The starting point for the present analysis is given by the conclusions of the 2015 RRT where only calm water conditions were addressed. A general outcome was that average values of power and thrust showed small discrepancies among facilities, whereas larger differences were observed in the time-fluctuating series. Such data scattering was related to different turbulence levels in flumes and towing tanks and carriage vibrations observed in some of the towing tank tests.

The extension to consider wave/current interaction in the present RRT revealed a more complex phenomenology and much larger scattering among data from different testing environments. A key finding is that time-averaged turbine performance results in wave/current conditions present differences up to 15-25% for the peak power coefficient depending on the facilities and flow conditions. Quite larger differences are observed for the standard deviations, as shown in Figure 5.

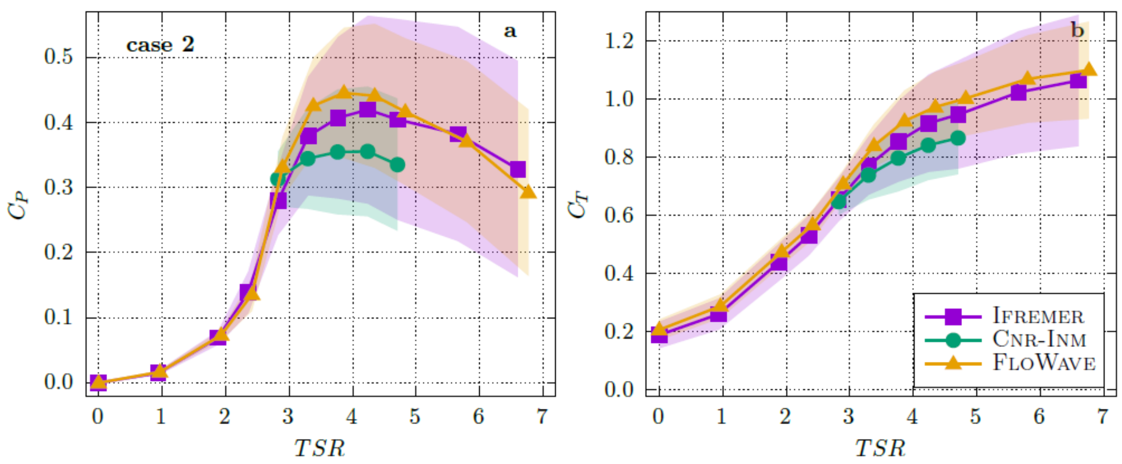

Figure 5 Turbine power (left) and thrust (right) coefficients for wave/current testing conditions no. 2.: average values and standard deviation. (From [3])

These differences are strongly correlated with the different flow characteristics generated. In order to understand the causes of such discrepancies, three main aspects have been investigated: blockage, turbulence, and wave/current interactions.

Regarding blockage, results from the present RRT confirm the conclusion from the 2015 RRT that blockage effects are not negligible even if the facilities are among the largest of their types existing globally, and the blockage factor with a D ≈ 0.7 m turbine was below 5%. Standard correction formulas (e.g., Bahaj et al. [6]) can be used to filter flow confinement effects on turbine performance measured in flume and towing tanks. The application of this approach to tests carried out in other facilities, as the FloWave circular wave/current tank, introduces uncertainties, as clearly shown in Figure 6, where blockage correction factors are compared.

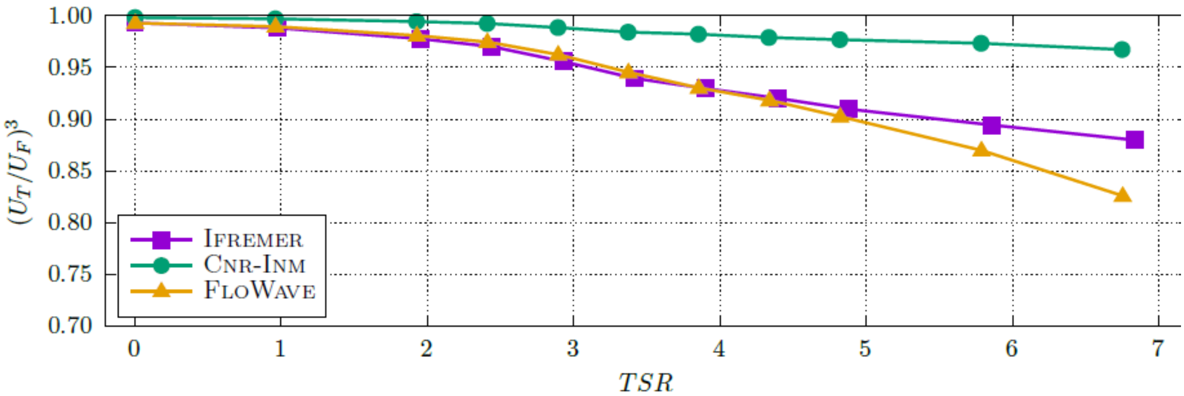

Figure 6 Comparison of blockage correction factors in the three facilities (From [3]).

Considering turbulence, calm-water measurements in the present RRT confirmed trends observed during the 2015 RRT. Wave/current testing revealed a new phenomenology, with significant discrepancies of data among facilities. In the flume tank installation at IFREMER, the wavemaker paddles interfere with the onset flow and act as turbulence generators. As example, a 8% increase of CP mean value at design TSR and 7 times higher standard deviation compared with calm water was observed. This effect is less evident in the circular wave/current basin at FloWave, while is absent in a towing tank installation where the wavemaker forces oscillations of water at rest.

Different ways used to generate currents and waves is another source of onset flow differences among the facilities. A key difference is that in flume and wave/current tanks the wave maker interacts with the onset current, while in a towing tank, waves are generated in calm water. This yields different mechanisms by which the current modifies wave amplitude and length and also, wave-induced vertical velocity profiles. In particular, in installations where waves are generated on a streaming flow, significant differences between imposed and realized wave patterns and deviations of the vertical velocity profile with respect to the theoretical pattern were observed. Flow velocities up to 10% higher than the nominal values and wave amplitudes higher than the target values by up to a factor of 2 were measured. The repeatability of wave patterns is also affected. These effects are negligible in a towing tank installation. Another source of differences is related to the wave absorption technique used in the facility.
An example of velocity fluctuations and the effects on measured turbine power, with larger standard deviation observed in flume tanks is given in Figure 7

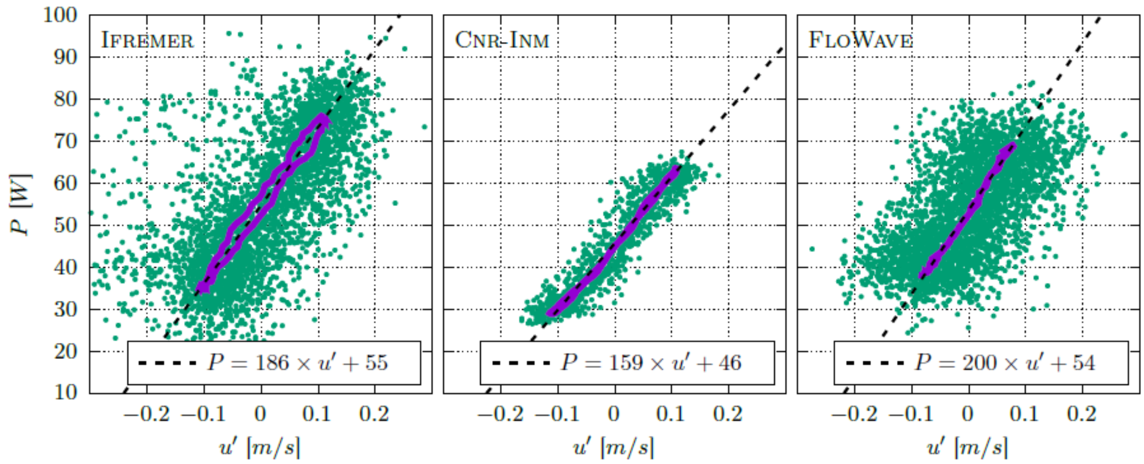

Figure 7 Correlation between measured power and wave-induced velocity fluctuation in the three facilities: raw data (green), and wave phase average of the power versus the wave phase average of the fluctuating velocity (violet) (From [3]*).*

Variations of flow speed intensity across the vertical profile have further consequences when disc-integrated velocity values are used to determine non-dimensional coefficients of turbine thrust, torque and power. Differences in disc-integrated velocity contribute to increase the discrepancies among power coefficients determined from each facility. For example, Figure 8 compares different velocity profiles across the rotor disc vertical span.

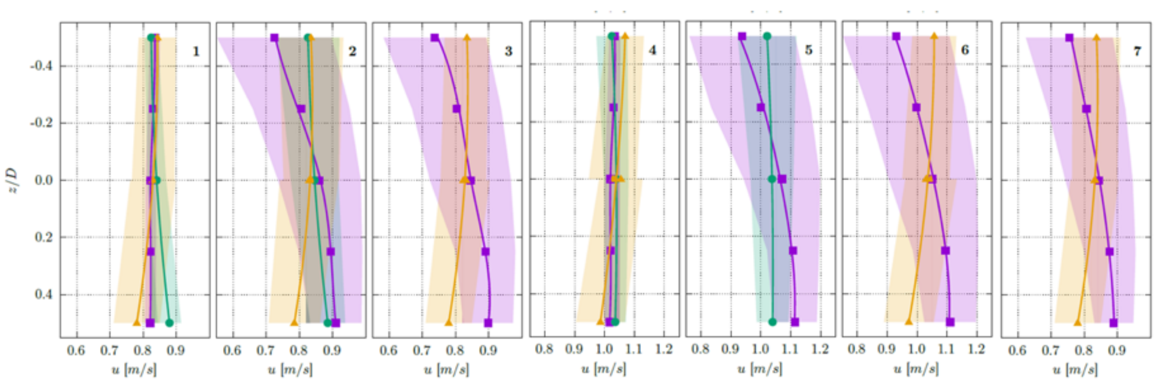

Figure 8 Vertical profiles of the average and standard-deviation of the axial velocity component across the rotor disc: IFREMER (blue), CNR-INM (green), FloWave (Orange).

2.2.2 Laboratory to sea transition testing results

Analysis of the power characteristics relative to rotor speed has been undertaken and presented as mechanical power capture and electrical power output, as shown in Figure 9. This presents Power Coefficient (Cp) against rotor speed (lambda) from all test runs using the mean of the complete unfiltered and depth averaged velocity data for each run and mechanical or electrical power. All Cp values rise from a TSR of 1 and maximum power is achieved around a TSR of 3. Mechanical power is consistently 30% higher than electrical power. The consistent variation between mechanical and electrical power is due to the lower part load efficiency of the electrical generator unit. Up to a TSR of 3, data evaluated using the Vector compare well to the Aquadopp data and show little scatter. For TSRs above

3 scatter increases and Vector data consistently predicts higher power values than the Aquadopps. Overall, this rough analysis without further data selection or filtering already provides a good idea of turbine characteristics. In the following sections we will investigate the influence of different filters and data selection strategies.
Remarkably, some of the runs performed at the lowest and highest velocities yielded excellent agreement around the peak Cp values of 0.3 at TSR 3 to 4.

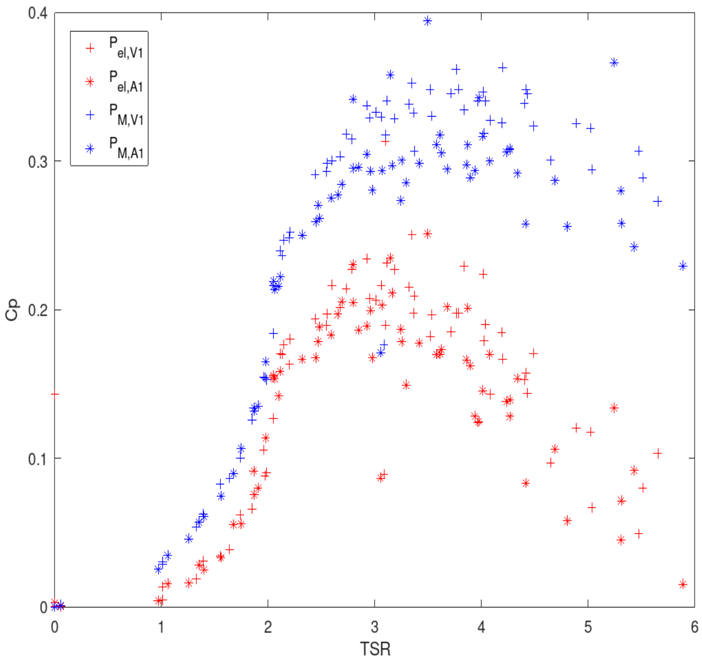

Figure 9 Mechanical and electrical ouput relative to rotor speed

Following the evaluation of the part load efficiency impact on Cp data, a correlation was established and data is presented for mechanical power capture by the turbine rotor. Figure 10 presents data split by test location, Channel and Lough. The Channel data represents the turbine being ‘pushed through turbulent flow conditions, while Lough data represents the turbine being ‘pushed’ through stagnant water. The resulting Cp − λ curves are similar, with neither scatter nor power levels noticeably affected by location. Turbulent kinetic energy levels encountered during testing do not seem to influence Cp values either with values evenly distributed across the entire TSR range and outliers not showing a clear correlation with extreme values of k.

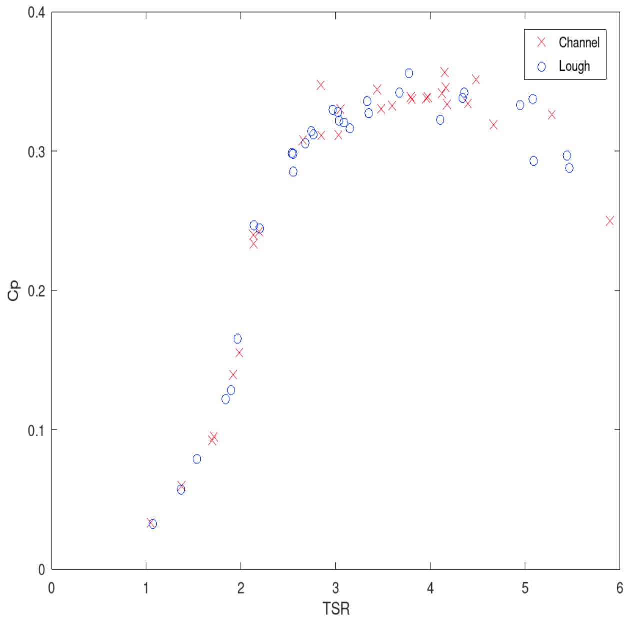

Figure 10 Turbine power characteristics against rotor speed when operating in turbulent and calm flow conditions

Comparison with laboratory and sea testing and simulated numerical rotor performance is displayed in Figure 11. The Cp − λ data and fitted curves from sea (V1) and laboratory testing with blockage correction applied to the laboratory data ($TankBC_{TP}$) [6], [7]. Both the sea and laboratory testing compared favourably with the predictive performance using University of Strathclyde in-house Blade Element Momentum Theory model (BEMT). This provides high confidence in the use of BEMT to inform typical expected performance.

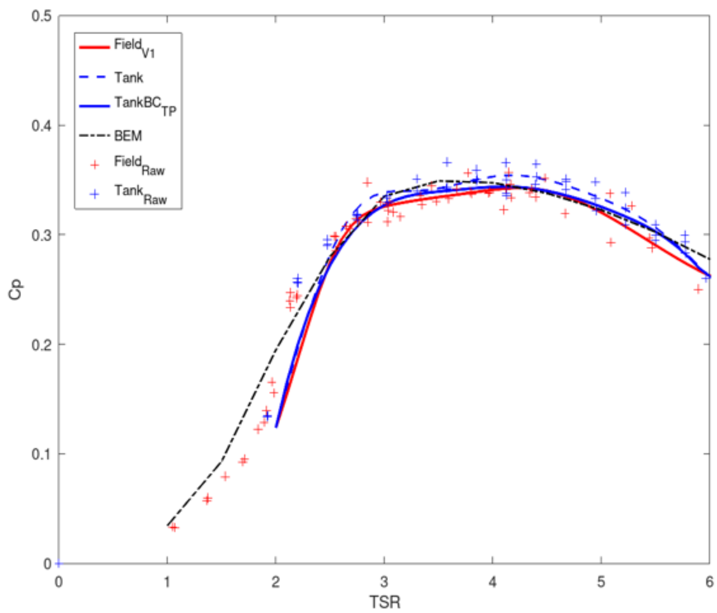

Figure 11 Power performance analysis for both laboratory and sea testing comparison with numerical simulation predictions

2.3 Lessons learned and recommendations for standardised testing

The analysis of results from the tidal Round Robin test in waves clearly shows that turbine performance measurements can be largely affected by the quality of wave/current conditions that are realized. The phenomenology is quite different from calm water testing, where significant deviations among results from different testing environments were observed only for standard deviations of raw data. In fact, when a combination of current and waves is considered, testing environment characteristics largely affect also the average values of turbine performance coefficients. Moreover, important differences have been noticed between flume and towing tank tests.

Regarding the characterization of the current intensity, recommendations are similar to those derived in the 2015 RRT for calm-water testing.

2.3.1 Velocity measurement

Default accuracy of ADV instruments is typically reported as ±1% of the measured value. However, the quality of measurements is sensitive to the the density of seeding particles in the water. In towing tank tests, the nominal onset flow speed is given by the carriage speed which is generally measured with high accuracy (e.g., ±0.1% of the measured value, at CNR-INM). Comparing measures from different sensors (i.e., Pitot tubes or PIV systems) should be considered. The measurement of onset flow turbulence intensity is fundamental for a correct interpretation of turbine performance data.

The choice of the flow speed measurement point is also important. A distance of 2D upstream of the rotor plane at rotor-axis depth can be taken as a compromise between a larger distance to reduce the effect of turbine-induced perturbations, and a shorter distance to maximize the correlation between flow speed at the measurement point and at the rotor plane. It should be noted that the definition of the nominal flow speed affects the quantification of turbine performance by means of non-dimensional coefficients for thrust, torque and power. As example, a 1% difference in the definition of the nominal flow speed determines a 3% variation of the calculated power coefficient. The actual vertical velocity profile during tests in waves is an additional source of reference velocity uncertainties.

2.3.2 Testing blockage ratio influence

The ratio of the area of the turbine rotor to the cross-sectional area of the testing environment can influence the results. The larger this ratio value, the greater the influence. This requires blockage correction to be applied to the turbine data. Standard correction formulas (e.g., Bahaj et al. [6]) have been derived for flume and towing tanks. The application to tests carried out in circular wave/current tanks yields some uncertainty in the definition of input quantities as the test section dimensions.

2.3.3 Wave measurement

Dealing with measurements in wave/current conditions, special care should be devoted to analysing the realised wave pattern. In flume tank environments, imposed and realised conditions can significantly differ and discrepancies must be accurately quantified. Different wave probe types could be used to assess surface elevation and wave periods. Probe choice should be such that the operating range adequately matches the requested wave climates. In general, the use of ultrasound and dynamic wave gauges is recommended. In case of test campaign lasting for several days, probe calibration done in the first day of tests, should be repeated to ensure data consistency.

2.3.4 Data collection and timings between test cases

The acquisition time for a single condition (wave climate, flow speed, turbine performance) should be sufficiently long to make possible a sound statistical analysis of raw data and determine quality time averages and standard deviations. In a flume tank, durations of 2-3 minutes are acceptable, although this period can be optimized on the basis of the conditions to be tested. Towing tank testing implies a limitation to acquisition time related to the extension of the tank. Round Robin tests showed that at least 20 wave periods per run should be collected.

Suitable downtimes are to be considered between two runs. In flume tanks this is important when flow conditions change. The duration of this waiting time depends on the effectiveness of wave absorbing devices in the facility. This aspect is of primary importance in towing tanks where, ideally, each run should start from calm water and no-wave conditions. Depending on test conditions and the wave absorbing device, downtimes can last for 30 to 45 minutes. Monitoring of wave elevation signals can be useful to optimize these timings.

When possible, runs should be repeated. This information is deemed necessary to undertake an uncertainty analysis based on a combined expanded uncertainty using precision and bias errors.

Dealing with data acquisition, data sampling frequency should be chosen by considering the variability of physical quantities to be monitored. Automated synchronization of signals output from sensors directed to different acquisition units should be obtained by a shared trigger signal.

2.3.5 Data processing and correction

Considering the complex phenomenology of turbine performance tests in waves, particular attention should be also given to implement a sound data processing strategy. Derivation of time-averaged and standard deviation values for all the observed variables is straightforward in case of stationary flow conditions in calm water. In case of wave-induced transient-flow forcing, data averaging has to be generalized to address periodic signals. The Hilbert transform technique used in [3] is an example.

The application of a blockage correction factor to test data recorded during laboratory testing provides an excellent agreement attained between sea testing using a propelled Barge ‘pushing’ the turbine through the water.

2.3.6 Transition to sea testing

Finally, a self-propelled Barge 'pushing' the turbine through the water for sea testing demonstrated both a controllable, flexible, and efficient way to transition from laboratory to sea testing to characterize a tidal turbine performance. Barge based propulsion testing also provides an effective technical, cost, time, and regulatory efficient form of sea testing.

2.4 Recommendations for future round robin activities

Future work in relation to implementing and developing the outputs from this round robin research would be the evaluation and establishment of an integrated infrastructure correlation coefficient (IICC). An IICC would be established for each testing infrastructure and would be applied to the test data in order to provide fully comparable inter-infrastructure data. This would allow performance data produced at one testing facility to be compared and benchmarked against performance data from another testing facility.

The next stage in advancing round robin testing would be the enhancement of the laboratory to sea transition testing to be more comprehensive and representative in supporting technology innovation and development when evolving from TRL 4/5 to TRL 6/7.

A general conclusion from the present tidal round robin test is that further studies are required to fully understand the relationships between wave and current flow conditions and turbine performance. In particular, the analysis of single blade loading might be helpful to clarify the relationship between onset flow variations and differences among measured performance data from the different testing environments.

2.5 Description of open access dataset

Recalling the objective to design and implement the MaRINET-2 e-infrastructure carried out in WP6, results of the tidal Round Robin test have been collected and stored to secure their interoperability and long-term preservation.

Following the approach establised in WP6, the tidal Round Robin test data are being made available on the SEANOE platform (seanoe.org). This allows a long-term preservation of datasets and provide a specific DOI for each dataset with proper links with MaRINET2 sites DOIs and program (OpenAIRE metadata).

Specifically, the following dataset was published on SEANOE:

Gaurier Benoit, Ordonez-Sanchez Stéphanie, Germain Gregory, Facq Jean-Valery, Johnstone Cameron, Salvatore Francesco, Santic Ivan (2018). MaRINET2 Tidal "Round Robin" dataset: comparisons between towing and circulating tanks test results for a tidal energy converter submitted to wave and current interactions . SEANOE. https://doi.org/10.17882/58265

The dataset is open for access and assigned the DOI 10.17882/58265.

More details on data preservation and access policy for the results of the MaRINET2 tidal round robin tests are given in MaRINET2 Deliverable 6.3 [10].

3 Wave round robin

3.1 Wave round robin summary

The wave round robin campaign conducted in MaRINET2 involved selecting and testing two different wave energy converters (WECs) in several basins in Europe: Centrale Nantes (ECN), University College Cork (UCC), University of Plymouth (UoP) and University of Edinburgh (UoE). MaRINET2 partner IHCantabria (IHC) acted as witness to the tests. The devices chosen were a low TRL fixed oscillating water column (OWC) and a higher TRL hinged raft (~TRL 3). The following section provides a summary of the wave round robin campaigns. For a more complete description of the campaigns, please refer to MaRINET2 open-access publications [11], [12] and [13].

3.1.1 Campaign objectives

The objectives of the wave round robin campaign were to

1. Test two different devices (a fixed OWC and a hinged raft) in several test facilities around Europe
2. Assess the impact that the facility itself has on the results of experimental testing
3. Document differences in laboratory process and assess the impact on test results
4. Make recommendations on methodologies for laboratory testing
5. Produce an open-access dataset that ascribes to FAIR principles.

3.1.2 Facility details

The main features of each facility involved in the wave round robin are given in Table 4. The fixed OWC was tested at 1m water depth in UCC, ECN and UoP. The hinged raft was tested in a range of water depths (2-5 m) in basins at ECN, UCC, UoP and UoE as illustrated in Figure 12.

Table 4 Features of wave round robin facilities

Infrastructure	ECN	ECN	UoP	UCC	UCC	UoE
Tank Name	HOET		COAST	Lir DOB	Lir OB	FloWave
Tank Shape	Rectangle		Rectangle	Rectangle	Curved	Circle
Length (m)	46		35	35	25	25 (diam.)
Width (m)	30		15.5	12	1	25 (diam.)
Depth (m)	5	1	3 (1m for OWC)	3	1	2
Active absorption	No		Yes	Yes	Yes	Yes
Device tested	Raft	OWC	Raft, OWC	Raft	OWC	Raft

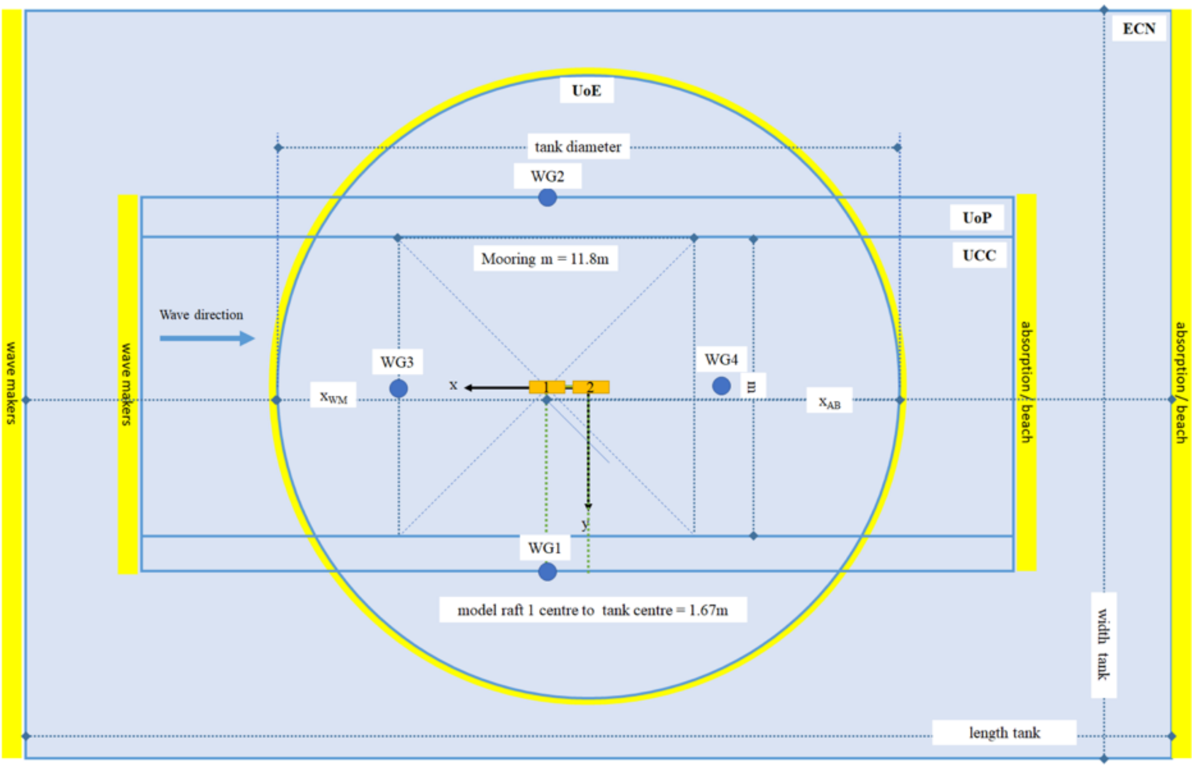

Figure 12 Wave basins used for the wave round robin campaign (hinged raft)

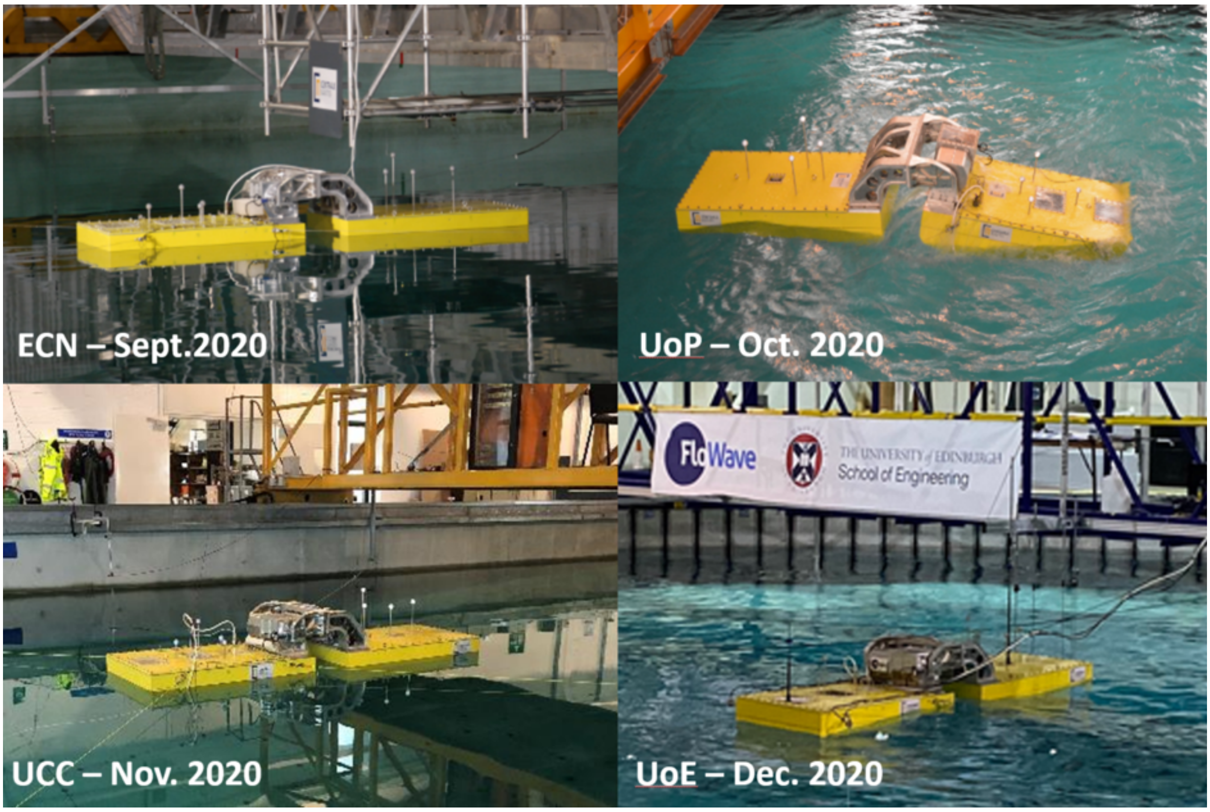

Figure 13 Hinged raft being tested at ECN, UoP, UCC and UoE.

3.1.3 Model details

Two devices at different TRLs were tested as part of the wave round robin: a low TRL fixed oscillating water column (OWC) and a higher TRL hinged raft wave energy converter.

3.1.3.1 Hinged raft

A 1:25 scale, deep-water, two-body hinged raft was selected to be the higher TRL concept for the MaRINET2 wave round robin tests (~TRL 3). This device includes a PTO emulator that produces a controlled torque. The depths of the wave tanks involved vary (from 2-5 m), and therefore the corresponding full-scale configurations will have different depths. For most of the tests, the waves of interest are deep-water waves in the different tanks.

Preliminary numerical simulations of the model and its PTO were performed using InWave and OrcaFlex software, as well as Centrale Nantes internal codes. Several iterations of calculations were performed to reach a design at model scale with a natural pitch period of approximately 1.5 s and a maximum torque at the hinge of approximately 70 Nm.

Table 5 Raft dimensions

Features	Full scale	Model scale
Length (m)	36	1.44
Width (m)	21.75	0.87
Height (m)	7.65	0.306
Gap between floaters (m)	8	0.32
Mass	3125 tonnes	200 kg

The raft main dimensions are given in Table 5. The front floater includes the control and monitoring system and the motor. The back floater contains a set of lead weights placed to balance the model. The centres of gravity of each floater were measured with a three-point load measurement system.

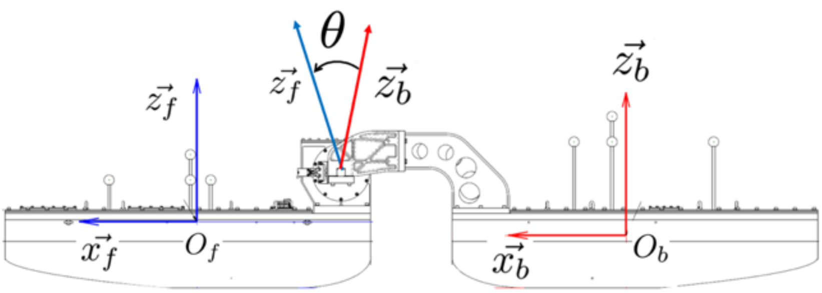

Figure 14 Hinged raft schematic

The model is moored with four aerial lines connected to four mooring points on the front floater. The same mooring setup is reproduced in all facilities with anchoring points at the corners of a square with 11.8 m sides, cantered on the middle of the front floater (as shown in Figure 12). Each mooring line is composed of a stiff rope made of polyethylene fibres and one calibrated spring with 27 N/m stiffness.

3.1.3.2 OWC

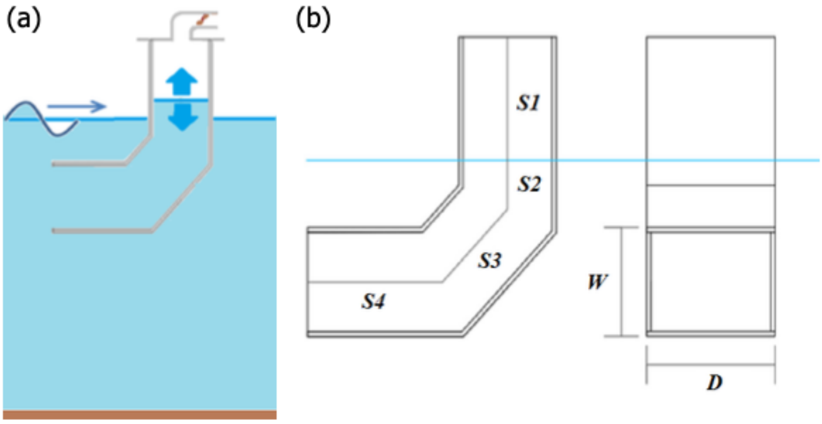

Dimensions [m]	1 :30	Full scale
D (external)	0.300	9
W (external)	0.236	7.08
Wall thick.	0.008	0.24
S_1	0.260	7.8
S_2	0.103	3.09
S_3	0.217	6.51
S_4	0.318	9.54
depth	1.000	30

Figure 15 OWC schematic and dimensions

The OWC tested during the round robin campaign was a 1:30 scale fixed nearshore bend-duct OWC with a low TRL. The device was constructed out of perspex and fitted with wave probes, pressure sensors and a 15 mm diameter orifice. A fixed wave energy converter was chosen for the round robin as it eliminates any uncertainties linked to the motion of the device.

3.1.4 Test campaign description

3.1.4.1 Raft test plan

The model was tested over a range of regular and irregular waves. For regular waves, four different target wave heights were generated (0.05 m, 0.1 m, 0.15 mand 0.2 m) for a set of 13 periods between 1 s and 2.4 s, with a focus around the natural pitch period (~1.5 s). The list of regular waves produces different wavelengths over the different facilities, because of the differences in water depth listed in Table I. These differences in wave length arise for periods longer than 1.8 s. For the facilities with shallower tanks (UCC, UoP and UoE), additional tests were carried out where the periods greater than 1.8s were adjusted to produce the desired wavelengths; however, it was found that these differences did not lead to any discernible discrepancies in the results.

The irregular wave test list consisted of three different target significant wave heights (H_s = 0.05m, 0.1m and 0.15m) for a set of four peak wave periods (T_p = 1.3 s, 1.55 s, 1.8 s and 2.05 s). These were generated with JONSWAP spectra with a gamma value of 3.3.

3.1.4.2 OWC

The test campaign for the OWC consisted of a range of regular and irregular sea states presented in Table 6 and Table 7 respectively. The regular wave test durations varied according to each facility’s standard process but was a minimum of 20 periods. The irregular sea states were chosen based on measurements made at the port of A Guarda in northwest Spain for a breakwater integrated OWC at the port.

Table 6 Regular sea states for OWC

H (m)	T (s)								
0.025	0.73	0.91	1.10	1.28	1.46	1.64	1.83	2.19	2.56
0.050	0.73	0.91	1.10	1.28	1.46	1.64	1.83	2.19	2.56

Table 7 Irregular sea states for OWC

Hs (m)	Tp (s)
0.025	1.72
0.042	1.32; 1.72; 2.13
0.058	1.72; 1.93; 2.13
0.075	1.93
0.092	1.72; 2.13
0.108	2.33
0.125	1.93
0.158	1.93; 2.33
0.192	2.53

3.2 Hinged raft results

3.2.1 Impact of analysis interval and wave height on regular wave results

There are two major criteria which must be considered when selecting the time interval over which a set of regular wave test results are analysed, namely:

- The quality of the wave signal: i.e. the duration over which the incoming regular wave is not affected to a significant degree by reflections
- The steadiness of the response signals which is obtained when all transient effects in the response have vanished.

To determine the impact that the analysis period had on the results from different basins, the regular waves were analysed with three different time interval selection strategies:

- **Long:** the interval chosen is long enough to capture most of the transient effects. The quality of the calibrated wave is checked visually: a portion of the interval will be contaminated with reflections, but as long as these do not clearly impact the wave elevation signal at the reference position then the influence of reflections is deemed acceptable. This results in an interval that usually includes between 15 and 20 wave periods. This interval selection strategy is generally appropriate for facilities with active absorption.
- **Short:** The interval chosen consists of the fully developed wave that precedes the arrival of the reflected wave. The duration of this interval depends on the wave period, the group velocity and the distance between the reference position and the end of the basin.

- **Usual:** This strategy represents the method for interval selection that is usually adopted at each facility.

Figure 16 illustrates how generated target wave signals can differ, depending on how the calibration was done and the analysis interval selected. Figure 17 shows how the interval selection can impact the results, in this case the capture width ratio (CWR). For a detailed discussion on how the interval selection can affect the results, refer to [11].

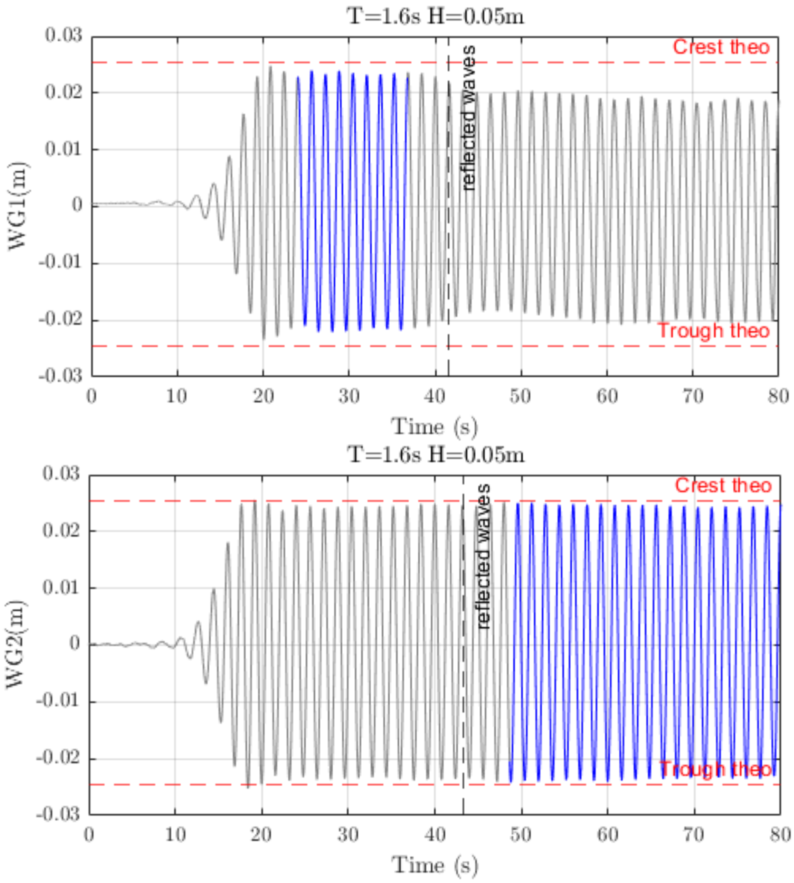

Figure 16 Wave gauge signals for the same target wave generated in two different facilities illustrating the 'short' and 'long' time interval selection (blue).

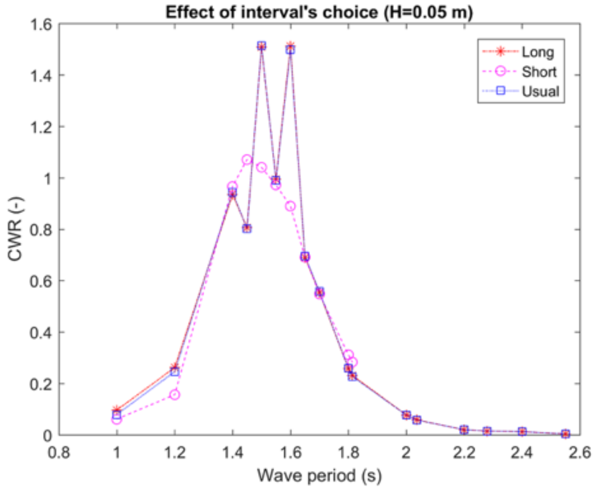

Figure 17 Effect of interval selection on CWR results at one facility

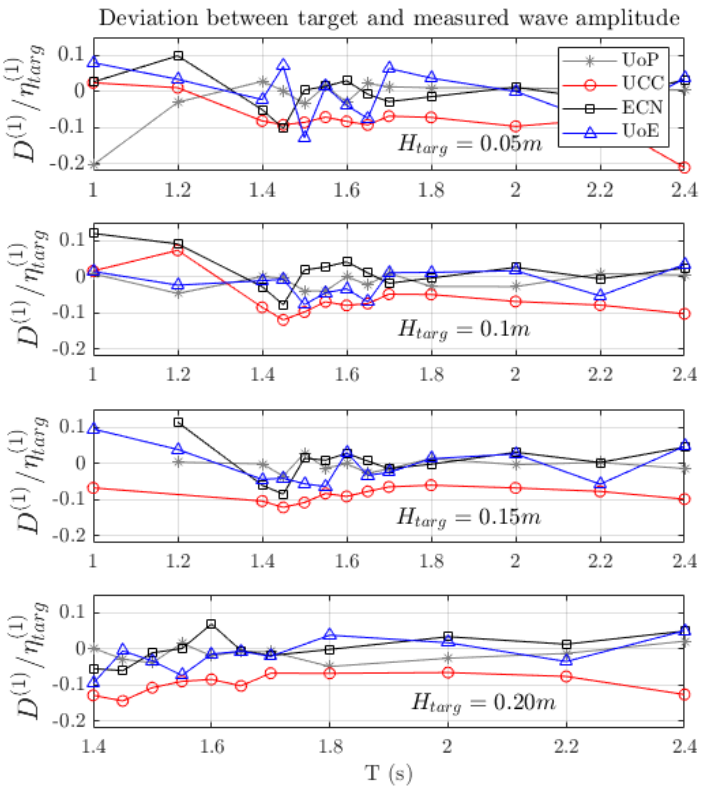

Figure 18 Comparison of the difference between achieved and target wave heights at each facility for target wave heights of (top to bottom): 0.05m, 0.1m 0.15m and 0.2m, where D = η_{meas} - η_{targ} in which η is the amplitude.

Figure 18 shows the deviation in achieved wave height across all facilities. It can be seen that aside from the discrepancies between facilities, consistent wave heights across wave periods in individual basins was difficult to achieve.

For the regular wave results, the capture width ratio (CWR) was calculated across all facilities. Figure 19 displays the averaged results from all facilities (solid lines) as well as the standard deviations above and below the average (dashed lines). From this figure it can be seen that for periods below 1.2 s and above 1.8 s, linear behaviour is observed where the wave height does not affect the CWR. Between 1.2 and 1.8 s however, the model behaves in a non-linear way with a high sensitivity to wave height, with notable discrepancies between facilities, particularly for smaller waves.

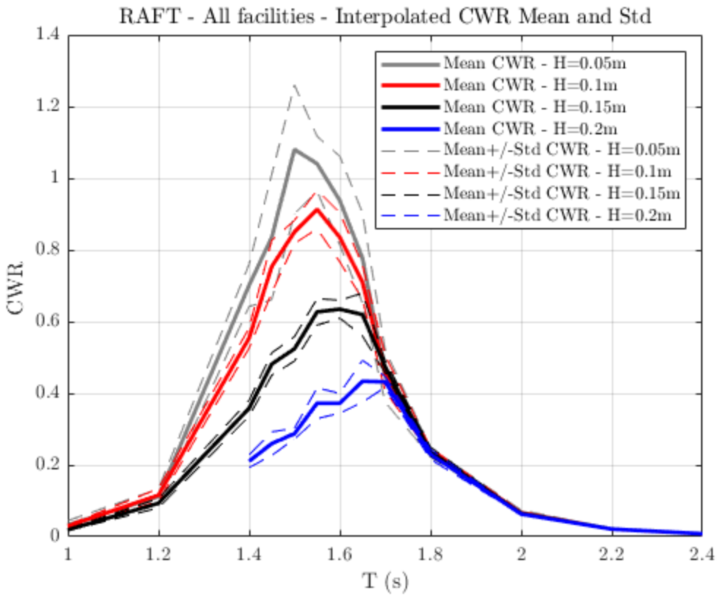

Figure 19 Mean CWR and standard deviations for all facilities

3.2.2 Irregular sea state comparison

The sea states were calibrated based on the wave gauge (WG2) at the nominal location of the model, without the model in place. The measured spectra for Hs=0.1 m are shown in Figure 20. For visualisations of the comparisons between facilities for other sea states, refer to [12]. It was found that the wave periods were generally consistent across facilities with some under-generation noted, particularly for larger wave heights.

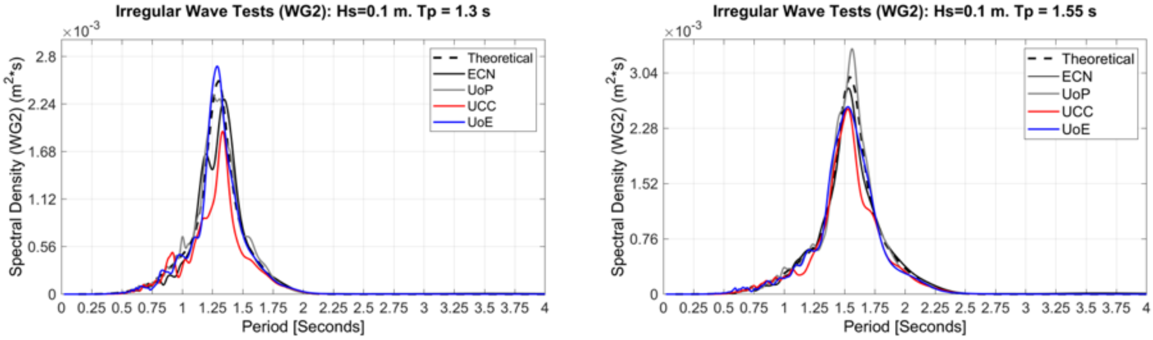

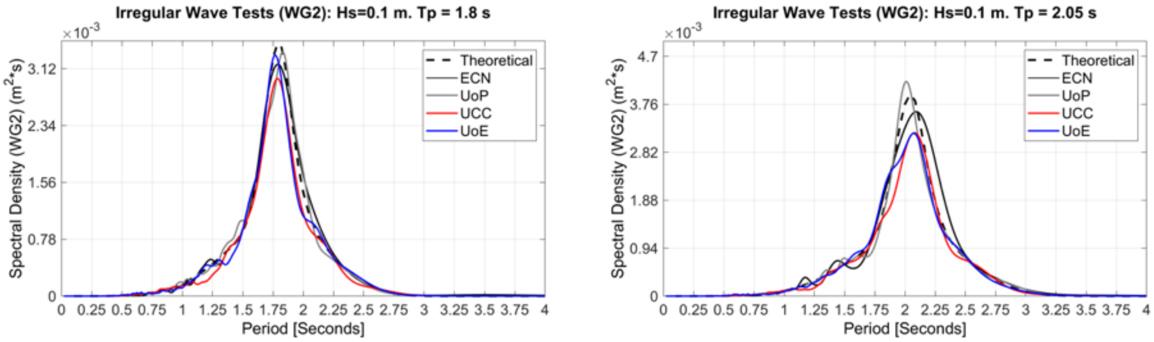

Figure 20 Wave spectra measured at nominal model location for Hs=0.1m and four different periods across all facilities (Theoretical – dashed; ECN – black; UoP – grey; UCC – red; UoE – blue.)

3.2.3 Hinge position

The hinge position, or relative pitch, is simply defined as the relative angle between the fore and aft bodies, with 0 degrees being the still water "flat" state. It was found that good agreement existed across facilities for the significant values (approximately 3% spread in the results), but a considerably greater spread was found in the comparison of the maximum values (approximately 35% in the case of the 1.8 s period seas). The comparison between significant and maximum values for Hs=0.1 m is presented in Figure 21. Similar behaviour was observed across all significant wave heights, and reflects the discrepancies in the achieved wave heights (Figure 5 in [12]).

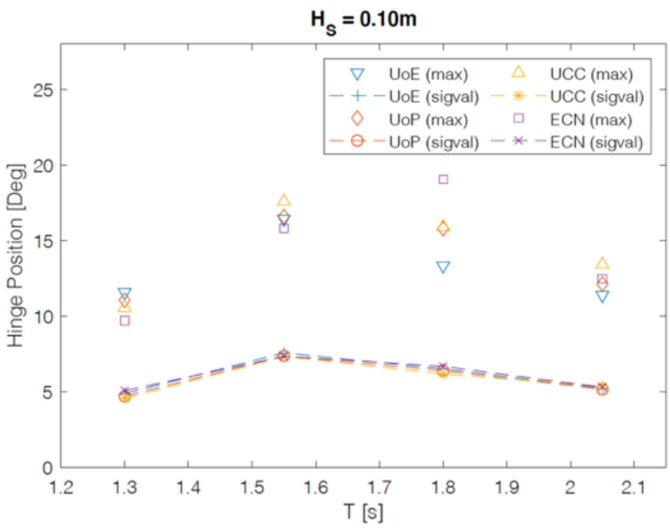

Figure 21 Hinge position significant and maximum values across facilities for Hs=0.1 m

3.2.4 Platform motions

RAOs were calculated for pitch, heave and surge; it was found that similar behaviour was exhibited across all facilities, with the exception of forward raft heave (likely due to splashing of the motion capture markers, which is discussed in [12]). A comparison of the results for heave is presented in Figure 22. For full results, please refer to [12].

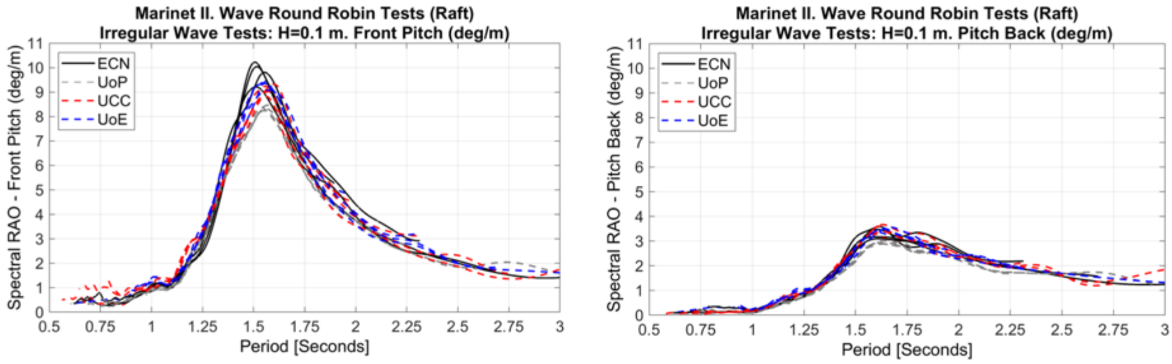

Figure 22 Pitch RAO for Hs=0.1 m for all facilities

3.2.5 Key learnings from hinged raft round robin

3.2.5.1 Regular wave generation

The way in which regular waves are generated is not uniform across all basins. Some basins are equipped with wave flap generators that allow for wave absorption, others are not. Not all basins will rely on their beach to reduce the reflection of the regular wave. Basins that do not use wave absorption or judge their beaches not efficient enough to limit reflection will favour short tests. Basins that believe in their ability to limit reflection by active flap control or by the efficiency of their beach choose to run regular wave tests for a longer duration than those who do not. This is done to allow enough time for the wave conditions to stabilise (with reflection) in the basin. These two opposite perceptions lead to the choice of distinctive approaches for the analysis of the regular wave tests, as well as distinctive approaches to wave calibration.

3.2.5.2 Variability of motions, loads and power

In broad terms, the agreement across the facilities was good and the fundamental behaviours of the WEC were consistent across test programmes. This was observed both in the frequency domain characterisation (RAOs) and summary parameters (e.g. mean, median, significant value). Where significant deviations did occur (e.g. forward raft RAO at higher wave heights) this could often be traced to measurement issues, rather than a change in response of the WEC itself. Significant deviations were observed in the power output for waves matching the resonance period of the device (e.g., small regular waves). These deviations could be traced back to differences in some of the main wave characteristics (height and steepness).

For this device, the motions and power output showed the least variability. Ideally, data from more than four facilities would be available to give more reliable quantification, but there are clear practical and financial challenges in achieving even larger multi-facility deployments. However, in the case of mean power it is suggested that a variation of 5-10% can be expected for facilities operating to their own practices. Similar variability is present in the motion outputs. Interestingly, the influence of depth, and therefore wavelength, is not a clear influence on the response in this programme. The facility depths range from 2m to 5m, which at the T_p values in question, span deep to intermediate water depth. However, at the "borderline" intermediate water depths in question, the change in the power resource is expected to vary between 1-5% for the tested range of periods, based on the method outlined in [14]. While this is similar to the observed variability, there is no clear trend to suggest it is the dominant factor, either across facilities or across the periods (the depth effect would be strongest at higher periods). It is also noted the dry station-keeping system deployed for these tests has a geometry that is independent of water depth, as opposed to, e.g., a catenary system. This will further reduce the influence of water depth on the WEC's behaviour. In the regular wave test programme [11], the wave periods were adjusted to provide the same wavelength across facilities with no discernible difference in the results.

The clearest deviations were seen in the measurement of mooring loads, in particular the static loads. The trends in the dynamic loads (i.e. the loads induced by the response to wave environment) are similar, suggesting that inter-facility variation is less significant than test setup and configuration.

It is noted that the uncertainty appears to be lower in the irregular seas than the regular tests from the same experimental programme, provided in [11]. It is suggested that in regular wave testing any variation in individual wave heights (e.g. due to reflections) are much more apparent, and the results are more sensitive to decisions on the sampling window for each facility.

3.2.5.3 Influence of experimental setup and calibration

All facilities calibrated the sea states without the model in the basin and with a gauge deployed at the nominal model location. Appropriate gain corrections were then applied to achieve the correct significant wave height. The wave period does not typically require correction due to the deterministic frequency control employed by the wave tanks in this experimental programme. Nevertheless, deviations in H_s were noted across the facilities when the data was analysed using a common method. In this case, this appeared as under-generation of the target wave height in the order of 10-15% in the worst cases. Several factors contributed to this variation:

- Operational calibrations conducted using spectra averaged across multiple gauges to minimise the influence of hotspots and reflections.
- Inconsistency in facility procedures between using incident spectra (obtained through multi-gauge reflection analysis) vs. total spectra.
- Differences in facility procedures in terms of accepted uncertainty.

3.3 OWC results

3.3.1 Wave calibration

Each facility carried out one iteration of wave calibration without the OWC in the tank with a wave gauge at the OWC location in addition to a number of gauges around the model. The resulting measured wave height against wave period at the location of the OWC model are shown in Figure 23 for a target height of 25 mm and Figure 24 for a target height of 50 mm. In most cases, the generated wave height is within 10% of the targeted 25mm or within 5% of the targeted 50mm. This is equivalent to a wave height difference of less than 3mm, which is acceptable but can lead to differences in results on the OWC performance.

Wave periods beyond 1.83 seconds were not tested at ECN due to the tank length not being sufficient to allow the analysis of waves and OWC parameters before time before reflections returned to the OWC location. Similarly wave periods beyond 2.19 seconds were not tested at UCC.

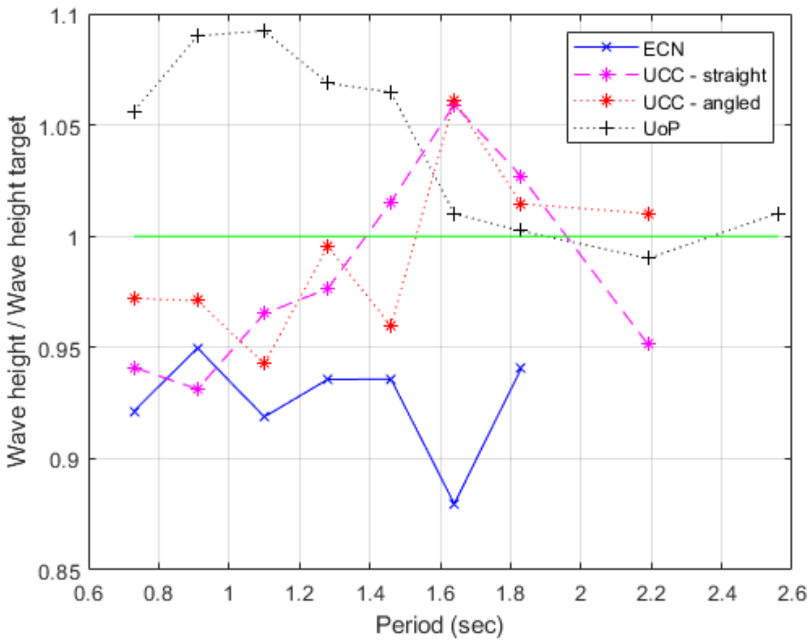

Figure 23 Measured regular wave height at location of model. Target wave height was 25 mm.

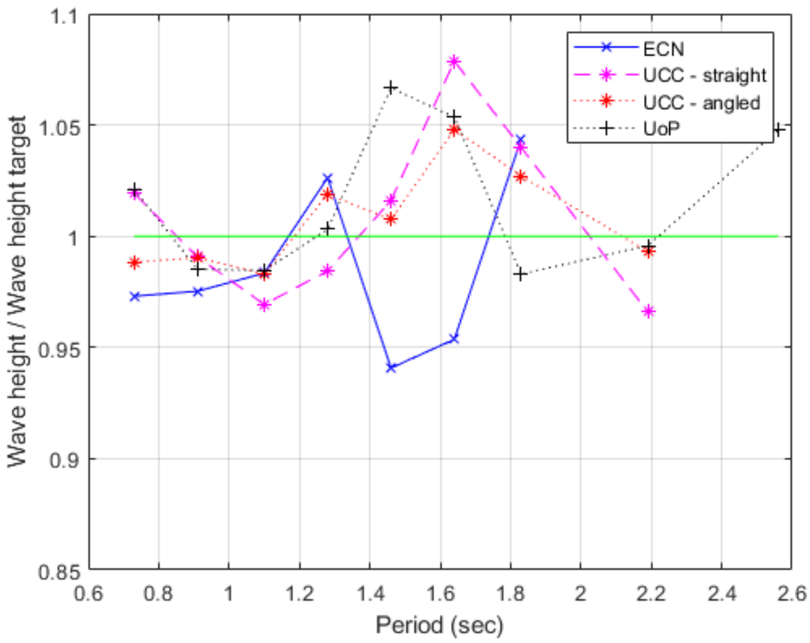

Figure 24 Measured regular wave height at location of model. Target wave height was 50 mm.

3.3.2 Water column RAO

The water column displacement RAO is a common parameter describing the behaviour of the water column. It is the ratio between water elevation inside the water column and the wave height measured at the OWC location during wave calibration. The results are presented in Figure 25.

At wave periods greater than 1.10 s, there is a significant difference between results for 25mm and for 50mm wave height. The water column displacement RAO decreases when the wave height increases. This is mainly due to the influence of air compression due to the presence of the orifice being more significant at larger wave heights. There is also a 15% difference of RAO in all facilities compared to the inter-facility average RAO.

This is not only due to the variation of wave height between facilities. For example, the generated wave heights at ECN in the 25mm series is always smaller than in other facilities but the water column RAO is not higher than in the UoP tests.

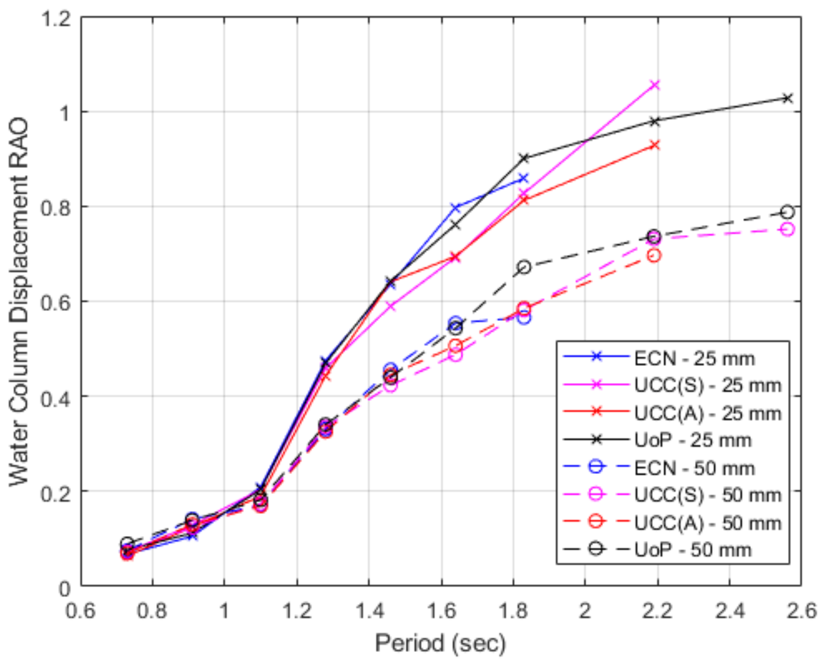

Figure 25 Water column displacement RAO from all regular wave experiments

3.3.3 Capture width ratio

The OWC capture width ratio (CWR) obtained from all regular tests are presented in Figure 26. At wave periods greater than 1.10 s the CWR generated by the 25 mm wave heights are consistently higher than at 50 mm.

There is also a 15% difference of CWR in all facilities compared to the inter-facility average CWR.

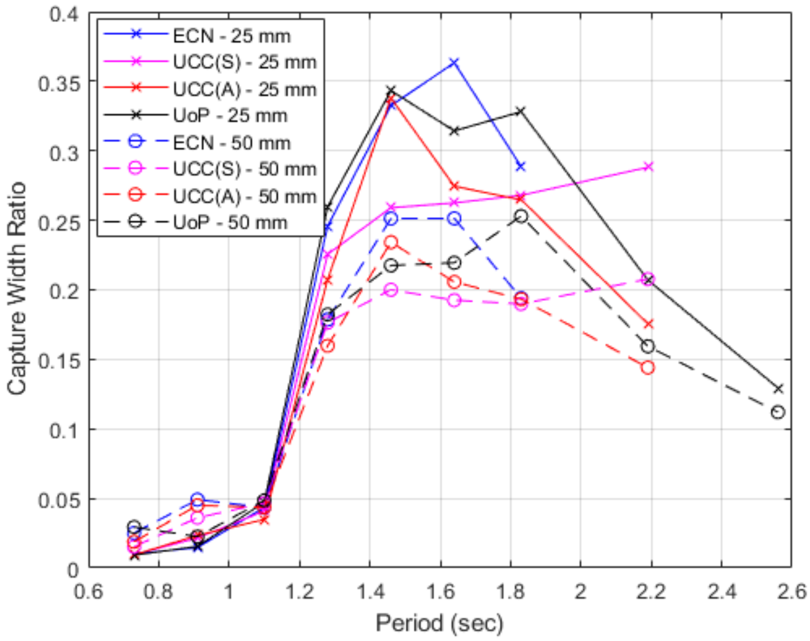

Figure 26 Measured capture width ratio from regular wave experiments conducted in all facilities.

3.3.4 Key learnings from the OWC round robin tests

Large differences were observed on the results of the four test campaigns in the OWC round robin. This was not expected because the OWC round robin project was designed to limit the uncertainty parameters:

- The model is fixed and its position in each wave tank could be set accurately.
- There are no moving parts so the characteristics of the model could not change between facilities.
- The same sensors were used in all facilities.
- The wave gauges in the model were calibrated before each test campaign
- The pressure sensors were calibrated before the first and the third test campaigns, at ECN and UCC, the calibration results did not differ significantly.

Therefore, the differences in test results can only be caused by the characteristics of the waves generated, assuming the data acquisition system accuracy was much higher than the differences observed in the results. The acquisition systems used are usual accurate with errors much lower than the 1% and the differences in the two test campaigns results in UCC are in the same range as the other facilities.

The main uncertainty is on the generate wave heights or wave spectrums differ in each facility and reflected waves; the forward bend OWC chamber is highly sensitive to wave direction. For regular waves, it was decided to estimate the wave height before beach reflected waves reach the model. This avoids uncertainty due to the influence of reflected waves but reduces the time interval and number of waves that can be analysed. In irregular waves, the test duration required to represent a full wave spectrum is too long to test in the time interval with only incident waves. It is particularly important in wave basins with a wavemaker that do not have an active absorption system.

Large variations on the generated wave heights were observed in percentage, although it is only 2 to 3 mm absolute difference. The time required to further

reducing the difference between generated and target wave height can be long and this type of difference usually is accepted in commercial projects. This is a significant learning from the OWC round robin.

3.4 Lessons learned and recommendations for standardised testing

It is noted that the clearest source of inconsistency between laboratories is in the calibration of sea states. The effect of this is exaggerated in this study as several outputs (e.g., mean power) are being compared with no reference to the measured wave parameters. Outputs such as RAOs, when calculated using measured, rather than target, spectra are less affected in this regard and are therefore deemed more useful when comparing results from different laboratories. In making recommendations we distinguish between 'characterisation' and 'calibration'. The former is obtaining an accurate measurement of the test environment, while the latter is the extension of this where the input variables are iterated to meet a specific target.

Based on the experiences of the wave round robin campaign, the following recommendations are made to ensure consistency when conducting scaled testing of WECs.

- Sea state characterisation should be clearly reported along with the facility's methodology. It must be clear whether the values relate to total or incident spectrum.
- Where possible, the characterisation should be based on average measurements from 3-5 with no model in the basin ("open tank"). These gauges would typically cover the area occupied by the model, suggesting a footprint of 1-2 m. The gauges may be spaced to support reflection analysis, allowing the incident spectrum to be reported.
- As a minimum, H_s value from the total spectrum should be reported as averaged across the gauges. It is noted that wave periods in contemporary wave tanks are reproduced very accurately, nevertheless it may be desirable to report mean periods as a measure of quality assurance. Full reporting requirements are outlined in [15] as recommended by the IEC.
- A reflection analysis should be conducted if possible, and the incident parameters reported alongside the total spectrum. The reflection analysis methodology should also be referenced.

- Accurate characterisation of the sea state is considered as a prerequisite to any sea state calibration. An established facility with experienced operators is likely to be capable of producing sea states to within 5% of target values with minimal iteration. In a time-limited programme it may therefore be acceptable to run uncalibrated sea states, providing they are characterised as detailed above.
- Where sea state calibration is conducted, the methodology must be reported, in particular, the adjustments made to the input spectrum. For example, is the target H_s achieved through the application of a broad gain function, or is a frequency dependent gain function applied (adjusting each frequency bin individually)? The latter method is recommended where practical. It is suggested that a standardised procedure should be adopted (e.g. by the IEC) for sea state characterisation and calibration given its clear importance for maintaining consistency between laboratories. This influence was even more pronounced on the regular wave tests that reported in [11].
- The use of a design wave (i.e. recreating a specific time series at the model location) should be considered as a benchmarking tool to aid comparison between test programmes at different facilities.
- Assuming that the model itself maintains consistency between programmes, the key source of variability is the interface with the facility (e.g. the moorings). In addition to ensuring dimensional accuracy, it is suggested that pull tests are conducted to establish the stiffness of the system. Selecting sensors that are sensitive and robust enough for measuring the loads in the mooring lines over the whole round robin campaign is important for the comparison of mooring loads.

3.5 Recommendations for future round robin activities

Future round robin activities of this nature should take note of the learnings described in the previous section. A significant finding from the raft tests, at larger scale and representing higher TRL testing, was that the model performed consistently, and there was no clear influence relating to facility design or configuration. To some extent this might be expected, given that these facilities all use similar and modern wave making equipment and are designed to operate at similar physical scales. Nevertheless, they vary considerably in physical dimensions (including depth) and shape. Most of the variability therefore appeared to be related to non-standardised operation and sea state calibration. To some extent the ongoing activities of the International Electrotechnical Commission (IEC) may provide guidance here, but generally not at the level of technical detail that would have made any significant difference to these test programmes.

It is therefore suggested that future round robin R&D activities should explore operational and environmental reproduction techniques for hydrodynamic test laboratories. This could potentially be supported by a benchmarking process with a representative model (e.g., the hinged raft).

Specific areas to explore are:

- Establishing clear procedures and techniques for laboratory sea state calibration appropriate for the wave energy sector. These must:
    - Take account of reflection behaviour in the facility, in particular the requirement to calibrate on the total or incident spectrum.
    - Establish if the calibration process must be dependent on the device time. For example, the difference between an attenuator and point absorber class of device may be significant when considering the incident versus the total energy spectrum.
    - Produce guidance on sea state durations and other parameterisations to enhance consistency. These should aim to extend the IEC Technical Specifications (providing they are appropriate), rather than produce competing guidance.
- Investigate techniques beyond the regular and irregular wave systems, in particular the concept of a deterministic design wave (i.e., the recreation of a specific time series at the model location). This has a twofold benefit, allowing tank performance to be benchmarked more clearly, but also enabling time-domain comparison of the performance of the round robin wave device. This can be useful when investigating variability in the model itself, but also the device-tank interfaces such as moorings.
- The above work would also support extended work on analysis techniques, given that all test data would be produced to standardised method with identical analysis periods.
- Using a combination of multiple sea state calibration techniques and deterministic design waves provides more control on the experimental variables, especially when combined with a reliable and controllable WEC model. Usable uncertainty estimation techniques are still lacking for the wave energy tank testing sector. Existing guidance tests to be either difficult to apply or simply poorly populated. A structured study tracing the uncertainties from sea state calibration, model construction, test execution, through to analysis could be conducted to provide a more usable uncertainty estimation process. The outcome could be similar to the uncertainty estimations produced by NREL for floating offshore wind testing [16].

The key research outcomes from this work would be:

- Guidance and standardisation of sea state calibration and environmental replication for wave energy converter testing purposes.
- The production and evaluation of a design wave(s) for the efficient evaluation and benchmarking of facilities and WEC models. This would have lasting impact beyond any round robin activities and be usable by any laboratory in the future.
- Guidance on standardised analysis techniques for both regular and irregular sea state testing.

- Guidance on uncertainty for wave energy testing, appropriate to the staged development approach adopted by the IEC. This guidance should be accessible and simple to use by any laboratory or user group, with a key aim of identifying the elements contributing significantly to uncertainty at the experimental design stage.
- Development of improved methodologies for designing truncated mooring systems in smaller tanks.
- Develop recommendations for testing with wave directionality based on a round robin test examining calibration and measurement procedures for generating directional sea states.

Specific recommendations relating research involving OWCs are:

- Investigate influence of OWC alignment accuracy to support the theory that this may influence results.
- Use of controlled air volumes for testing OWCs to provide proper scaling of air compressibility. Providing evidence to support the reliability of this approach could be of use to the sector.

3.6 Published wave round robin research

Published papers documenting the wave round robin activities are available from the following sources:

Journal of Marine Science and Engineering:

Davey, T., Sarmiento, J., Ohana, J., Thiebaut, F., Haquin, S., Weber, M., Gueydon, S., Judge, F., Lyden, E., O'Shea, M., Gabl, R., Jordan, L-B., Hann, M., Wang, D., Collins, K., Conley, D., Greaves, D., Ingram, D. M., & Murphy, J. (2021). Round Robin Testing: Exploring Experimental Uncertainties through a Multifacility Comparison of a Hinged Raft Wave Energy Converter. *Journal of Marine Science and Engineering*, *9*(9), [946]. https://doi.org/10.3390/jmse9090946

EWTEC 2021 Proceedings[1]:

Ohana, J.; Gueydon, S.; Judge, F.; Haquin, S.; Weber, M.; Lyden, E.; Thiebaut, F.; O'Shea, M.; Murphy, J.; Davey, T.; Gabl, R.; Jordan, L.B.; Wang, D.; Hann, M.; Conley, D.; Collins, K.; Greaves, D.; Sarmiento-Martinez, J. Round robin tests on a hinged raft wave energy converter. In Proceedings of the EWTEC 2021, Plymouth, UK, 5–9 September 2021.

[1] Not yet published at time of writing.

3.7 Description of open access dataset

All data generated by the MaRINET2 round robin is available for download through the MaRINET2 e-infrastructure which can be accessed through www.marinet2.eu or through the OpenAIRE Explore website: https://explore.openaire.eu

3.7.1.1 Raft

Details of the dataset from the hinged raft test program are as follows:

Ohana Jeremy, Davey Thomas, Sarmiento Javier, Thiebaut Florent, Haquin Sylvain, Weber Matthieu, Gueydon Sebastien, Judge Frances, Eoin Lyden, O'Shea Michael, Gabl Roman, Jordan Laura-Beth, Hann Martyn, Wang Daming, Collins Keri, Conley Daniel, Greaves Deborah, Ingram David, Murphy Jimmy (2021). **Marinet2 - Datasets from the "Round robin" testing program on a hinged raft wave energy converter**.
SEANOE. https://doi.org/10.17882/85077

3.7.1.2 OWC

Details of the dataset from the hinged raft test program are as follows:

Lyden Eoin, Judge Frances, O'Shea Michael, Thiebaut Florent (2021). **Marinet 2 Fixed Oscillating Water Column Wave Energy Converter Test Data Set – UCC**.
SEANOE. https://doi.org/10.17882/80895

4 Wind round robin

4.1 Wind round robin summary

4.1.1 Campaign objectives

Scaled model testing is an integral part of the development process for many offshore renewable energy (ORE) technologies, not just offshore wind. Testing at small scale can be efficient and relatively inexpensive, while testing within a controlled environment enables experiments to be repeated for a range of parameters. An additional advantage of testing at small scales is that each individual subsystem can be independently tested. However, the effects that a facility or laboratory will have on the outcomes even when following the same methodologies are uncertain.

Research carried out within MaRINET2 [17], [18] identified a shortfall in the published guidance available for laboratory testing of floating offshore wind turbines (FOWTs). Much of the existing literature is derived from the oil and gas industry and published by the ITTC in the 7.5-02-07-03 series that deals with ocean engineering[2]. The ITTC guidelines are relatively high level and do not provide standardised procedures for laboratory testing or detailed guidance on different aspects of FOWT testing. Other sources of guidance for FOWT laboratory testing are published research articles that document individual tank testing campaigns but these are device and basin specific and may not provide relevant advice for an individual embarking on a tank testing campaign. Researchers involved in laboratory testing of FOWTs are often prevented from publishing detailed accounts and lessons learned from a test campaign by Intellectual Property (IP) restrictions. There is no published research on how the facility itself may impact the outputs of a laboratory testing campaign, and how to conduct tests in a way that the tester can have confidence that the results can be reproduced with good accuracy in another wave basin.

Therefore, the aims of the floating wind round robin campaign conducted within MaRINET2 are as follows:

- Test a generic floating wave platform in four basins around Europe using the same test plan
- Observe the differences in test procedures between individual facilities
- Identify the major factors that cause discrepancies in the results obtained from different facilities
- Produce an open access dataset that can be used by the wider offshore energy community.

This report summarises the wind round robin campaign. For detailed discussion and analysis refer to the papers published in the MaRINET2 special edition of the Journal of Marine Science and Engineering, i.e. [19] and [20].

[2] Register of ITTC guidelines available at https://www.ittc.info/media/4251/register.pdf

4.1.2 Facility details

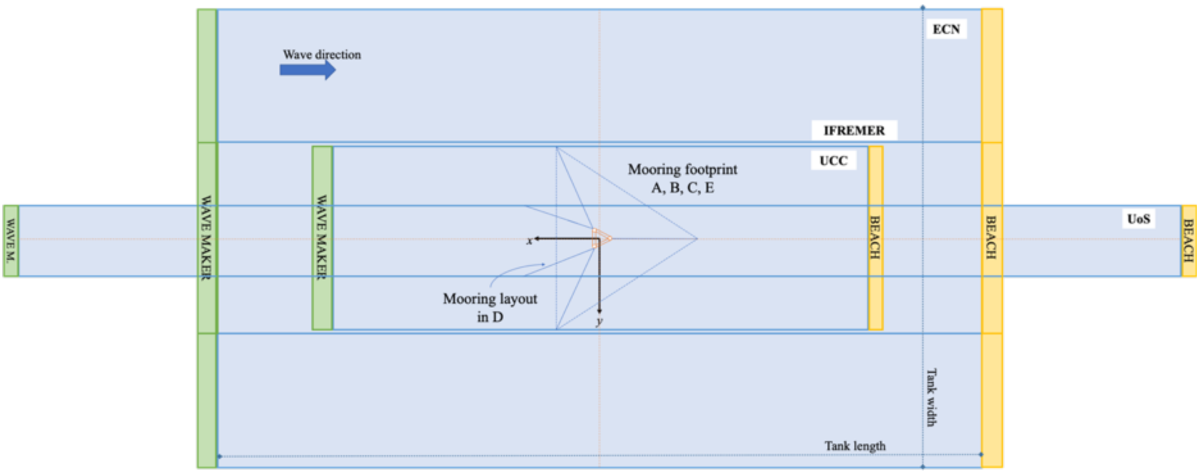

Figure 27 Layout of each of the four test facilities

Five tests at four facilities were carried out as part of the round robin test program: Ifremer, Centrale Nantes (ECN), the Kelvin Hydrodynamics Laboratory (KHL) at the University of Strathclyde (UoS) and two tests at University College Cork (UCC). The primary purpose of the second test campaign at UCC was to test a second method of wind emulation a number of months after the original test. However, the original test plan with (and without) the thruster was also partly repeated. These latter results comprise the fifth dataset used in this report. The main features of the wave basins in each facility are illustrated in Figure 27. ECN, UoS and UCC are all fresh water basins, whereas Ifremer is filled with salt water. Additional masses were added to the platform at Ifremer to achieve the same inertias calculated for fresh water. For the rest of this report, as well as the research presented in [19] and [20], the datasets are referred to as indicated in Table 8.

Table 8 Dataset reference

Facility	Ref
ECN	A
Ifremer	B
UCC Campaign 1	C
UoS (KHL)	D
UCC Campaign 2	E

4.1.3 Model, setup, and instrumentation

The model chosen was based on the 10 W semi-submersible floating horizontal axis turbine, designed originally by CENER as part of the INNWIND.EU project [21]. The structure comprises three cylindrical columns connected by horizontal rectangular pontoons. The turbine tower is mounted on the aft column and is designed to host a variety of turbine simulators. The 1/60th scale model has an aluminium hull with a carbon fibre composite tower as shown in Figure 28 with dimensions shown in Figure 29.

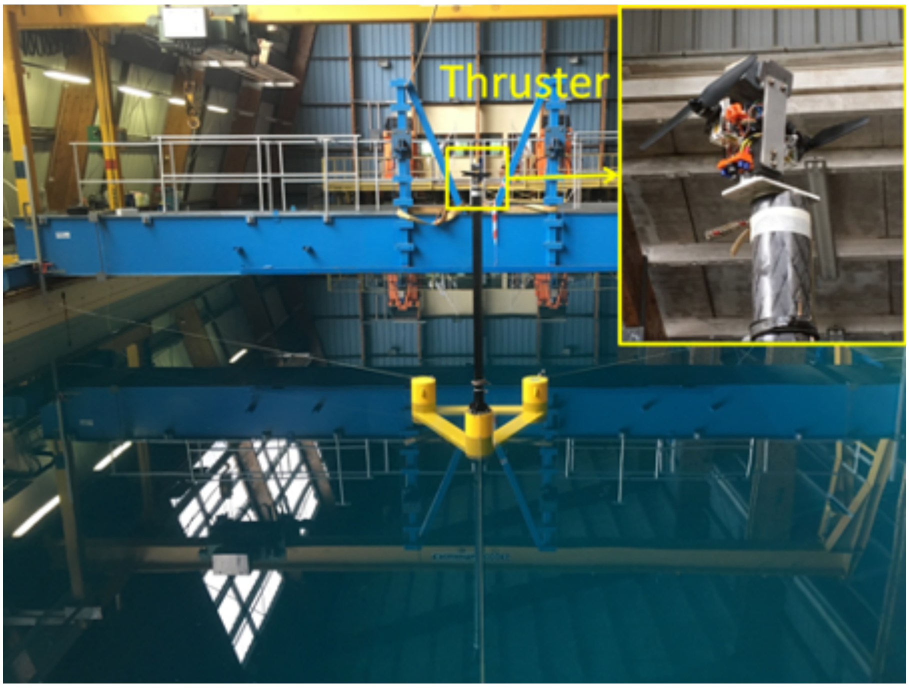

Figure 28 Model, mooring system and thruster installed in the basin at Ifremer

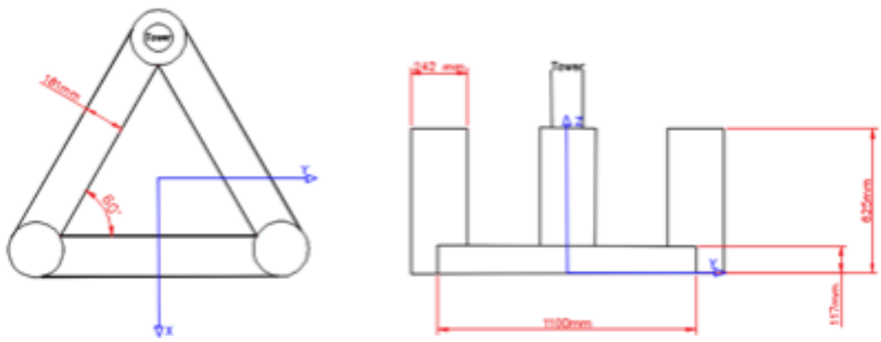

Figure 29 Model dimensions at 1:60 scale

A linear aerial mooring system was chosen for the round robin campaign as it is independent of water depth and could be installed in each of the facilities that participated in the round robin programme. The mooring system consisted of three lightweight inextensible ropes attached in series to linear springs. Each mooring line extended horizontally above the water surface from each of the model towers to an anchoring point in the basin (see Figure 28). For the three wider basins (Ifremer, ECN and UCC), an aerial mooring system with a spread of 11.8 m was implemented, whereas in UoS, a mooring system with a smaller footprint was installed (see Figure 27).

Each facility provided their own wave gauges which were arranged either side of and directly in front of the model (between the model and the wave maker). A wave gauge was installed at the model location for wave calibration in each facility. Some facilities deployed additional gauges to facilitate an analysis of the reflections in the basin.

The model was fitted with four reflective markers for tracking the motions of the device using Qualisys, which was available in all facilities: one on each of the aft towers and two on the mast.

Load cells were fitted to each of the mooring lines. The load cells, as well as the mooring lines themselves were supplied by Ifremer and travelled with the device to each facility.

Wind emulation at each facility was provided by means of a thruster supplied by Ifremer, with pre-programmed thrust levels of 3, 5, 7 and 8 N. In addition to the thruster, other methods of wind emulation were implemented as follows:

- Weighted pulley at UCC (Dataset E)
- Scaled rotor used in conjunction with fan at Ifremer

4.1.4 Test campaign description

The test plan was developed by Ifremer, who performed preliminary computations of the RAOs using Bureau Veritas' Hydrostar software. The results of these computations were used to help select the wave parameters for the physical tests. The test plan for the wind round robin included the following elements:

- Hydrostatics: check of water draft and Metacentric Height (GM) moduli (with and without mooring)
- Mooring stiffness: check surge and sway stiffness
- Decay tests in calm water: without moorings (heave, pitch and roll only) and with moorings (all motions)
- Regular wave tests: without wind thrust (see Table 9)
- Irregular wave tests: with and without wind thrust (see Table 10).

Table 9 Regular wave list at model scale

T (s)	*H* = 0.05 m	*H* = 0.10 m	*H* = 0.15 m	*H* = 0.20 m
0.86	X			
1.03	X			
1.29		X		
1.8		X	X	
2.39	X	X	X	X
2.56	X	X	X	X
2.71		X		
2.74	X	X	X	X
2.78	X	X	X	X
2.86	X	X	X	X
2.94		x	x	
3.33	X	X	X	X
3.45	X	X	X	X
3.56	X	X	X	X

Table 10 Irregular wave list at model scale

Spectrum details	*Tp (s)*	*Hs*	*Wind thrust (N)*	Facility ref.
JONSWAP (γ=3.3)	1.29	0.05	0, 5, 7	A, B, C, D
JONSWAP (γ=3.3)	1.29	0.05	3, 8	D
JONSWAP (γ=3.3)	1.29	0.075	0, 7	A, B, C, D
JONSWAP (γ=3.3)	1.29	0.075	3, 5, 8	D
JONSWAP (γ=3.3)	1.81	0.1	0, 7	A, B, C, D
JONSWAP (γ=3.3)	1.81	0.1	5	A, B, D
JONSWAP (γ=3.3)	1.81	0.1	3	C
JONSWAP (γ=3.3)	1.81	0.1	3, 8	C
JONSWAP (γ=3.3)	1.81	0.15	0, 7	A, B, C, D
JONSWAP (γ=3.3)	1.81	0.15	5	A, B, D
JONSWAP (γ=3.3)	1.81	0.15	3	C
JONSWAP (γ=3.3)	1.81	0.15	3, 8	D
JONSWAP (γ=3.3)	2.58	0.10	0	A, B, C, D
JONSWAP (γ=3.3)	2.58	0.10	3, 5, 7, 8	D
JONSWAP (γ=3.3)	2.58	0.15	0	A, B, C, D
JONSWAP (γ=3.3)	2.58	0.15	3, 5, 7, 8	D
JONSWAP (γ=3.3)	2.58	0.20	0	A, B, C, D
JONSWAP (γ=3.3)	2.58	0.20	3, 5, 7, 8	D
Pink noise			0, 3, 5, 7, 8	D, E

4.2 Wind round robin results

The main results and findings from the wind round robin are presented and discussed in the following sections. Note that detailed analyses of the mooring system characterisation, and the results in irregular waves are presented in [19], [20], and summarised below. The research presented in [20] outlines metrics that can be used for a more straightforward comparison of the irregular wave test results from each facility. The detailed numerical results from the irregular wave tests using these metrics are included in the Appendix to this report.

4.2.1 Mooring system characterisation

The mooring system was characterised using static load tests which involved applying constant loads to the floater in still water and recording the equilibrium position with a focus on the surge direction. This was achieved by attaching wires to the floater guided by pulleys so that a horizontal force could be applied at the centre of gravity. Figure 30 shows the setup for this test at Ifremer. For a detailed description on mooring load characterisation the reader should refer to [19].

The results obtained for the measured surge (K_{11}) and pitch stiffness coefficients (K_{55}) are given in Table 11 and Table 12 respectively. The results show good agreement in general; the K_{11} value for facility D (UoS) differs significantly as azimuth angle of the mooring footprint was reduced to fit the mooring lines into the basin footprint (see Figure 27).

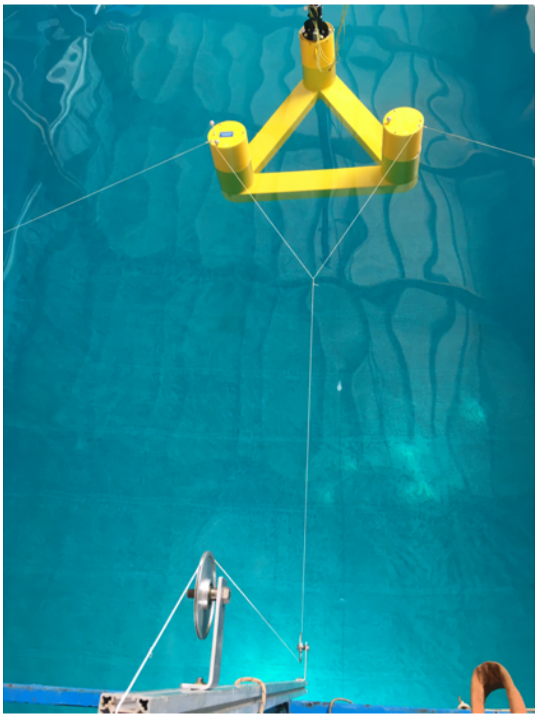

Figure 30 Static load test to characterise the mooring system stiffness

Table 11 Measured surge stiffness coefficients (K_{11})

Campaign Ref.	Mean K_{11} (N/m)	Std. dev. (N/m)	Std. dev/Mean (%)
A	22.36	0.58	
B	23.37	0.71	
C	23.54	0.48	
D	34.32	0.71	
E	22.50	0.40	
All (A, B, C, D, E)	25.22		18.7
Excl. UoS (A, B, C, E)	22.86		3.0

Table 12 Measured pitch stiffness coefficients (K_{55})

Campaign Ref.	Mean K_{55} (N.m/deg)	Std. dev. (N.m/deg)	Std. dev/Mean (%)
A	3.87	0.07	
B	4.01	0.07	
C	4.11	0.07	
D	3.95	0.07	
E	3.93	0.08	
All (A, B, C, D, E)	3.97		2.7
Excl. UoS (A, B, C, E)	3.97		2.7

4.2.2 Decay tests

Decay tests for the 6 DOFs of the moored system were carried out in all basins, with some additional tests carried out at certain facilities without the thruster power cables attached. The purpose of these tests was to measure the natural period of the motion mode which is predominantly responding to the position offset. The second objective was to assess and quantify the nature of the damping acting on the moored platform, through a P-Q analysis.

Consistent results were generally obtained across the facilities, except for facility D again where a different (stiffer) mooring setup was implemented. The largest differences were observed for the surge natural period, differences which were largely attributed to the power cable stiffening the system. Quadratic damping was found to be dominant in surge, with a lesser contribution from linear damping acting on the platform. For heave, very consistent results were obtained across all facilities, and the damping in heave was noted to be fully quadratic. This was also the case for the damping in pitch. For the other three DOFs, the results for the sway were very similar across facilities (except for facility D), and consistent results were also achieved for the roll natural period; however, large variations were observed between facilities for the natural periods in yaw.

4.2.3 Regular wave results and discussion

The list of tests performed is presented in Table 9, for a set of selected periods, regular waves are generated with various waves heights in order to investigate the non-linear response. Some facilities did not perform all the tests listed in Table 9 and some did additional cases. Figure 31 and Figure 32 show the results from ECN measurements. The heave motions present a linear behaviour for the shortest and longest periods and non-linearity is observed around the cancelation period T≈ 2.4s and resonance period T≈2.66s. On the pitch motions RAO, the non- linearity is also located around the resonance period T≈3.38. Finally, on Figure 32, even if the surge motions response is more scattered for period above 2.3s, a quite linear behaviour is observed in the considered period range. This linear response was expected since the resonance period is much longer for surge T≈19s.

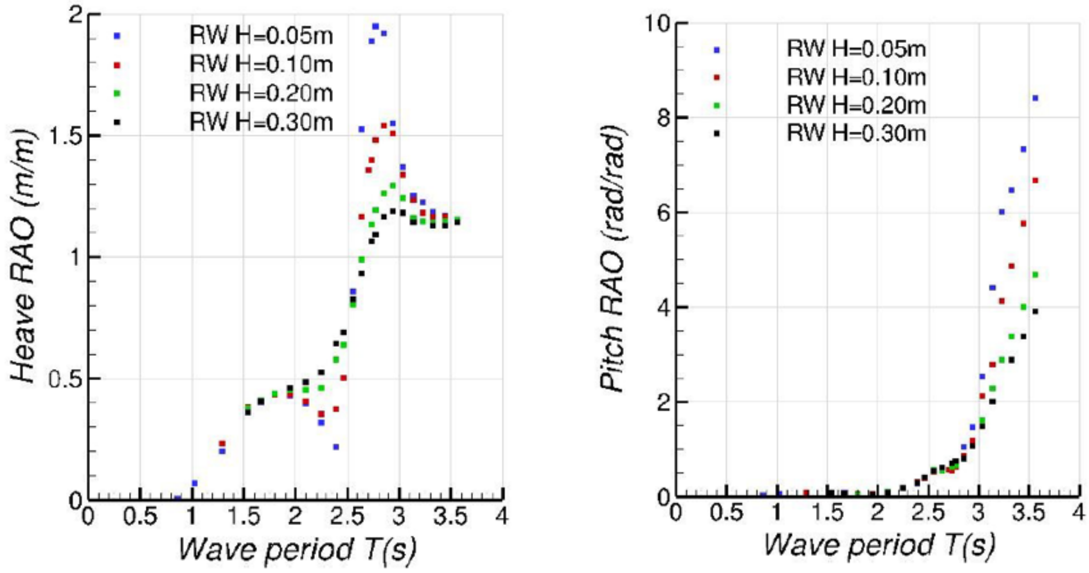

Figure 31 Heave and pitch response amplitude operator measured in ECN

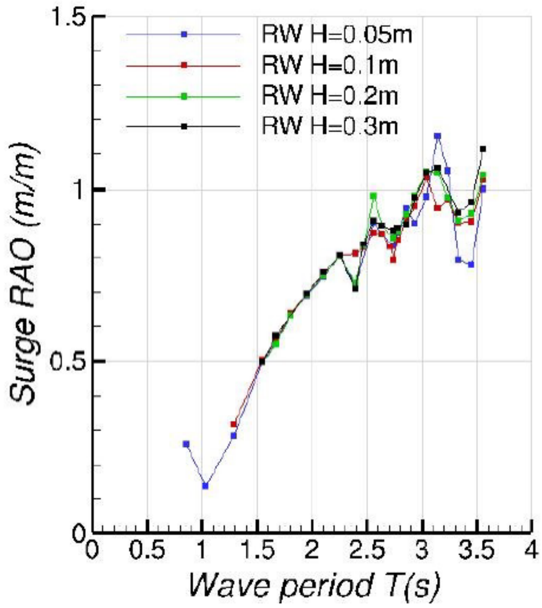

Figure 32 Surge response amplitude operator measured in ECN

The four facilities results are compared for heave and pitch motions on Figure 33. For both heave and pitch motions the values collected across facilities are quite similar except around resonance periods. As discussed just above, in these specific cases, the model response is non-linear, with a high sensitivity to the incident wave height. Therefore, potential differences in incident wave heights across facilities may cause the deviation observed around resonance period.

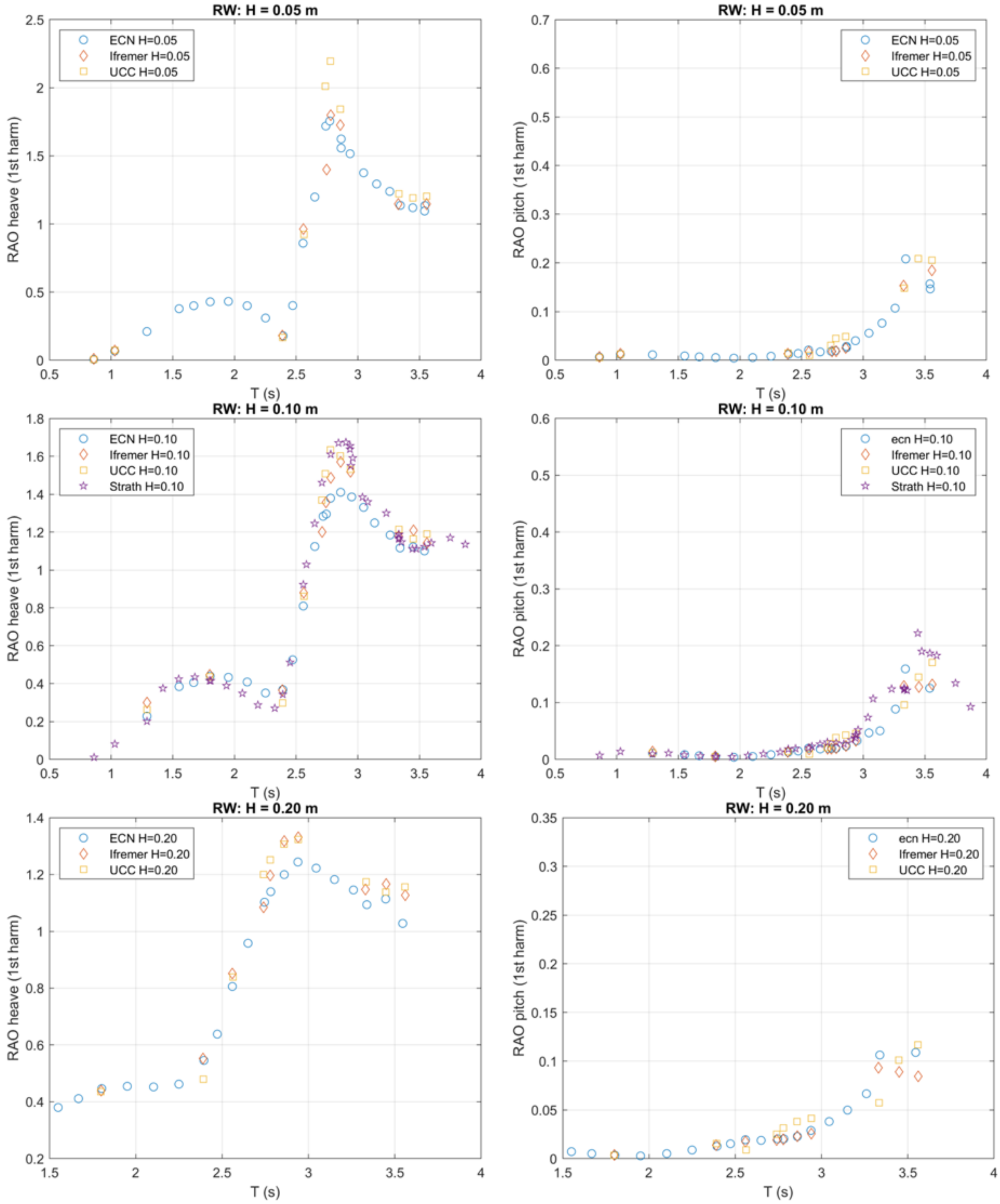

RW: H = 0.05 m
ECN H=0.05
Ifremer H=0.05
UCC H=0.05
RAO heave (1st harm)
RAO pitch (1st harm)
T (s)
RW: H = 0.10 m
ECN H=0.10
Ifremer H=0.10
UCC H=0.10
Strath H=0.10
ecn H=0.10
RW: H = 0.20 m
ECN H=0.20
Ifremer H=0.20
UCC H=0.20
ecn H=0.20

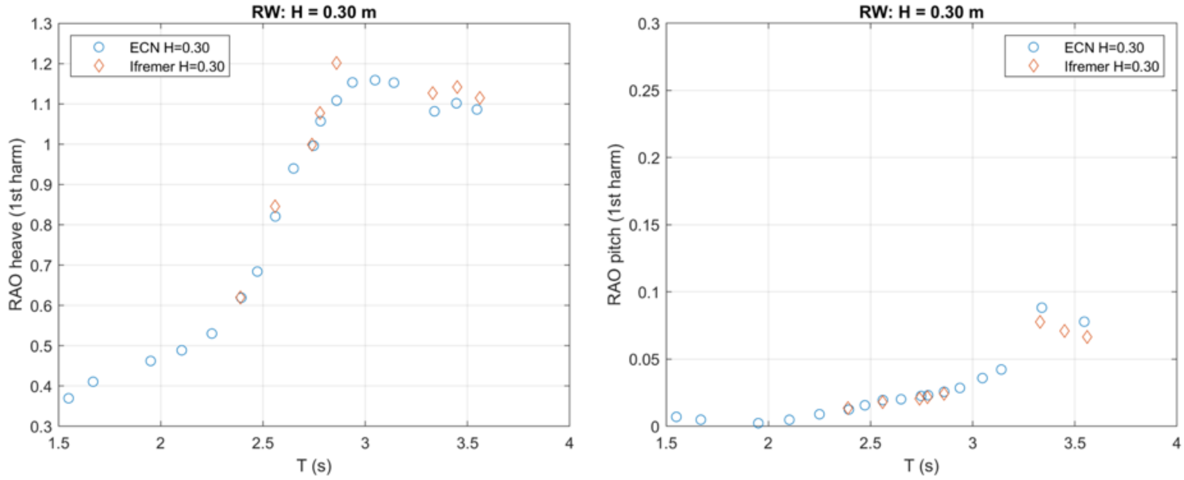

Figure 33 Heave and pitch RAOs in all facilities for incident wave heights of 0.05m (top row), 0.1 m (second row), 0.2 m (third row), and 0.3 m (bottom row).

A complementary analysis could be relevant to compare the wave calibration data collected in every basin without the model and would enable a better understanding of these RAO plots.

Nevertheless, even without the global view on wave calibration data across facilities, Figure 34 displays significant discrepancies on the time histories of wave elevation, heave and pitch motions. For these plots a regular test condition is specifically chosen at the heave resonance period.

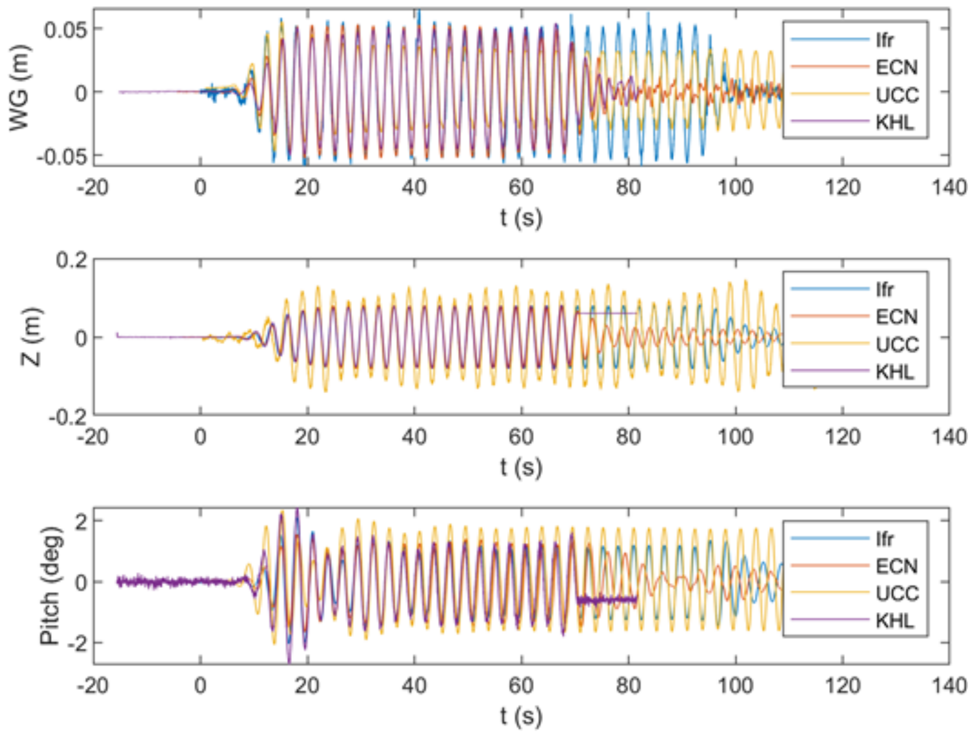

Figure 34 Time histories of wave elevation and heave and pitch motions for the regular wave test condition T=2.86s H=0.1m

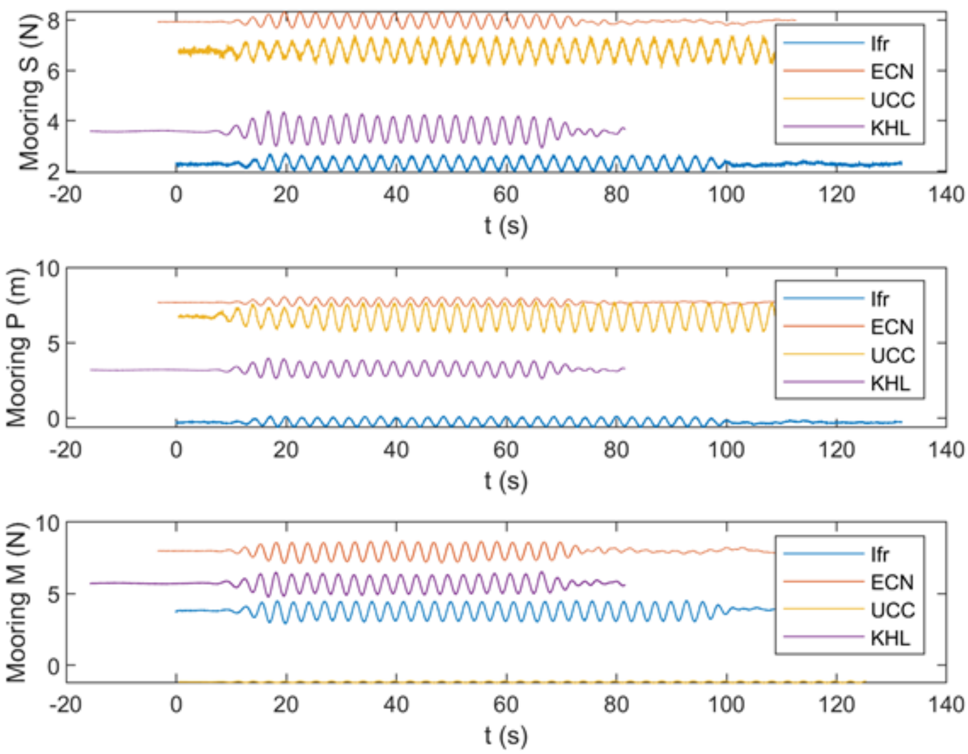

Figure 35 Time histories of the mooring lines loads for the regular wave test condition T=2.86s H=0.1m

Finally, Figure 35 shows the time histories for the mooring tension signals for the same specific regular wave tests at heave resonance period. The first observation is a large difference on mooring lines pretensions across facilities. These initial value differences may be due to an offset drift on the load cell signals. This electrical artefact is sometimes observed with some signal conditioners used to amplify strain gauges sensors. Signals from Ifremer and ECN have similar amplitudes. They cannot be compared to KHL signal since the mooring setup was different in this facility. However, mooring tensions recorded in UCC, with a similar mooring setup of Ifremer and ECN are distinct. The amplitudes are larger in the front lines, and the back line is slack.

4.2.4 Irregular wave results

Tests in irregular waves were carried out in all facilities. For a detailed analysis of the irregular wave results, refer to [19] which includes a discussion on the effect of the wave seed on the response. Detailed numerical results are provided in the Appendix.

Figure 36, Figure 37 and Figure 38 display the average RAOs for all the considered JONSWAP waves. In these plots, the 'average' is determined by taking the average of the RAOs from all basins for a specific JONSWAP wave. Each average RAO is surrounded by its envelope (shaded in grey) which allows visualisation of both the global trends and the spread in the results across all the facilities. These figures show that the same global RAOs were obtained, but with important variations.

Figure 36 shows that the variations in the surge RAO are amplified as the frequency decreases, exhibiting oscillations in the 0.3-0.5 Hz range. These oscillations are not equally sized for all facilities, and largely disappear above 0.8 Hz. They are largely attributed to reflections, which were significant in certain basins at lower frequencies.

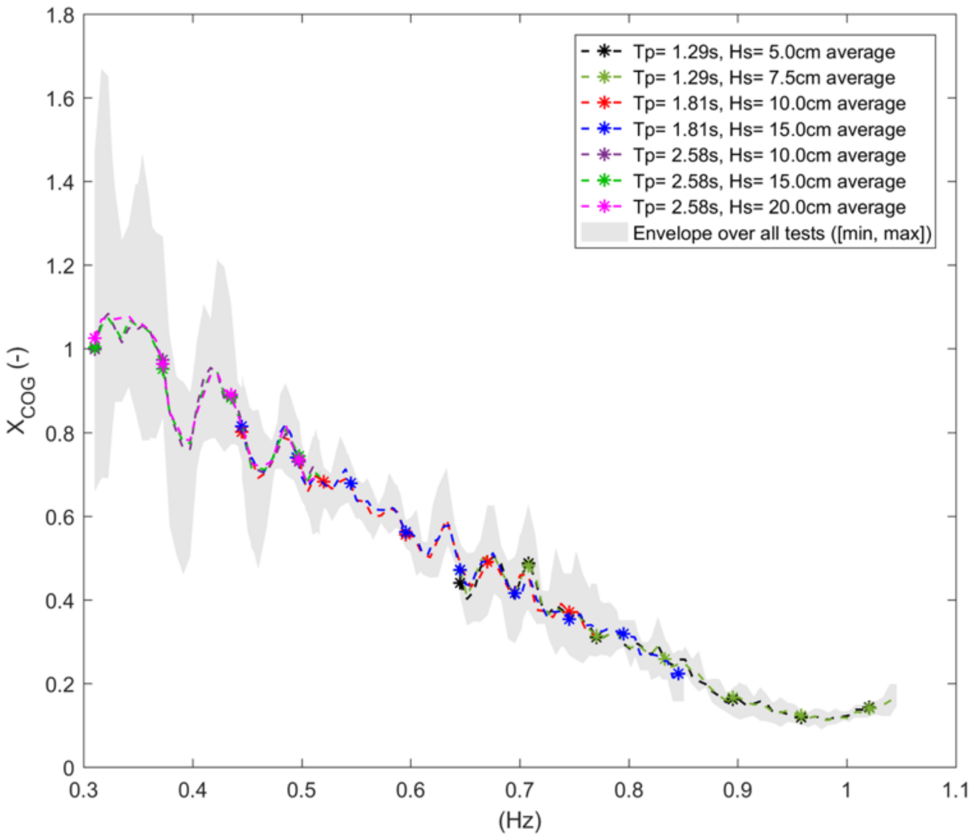

Figure 36 Surge RAOs for all JONSWAP waves: averages and [min max] envelope

The strongest agreement between facilities is obtained for the heave RAOs (Figure 37), evidenced by the relatively small spread in the results, particularly above 0.5 Hz. The RAOs of all basins capture the resonance peak (0.37 Hz) and the heave cancellation frequency (0.43 Hz) at the same frequencies. The variation in the RAO amplitudes is most pronounced around these two points.

The pitch RAOs were very similar across facilities (Figure 38). The prediction envelope was broader in the 0.3 to 0.45 Hz range. Note that the pitch eigen (natural) frequency of 0.29 Hz is close to the start of this range, and the effect of the wave height is strong at this frequency. Therefore, similarly to heave, the differences in achieved Hs between facilities for the same target wave lead to large discrepancies between RAOs close to the pitch resonance peak. As was the case for heave, the pitch response peak decreases with increasing Hs.

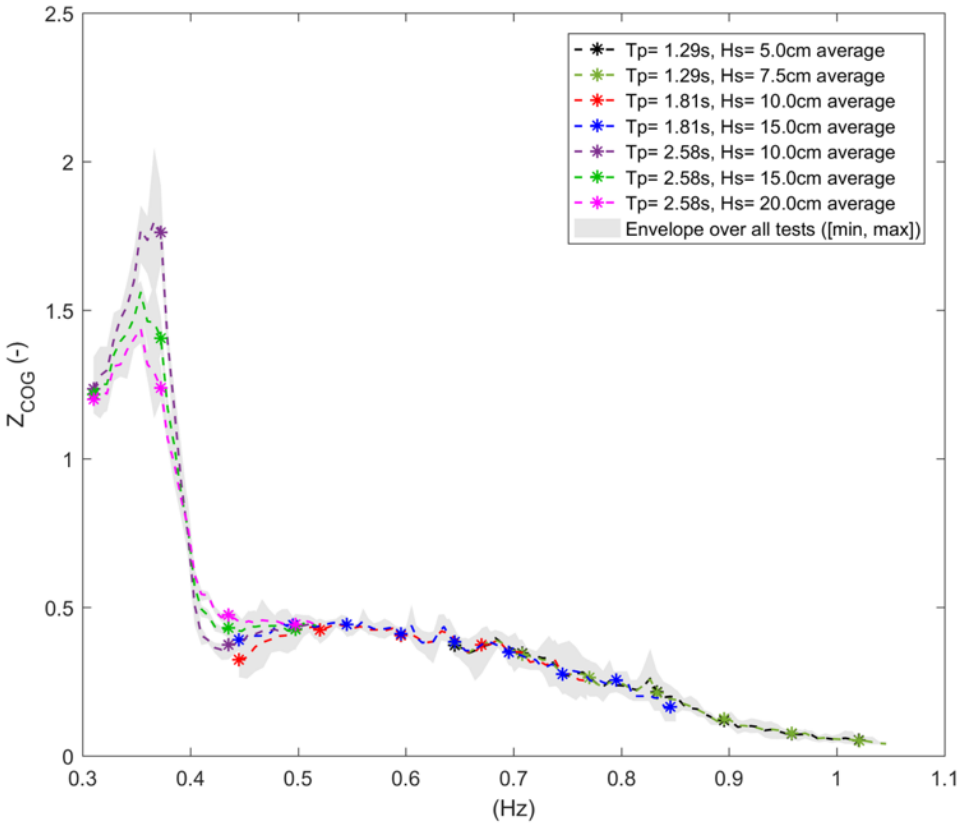

Figure 37 Heave RAOs for all JONSWAP waves: average and [min max] envelope

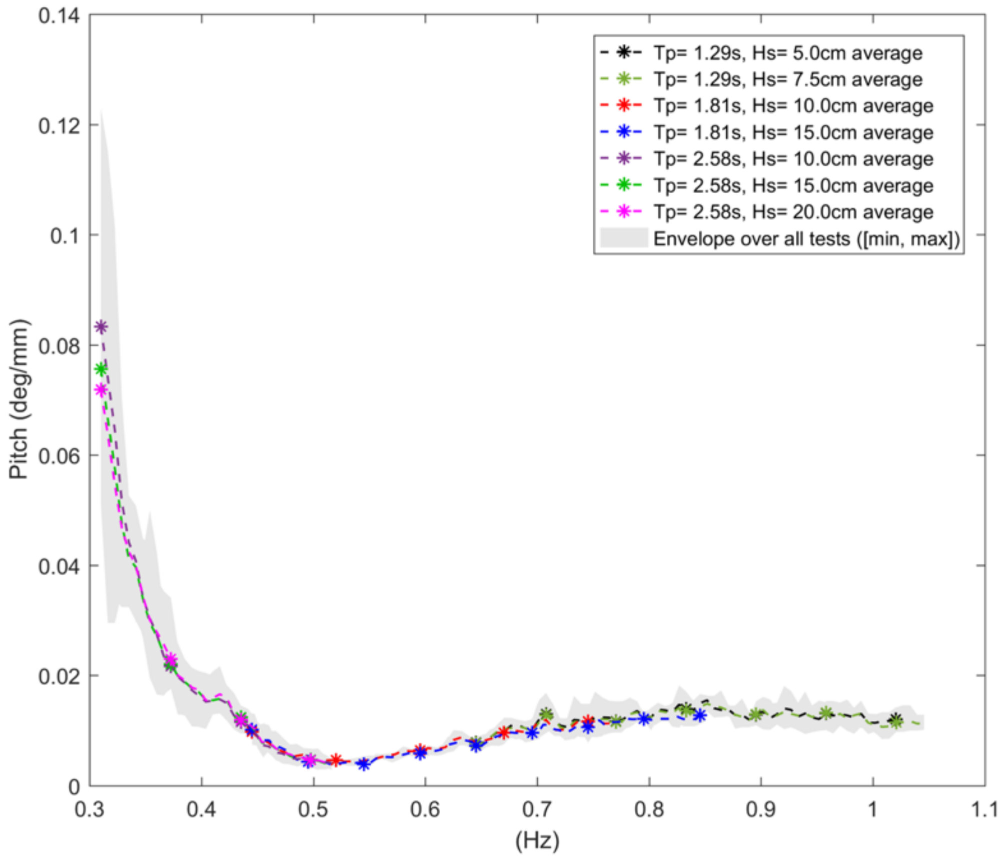

Figure 38 Pitch RAOs for all JONSWAP waves: averages and [min max] envelope

4.2.5 Impact of thruster on tests in irregular waves

When applying a thrust to the model during the decay tests, the increase in thrust leads to an increase of the horizontal mooring stiffness and a decrease of the surge natural period.

On irregular waves, the thrust action leads to the following remarks:

- the surge low frequency peak may differ from the natural period
- the heave and pitch peak periods are close to the natural periods
- long peak periods and pink noise have an influence on the pitch resonant response

4.2.6 Wind emulation comparison

Tests were run at Ifremer with a wind generator [22] and the DTU rotor [23]. The rotor was fitted at the top of the model mast in the place of the thruster used for other campaigns.

The aerodynamics depend on the Reynolds scaling and the seakeeping in waves depends on the Froude scaling. Combining both aerodynamics and hydrodynamics is a key point for a good representation of the floating wind turbine behaviour. For this purpose, the DTU rotor is designed to fit Froude scaling in terms of wind speed, rotating velocity, thrust… and the blades profiles are then different from the full-scale geometry.

The DTU rotor is controlled to fit the rotating speed and wind thrust. The Rotor at rest is located 3 m downwind from the wind generator.

The wind generator [21] can provide uniform wind, sheared wind (mix of 3 levels of constant wind) and irregular wind. In our case, irregular wind is generated according to Kaimal spectrum and formulation given by NREL [24].

While both wind and waves can be generated, a particular attention must be given to the repetition periods of the wind and waves sequences representing the target spectra. A common repetition period is used and sequences with longer durations are generated, as a consequence a common time interval can be selected for analysis.

The figures below illustrate the RAOs identified at Ifremer with the thruster (Figure 39) and with the DTU rotor (Figure 40).

The responses on JONSWAP spectrum sea states can be seen on the frequency interval f>0.55 Hz. The irregular wind induces more erratic RAOs calculated with the waves as reference.

During decay tests, the action of the rotor with or without wind increases the itch natural period and damping. The surge and pitch natural periods and damping are more erratic.

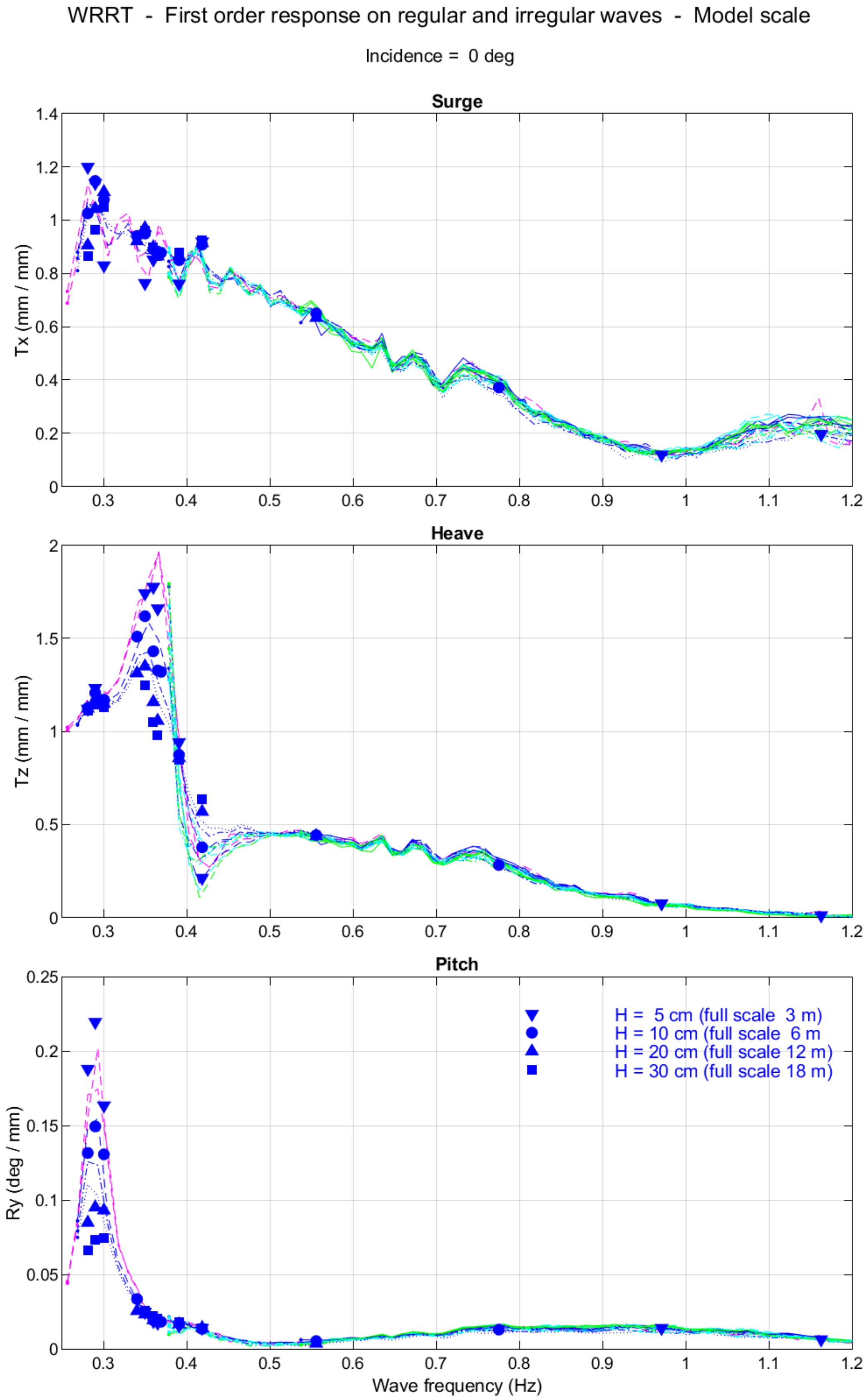

Figure 39 Tests at Ifremer without wind or with the thruster: Surge, heave, and pitch RAOs for regular waves (markers) and irregular waves (lines)

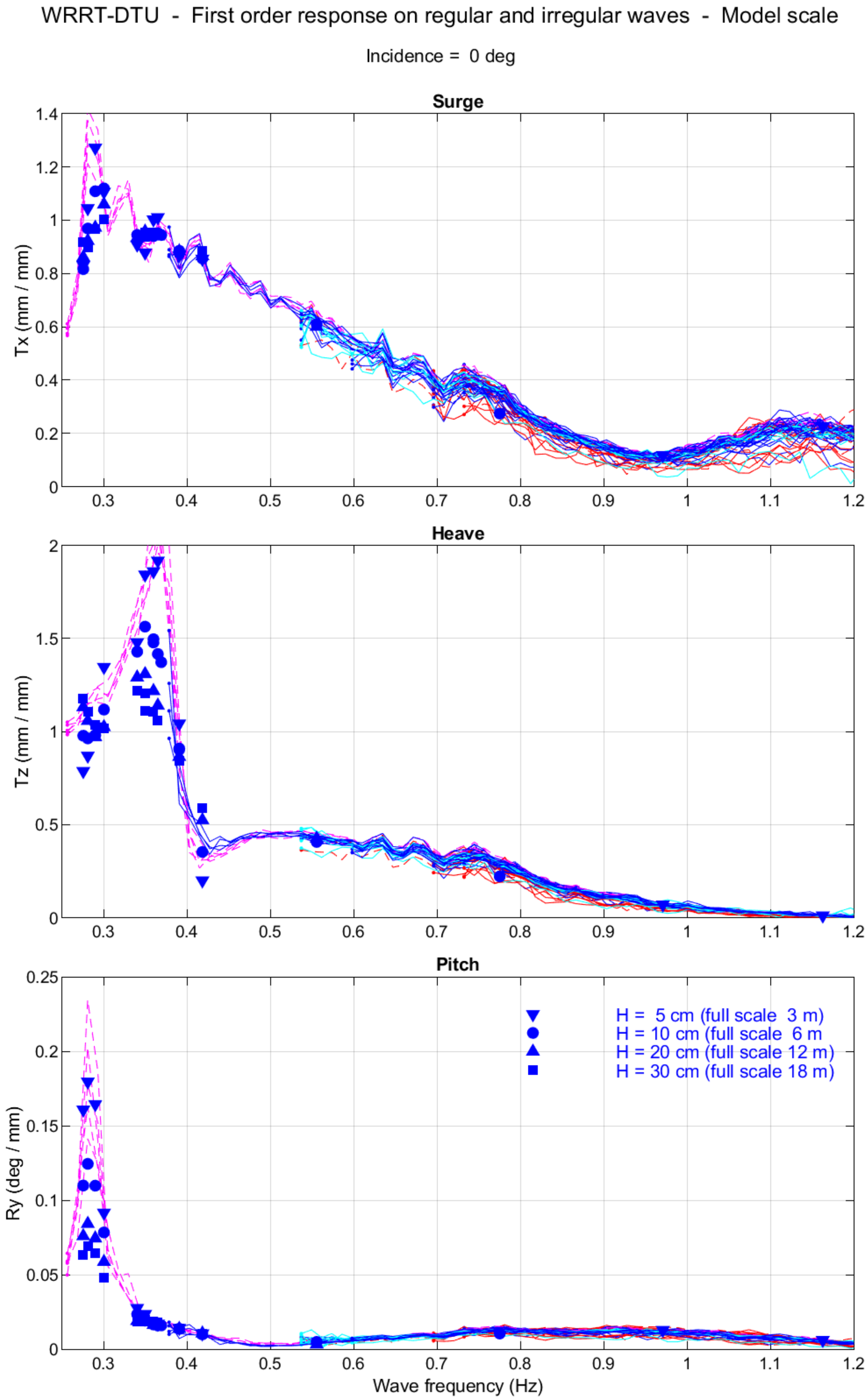

Figure 40 Tests at Ifremer without wind or with the DTU rotor: Surge, heave, and pitch RAOs on regular waves (markers) and irregular waves (lines)

4.2.7 Wind emulation using a pulley

After a first test campaign by UCC with the thruster, a second test campaign was carried out at UCC with an external load simulating the wind thrust. The load was applied using a weight connected to the top of the mast by a stiff rope running through a pulley.

For decay tests, the mass has a low influence on the natural periods but the surge and pitch damping are largely increased, most likely due to friction in the pulley.

On irregular waves, the resonant pitch response is decreased for sea states with pink noise spectrum and the low frequency surge response is decreased.

4.3 Lessons learned from the wind round robin campaign

4.3.1 Wave calibration

The processes by which waves were generated and calibrated were not the same for all facilities. This was generally due to the fact that the different physical characteristics of the basins (length, width, presence of active absorption etc.) guided different approaches to wave calibration and the selection of the analysis interval (particularly for regular wave analysis).

Ideally, more instructions would have been provided for the calibration of waves, e.g. the criteria for achieved significant wave height for regular and irregular waves, duration of the tests, the repeat time and the cut-off frequencies. Going forward, a minimum duration should be specified for the tests in irregular waves, and targets set for wave calibration, e.g. achieved JONSWAP spectra where the deviation of m0 is less than 5%.

4.3.2 Decay test methodologies and impact on damping

Different methodologies for carrying out decay tests were observed in the different facilities. Variations in the estimated damping coefficients were largely attributed to the way the decay motion was initiated, in particular the starting amplitude. Depending on the basin attributes, some operators initiated the decay motion while standing outside or over the basin, whereas others had to do so while on board a small boat adjacent to the model. In each case, the starting amplitude differed.

4.3.3 Irregular wave generation

The irregular waves produced in each facility were different, despite using the same target spectrum and Hs. This, combined with the sensitivity of the resonance peak to the Hs lead to the spread in the RAO results, particularly around the heave natural frequency and the cancellation frequency. Inconsistencies in the duration of the irregular wave tests across facilities is likely to have contributed to this discrepancy.

4.3.4 Impact of reflections

Reflections were very significant in certain facilities at certain periods. In some cases, there were insufficient wave probes installed to do a full reflection analysis.

Natural modes for the lowest water depths were observed. Although active absorption control procedures were available at UCC and UoS the impact of the natural modes is obvious when considering the transfer functions. For larger water depths at ECN and Ifremer and without active absorption the floater behaviour was less sensitive to the natural modes.

4.4 Recommendations for future round robin activities

4.4.1 Reflection analysis

Sufficient wave probes should be installed in all basins to facilitate an analysis of reflections and to determine the impact that they may have on the results. Full understanding of how reflections develop in a basin would give greater confidence in determining an optimal analysis period for each wave condition. Each wave condition should then be calibrated to an agreed level of accuracy for the selected interval. This would allow more like-for-like comparisons be made between facilities.

4.4.2 Decay test methodologies

It recommended that standardised procedures are developed for initiating motion when conducting decay tests. This may be achieved by measuring the displacement using a metre stick (if pushing down) or using a spring loaded gauge when lifting the model. The initial displacement should be agreed in advance of carrying out these tests. Care should also be taken to minimise motion in other DOFs than the one of interest.

4.4.3 Quantify the impact of the power cable

The power cable was found to be a source of discrepancy between round robin test campaigns. How the cable is supported and its impact on results should be carefully monitored in any future round robin activities, and guidance given on how it should be supported. Is it recommended that decay tests are carried out with and without the power cable attached to quantify its impact.

4.4.4 Parameter of irregular wave tests

It is recommended that care is taken to ensure that any irregular wave tests carried out are of sufficient duration to achieve convergence in achieved H_S. Tests should have a duration of 3 hours at full scale. Longer duration tests may be necessary to study the low frequency motions of the platform.

It is recommended that Pink Noise tests are included in the test plan, to enable assessment of how the device responds to as broad a range of frequencies as possible. To generate this type of wave series in a wave tank, the lower and upper frequency bounds should be set based on the capabilities of the wave maker.

4.4.5 Wind emulation

There are several different ways of emulating the wind thrust on a floating platform. The methods tested during the round campaign were:

- nearly constant thrust made possible by an onboard thruster or and external weight acting through a pulley
- wind generation and a controlled rotor capable of simulating the wind thrust in Froude scaling and variable pitch blades

Wind emulation with a thruster:

- When using “drone” components, high rotation speed may induce parasitic signals in force sensors.
- The alignment of the thruster onboard the model must be carefully checked.
- Calibration of the six components force induced by the thruster should be done with a six components gauge.
- The influence of gyroscopic effects should be investigated.

Wind emulation with a pulley and weight:

- When choosing a pulley, ensure the friction is a low as possible.
- The alignment of the pulling line with reference to the model and wave basin must be carefully checked.
- An initial estimation of the influence of the connected mass on the natural periods must be done as the external mass may modify the surge and pitch natural periods.

Wind emulation with a rotor and wind:

- a sufficiently large rotor diameter is necessary to minimize the Reynolds effects
- the wind generator must accordingly be able to feed the whole blades disk and the generated wind must be carefully calibrated
- sufficient time must be allowed to calibrate the rotor and its instruments prior to the tests
- generic studies should be organized for a better understanding of the damping and inertia effects during decay tests with rotor on
- a systematic protocol should be defined for the generation of both wind and waves
- combination of sea states and turbulent wind could be a scope of research on statistics and occurrence of coupled wind-waves parameters that may lead to “extreme” events.

4.5 Published wind round robin research

Two research papers describing the wind round robin tests have been published to date. Both appeared in the MaRINET2 special issue of the Journal of Marine Science and Engineering, details below.

Gueydon, S.; Judge, F.M.; O’Shea, M.; Lyden, E.; Le Boulluec, M.; Caverne, J.; Ohana, J.; Kim, S.; Bouscasse, B.; Thiebaut, F.; Day, S.; Dai, S.; Murphy, J. Round Robin Laboratory Testing of a Scaled 10 MW Floating Horizontal Axis Wind Turbine. *J. Mar. Sci. Eng.* **2021**, *9*, 988. https://doi.org/10.3390/jmse9090988

Gueydon, S.; Judge, F.; Lyden, E.; O'Shea, M.; Thiebaut, F.; Le Boulluec, M.; Caverne, J.; Ohana, J.; Bouscasse, B.; Kim, S.; Day, S.; Dai, S.; Murphy, J. A Heuristic Approach for Inter-Facility Comparison of Results from Round Robin Testing of a Floating Wind Turbine in Irregular Waves. *J. Mar. Sci. Eng.* **2021**, *9*, 1030. https://doi.org/10.3390/jmse9091030

4.6 Description of open access dataset

All data generated by the MaRINET2 round robin is available for download through the MaRINET2 e-infrastructure which can be accessed through www.marinet2.eu or through the OpenAIRE Explore website: https://explore.openaire.eu

Details of the dataset are as follows:

Gueydon Sebastien, Judge Frances, O'Shea Michael, Lyden Eoin, Le Boulluec Marc, Caverne Julien, Ohana Jeremy, Kim Shinwoong, Bouscasse Benjamin, Thiebaut Florent, Day Sandy, Dai Saishuai, Jimmy Murphy (2021). **Marinet2 - Datasets from the "Round robin" testing program on a floating wind turbine**. SEANOE. https://doi.org/10.17882/83063

5 Cross-cutting activities

5.1 Mooring and station-keeping solutions

Prototypes of MRE systems are commonly moored to the seabed using synthetic fibre ropes. This marked shift from conventional mooring methods employing chains and wire ropes is driven by the benefits associated to the use of synthetic fibre rope to energy take-off, reliability, and the consequent contribution to cost reduction.

Existing experience of fibre rope moorings in the offshore industry is primarily based on the operations in the offshore oil and gas industry for the past two decades. The application of this knowledge to MRE systems is limited since the loading regimes at O&G platforms beyond 1000 meters depth are significantly different from those experienced by MRE deployed at sites with depth in the order of tens of meters.

Additionally, due to the unique design requirements of mooring systems in offshore renewable installations, detailed numerical and empirical investigation as well as offshore experience is required to facilitate adoption and certification of fibre ropes in MRE.

Rope testing was conducted at the Dynamic Marine Component (DMaC) test facility in July to August 2019 and at IFREMER between August and December 2019. To ensure that the variable is limited to the facilities only, the same specimen is exposed to an identical test at DMaC and IFREMER to assess the differences in implementation and resulting experimental outcomes.

5.1.1 Test specimen

The round robin test specimen was a EUROFLEX® rope, composed of a combination of polyester fibres with a blend of polyolefin (PP+PE). It is a white twisted 3-strand rope with a yellow marker yarn manufactured by Lankhorst as a 32mm 3 – strand rope.

The minimum breaking force of the rope provided by the manufacturer is usually defined for the rope itself, without any terminations such as splices, or terminations formed with or without the use of additional fittings.

Five test samples per test facility were procured from Lankhorst Ropes with a length of 5 metres each. The rope length is 5 metres from bearing to bearing with approximately 0.6 m diameter eye each end and 1.12 m of splice coming from the bottom of each eye. This allowed approximately 2.5 m of unspliced rope for testing as required by the facility managers at DMaC and IFREMER.

The following length measurements were taken at the outset of each experiment with reference to the Minimum Breaking Load (MBL):

- L_T – Eye-to-eye length at reference tension (2% MBL)
- L_G – Gauge length at reference tension (2% MBL)

During the test set-up at DMaC, it was discovered that the polyolefin blend makes the rope more elastic than a pure polyester rope. Therefore, samples tested at DMaC were respliced to shorten the sample and compensate for the additional elasticity of the rope for break testing.

5.1.2 Experimental set up

5.1.2.1 Dynamic Marine Component (DMaC) test facility

The DMaC test facility is owned and operated by the University of Exeter. Constructed during 2010, its main role is to replicate the dynamic operational and fatigue loads that offshore components typically experience in service The facility, as shown in Figure 41, includes a hydraulically powered headstock for the application of user-defined loads (harmonic and irregular time-series).

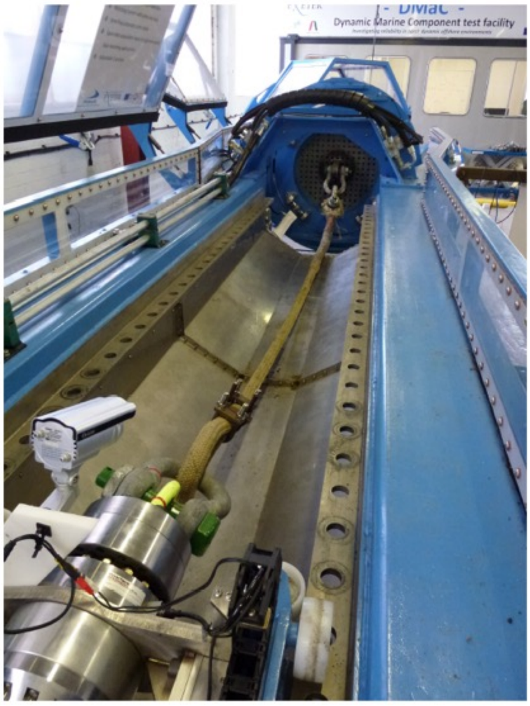

Figure 41 DMaC test facility at the University of Exeter.

It differs from existing tension test machines in that it also possesses a hydraulically powered tailstock, providing an additional three degrees-of-freedom (roll, pitch and yaw). This feature is particularly useful for the testing of subsea components which are subjected to bending or torsion at one end (for example cables, umbilical assemblies and risers). Additionally, the DMaC has been designed so that components can be fully submerged in fresh water during testing.

The DMaC machine comprises a synchronised control and data acquisition system which enables both specified and measured values to be appended, at each time step, to a single results file. For the tests reported here the axial load experienced by the main hydraulic cylinder (otherwise known as the 'Zram') and piston displacement were simultaneously logged at a sample rate of 50 Hz.

The load was measured by a DSCC pancake load cell manufactured by Applied Measurement Ltd, UK (serial number 50317); full-scale linearity of ±0.039%. Piston displacement was measured using a LM10 linear encoder manufactured by RLS Merilna tehnika d.o.o., Slovenia; resolution of 0.05 mm. The measurements were recorded using a National Instruments (NI) compact Reprogrammable Input Output (cRIO) 9022. Load measurements utilised a NI 9237 C-Series module and displacement measurements used a NI 9205 C-Series module.

In addition to data logging, the DMaC data acquisition system was used to monitor piston displacement and axial load during test setup, allowing the reference tension (2% MBL unless otherwise specified) to be set prior to testing.

An IP67-rated, WS12 draw-wire transducer manufactured by Applied Measurements was used to measure sample elongation during the bedding-in and dynamic stages of the ISO 18692:2007(E) at a sample rate of 50 Hz. The draw-wire transducer was record using the NI cRIO 9022 and NI 9205 C-series module. With the transducer body clamped to the sample using a custom-made clamp, the end of the draw-wire was attached to the sample using a bungee cord (via an additional length of wire) to provide a gauge length greater than 1.2m. In accordance with ISO 18692:2007(E) the attachment points of the transducer body and wire were at least three times the rope diameter from the end of the splices. The transducer has been used extensively for rope testing in the past and possesses a high level of measurement linearity (R2 > 0.99).

5.1.2.2 IFREMER

Two structural test frames, initially developed for rope testing, at The Marine Structures laboratory at L'Institut Français de Recherche pour l'Exploitation de la Mer (IFREMER) are available within the MARINET2 project:

- **1000 kN test frame.** 10 metre long tensile test frame, 8 meters long Piston one end, Course 1.5m, Possibility to wet during testing (spray with tap water) but not immersed. Possibility to heat central section. Displacement measured either by two digital cameras (non-contact) or wire displacement transducers fixed to rope. Break tests, Stiffness measurements, Creep tests.
- **300 kN Fatigue test frame**. 8 metre long flexural test frame (3 hydraulic actuators up to 3 metre displacement). Three operating modes: tension fatigue, cyclic bend over sheave and simulation of winch.

The tests described here were all performed on a 300 kN test frame at the IFREMER Centre in Brest, Figure 42.

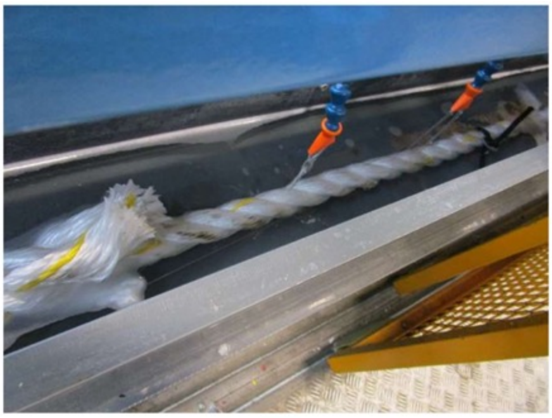

Figure 42 Rope sample in place on test machine at IFREMER, showing tap water spraying system.

The load cell is an AEP TC4 300 kN model. It is calibrated annually by an external company.

All samples were tested wet. This indicates that they were left fully immersed in tap water overnight without load for at least 12 hours before testing, then sprayed with water throughout the test except for the final ramp to failure.

Strain measurements were obtained from two wire displacement transducers placed at the two ends of the rope. They were mounted on an L-frame in order to be at the right height, Figure 43. At the fixed end of the rope the transducer was an ASM WS10-500mm displacement model. At the moving (piston) end an ASM WS10- 1250mm model was used.

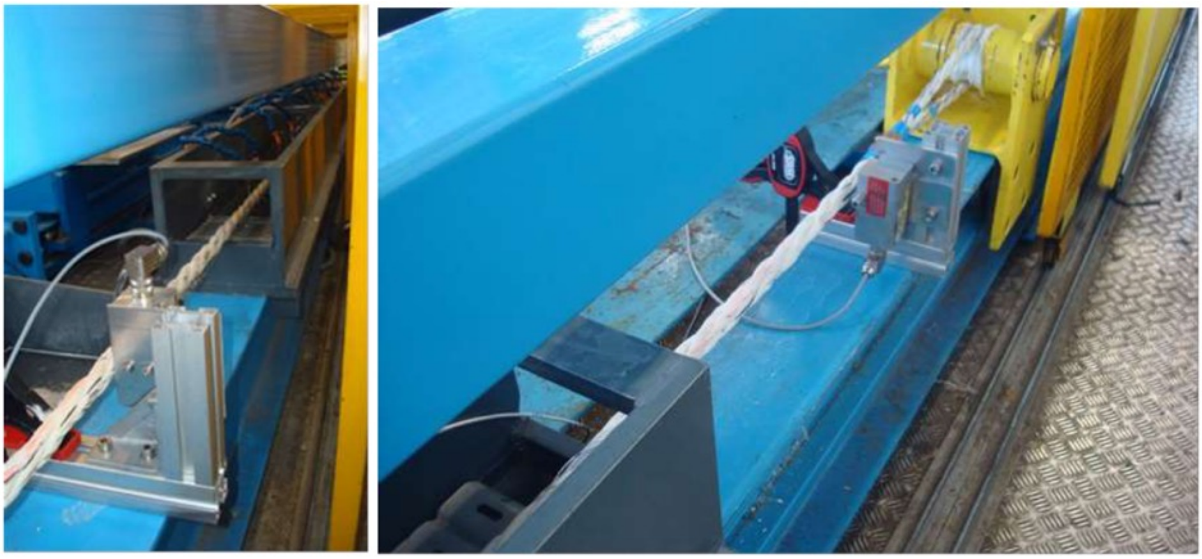

Figure 43 Wire transducer installation at ends of sample.

The ends of their wires were fixed to the rope in the central section using elastic loops. The distance between these two loops was measured accurately at the start of the test under a small load of 3kN, (2% break load) to define the reference length Lo. The strain was then determined as the difference between the two displacements divided by Lo. This strain value was used in all stiffness calculations. The two wire transducers were provided with supplier calibrations but both were checked manually before each test.

Piston displacement measurement was recorded throughout tests, using an SCAIME wire transducer model PT5DC-40. The MTS "MultiPurpose Elite" software controls the piston movement and allows test sequences to be recorded. It also allows continuous recording throughout each test of:

- Force
- Piston displacement
- Air and water temperatures
- External displacement transducers.

Data was recorded at two acquisition frequencies. A frequency of 1 Hz, to provide a first overview of the test, and higher frequency (5 Hz) for the dynamic stiffness measurements. The stiffness values given in this report were obtained from the data recorded at 1 Hz unless otherwise stated.

5.1.3 Test plan

The test plan is based on the recommendations for polyester fibre ropes for offshore station keeping by the International Standardisation Organisation, namely ISO 18692:2007(E) [25]. This standard is commonly used to develop the fatigue test procedure at both facilities.

The basic test plan, spanning over 5 h 50 min 20 s followed by a break test, is tabulated in **Error! Reference source not found.**. The table provides reference to steps detailed in ISO 1 8692:2007(E). Additionally, the complete test plan is divided into three sections. Section A involves bedding-in, Section B defines the quasi static and dynamic loading of the synthetic rope, whereas, Section C outlines the break test. Figure 44. illustrates a time series displaying these three sections.

Three testing regimes, agreed between IFREMER and the University of Exeter are described in Table 13 and an estimated test duration is also noted.

Table 13 Description and duration of the cyclic test regimes employed for round robin testing of a fibre rope.

Test Ref.	Test description	Test duration
Test 01 Test 02 Test 03	Phase A → Phase B	5 h 50 min 20 s
Test 04	Phase A → Rest 18 hours → Phase B	23 h 50 min 20 s
Test 05	Phase A → Rest 18 hours → Phase A → Phase B	34 h 50 min 20 s

Both establishments tested 5 identical samples based on the guidance provided by the same standard. For each test regime described in Table 13, a sample is tested at each facility to ensure repeatability of the process and increase confidence in the results. The initially discussed 24 hour resting period was limited to 18 hours once the working hour considerations were included.

The test regimes for these tests, defined in Table 13 include the repeats that are proposed. For Test 04 and Test 05, the samples were unloaded overnight, by removing the loading pin from the eye at the piston end of the rope, but the rope was left immersed at DMaC and wetting continued throughout at IFREMER.

Phase A includes the bedding-in, quasi-static stiffness measurements (10-30%), and dynamic stiffness values (15 s period) at three mean load levels (20-30%, 30-40% and 40-50%). Phase B is a linear ramp to failure under load control. Table 14 shows the steps in ISO 18692:2007(E) mapped to Phase A and B.

Table 14 Description of constituent steps in each phase of the test plan.

Phase	Steps	Description
Phase A	5-7	Bedding in (static)
	8	Bedding in (dynamic)
	9	Quasi-static loading
		Dynamic loading
Phase B	10	Load-to-failure

While piston and gauge displacement are recorded for Phase A at both test facilities, the transducers were removed prior to running the load-to-failure test stage to avoid damage to the transducer.

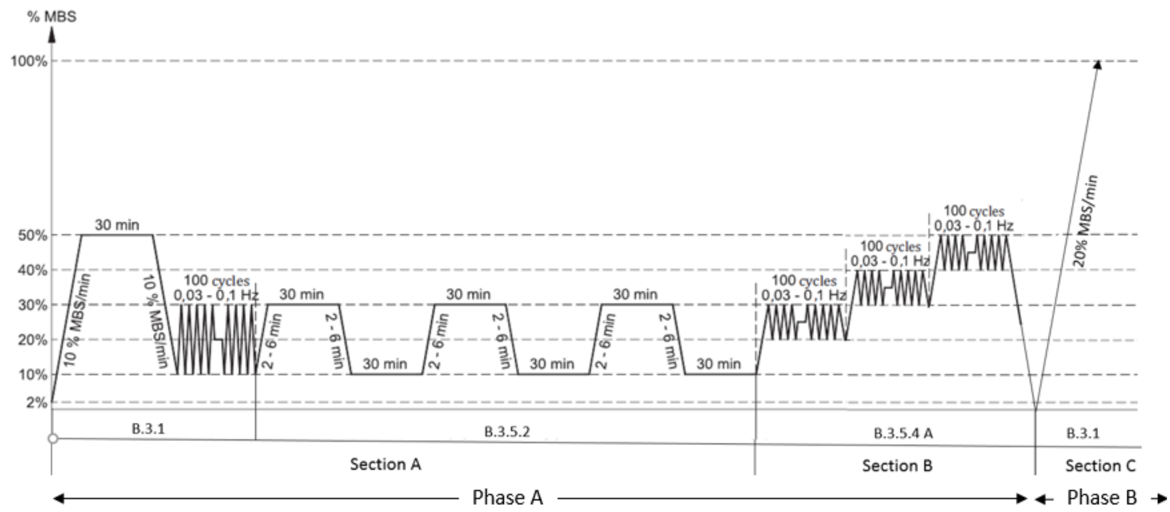

Figure 44 Input load time series distributed based on the sections and phases identified in Table 14 showing the bedding-in, quasi-static and dynamic loading as well as break testing

5.1.4 Test anomalies

5.1.4.1 DMaC

Test 01: OK

Test 02: OK

Test 03: OK

Test 04: Three attempts were made but sample did not break after leaving it immersed overnight in water. It was then removed from the test rig, left to dry and broken after Test 05 conducted. Therefore, the specimen was left for 48 hours (18 hours submerged and 30 hours dry) before the final break test.

Test 05: OK

5.1.4.2 IFREMER

There were some difficulties with the first test, due to a programming error and then with one of the wire transducers. A third problem was encountered during the ramps to failure, for which the initial hydraulic pressure was limited for 3 of the 5 tests, and had to be increased so the ramp was in two steps. These anomalies are detailed below.

Test 01: The bedding-in sequence was performed with 100 cycles from 10-20% instead of 10- 30%, and then the first QS cycle was loaded to 50% instead of 30%. The test was therefore stopped, the programme modified, and the QS cycles were restarted. There were also some problems with one of the wire transducers during certain stiffness measurements, as shown in Figure below.

During the break test on this sample there was insufficient hydraulic pressure to go beyond 188 kN, so the test was again stopped, then restarted with higher pressure and continued until failure at 218 kN.

Test 02: Once again pressure was insufficient to reach failure and the test was stopped at 200 kN, then restarted with higher pressure and continued to failure at 220 kN

Test 03: OK

Test 04: OK. During the ramp to break a load drop was detected at 158 kN. The test was stopped to inspect the rope but no sign of damage was visible so it was reloaded and finally broke at 176 kN.

Test 05: OK

5.1.5 Test results

The load time series applied to determine the stiffness characteristics of the sample is shown in Figure 45. The same load sequence is applied to all samples for Phase A at both test facilities based on the percentage MBL of 168 kN.

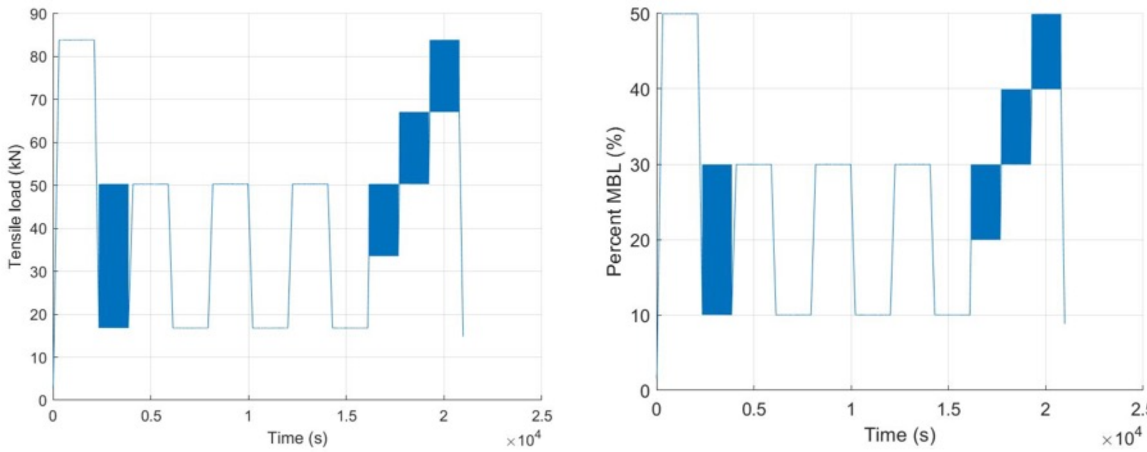

Figure 45 Load time series for Phase A displaying the applied load and % MBL.

5.1.5.1 Sample plots for Test 01 at DMaC

Two elongation measurements are recorded for Phase A of each test: piston displacement and changes in gauge length. Piston displacement and strain for Specimen 1 at DMaC are shown in Figure 46.

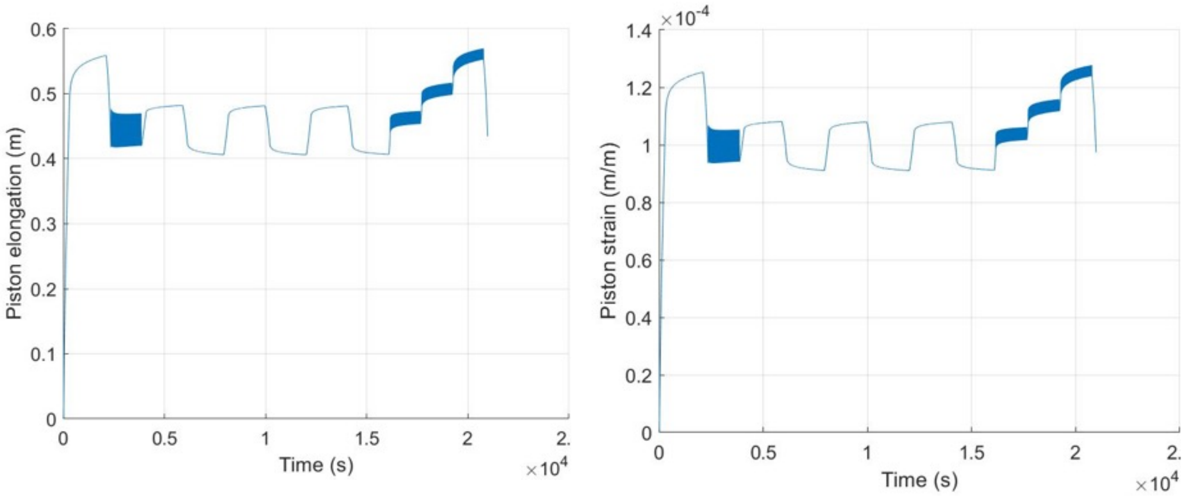

Figure 46 Piston elongation and piston strain for Test 01 at DMaC.

However, since the piston displacement includes the displacements of splices and end loops it cannot be used to determine stiffness values. Therefore, gauge measurements are used for determining stiffness parameters of the samples for steps in Phase A.

Gauge displacement and strain for Specimen 01 at DMaC are shown in Figure 47.

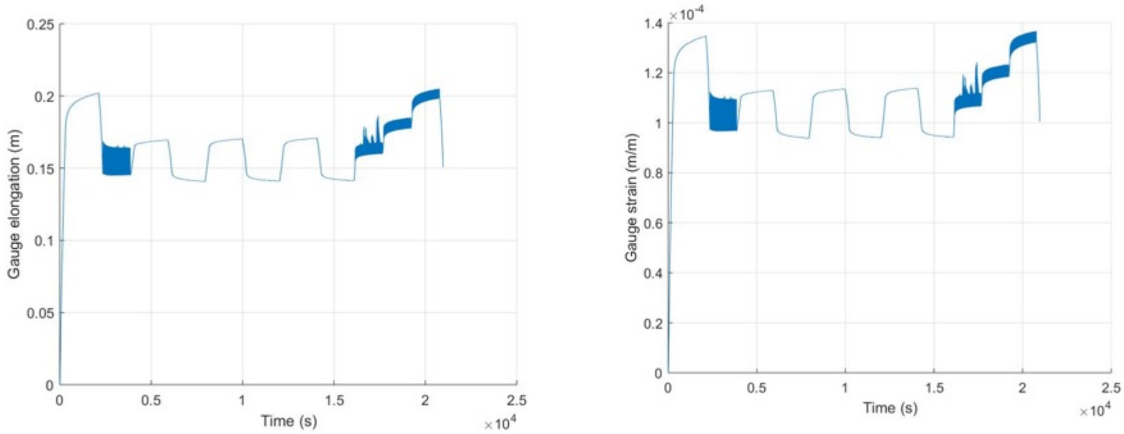

Figure 47 Gauge elongation and gauge strain for Test 01 at DMaC.

Since the transducer is removed for the break test, only piston displacement measurements are available for characterising sample elongation in Phase B. Time series for load and strain in the load-to-failure test of Test 01 are shown in Figure 48.

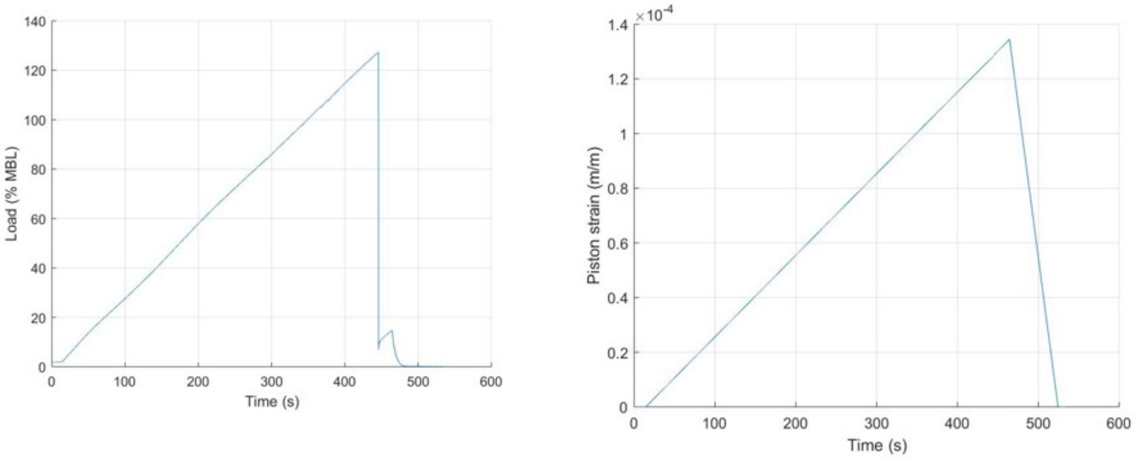

Figure 48 Load and piston strain time series for Test 01 at DMaC.

For each test, plots for load-piston displacement are produced for constituent steps based on the recommendation provided in B3.3. of ISO 18692:2007(E). Step 5-7, Step 8, Step 9 and Step 10 can be seen in Figure 49.

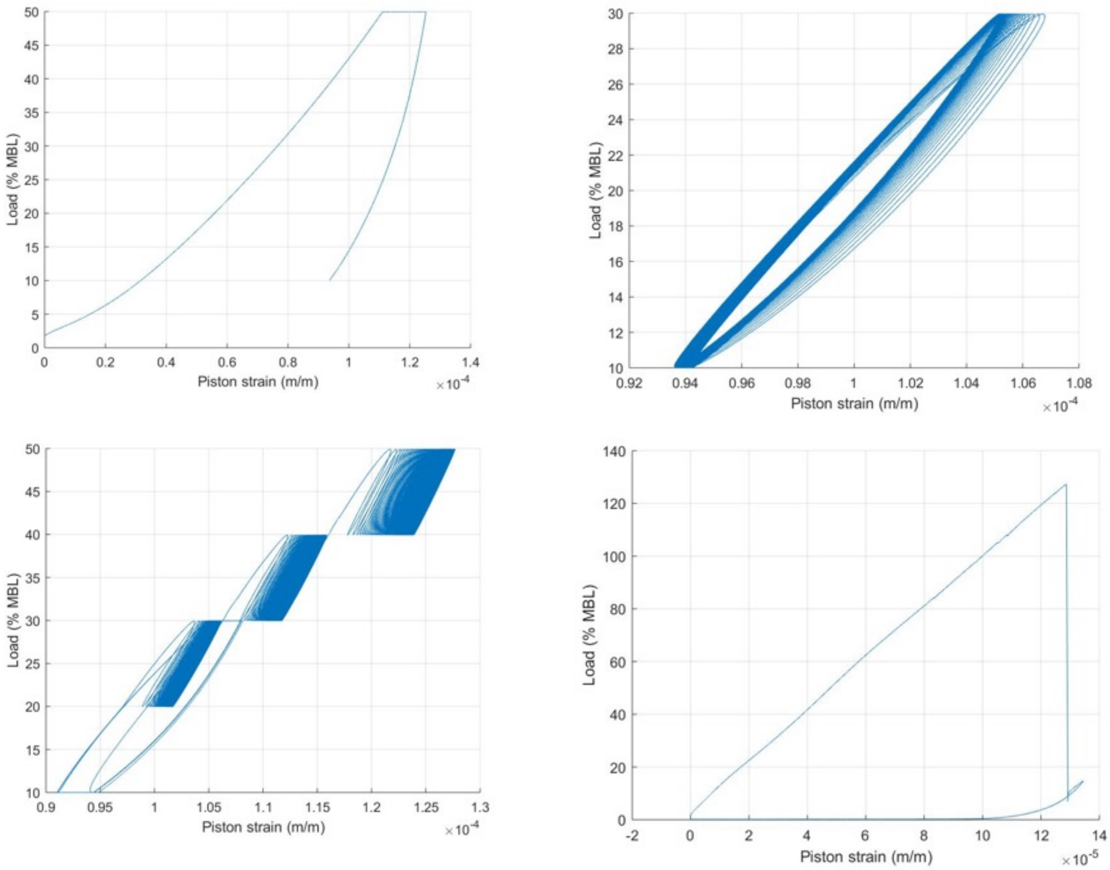

Figure 49 Load and piston strain plots for Step 5-7, Step 8, Step 9 and Step 10 for Test 01 at DMaC.

Similarly, load-gauge elongation plots for Step 5-7, last five cycles of Step 8 and last five cycle of each load range in Step 9 (dynamic), are shown in Figure 50, respectively.

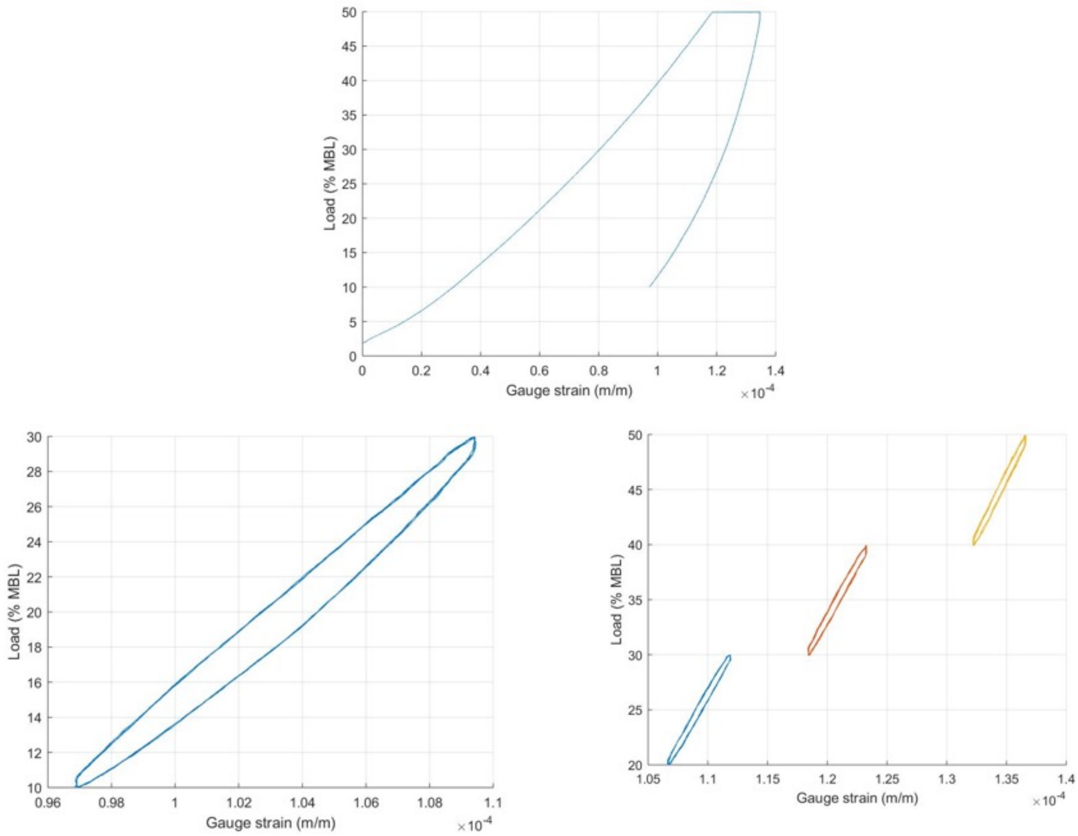

Figure 50 Load and gauge strain plots for Step 5-7, last five cycles of Step 8 and last 5 cycles of each dynamic load range in Step 9 for Test 01 at DMaC.

Finally, recommendation by ISO 18692:2007(E) is followed and load and elongation time series for quasi-static loading in Step 9 are shown in Figure 51.

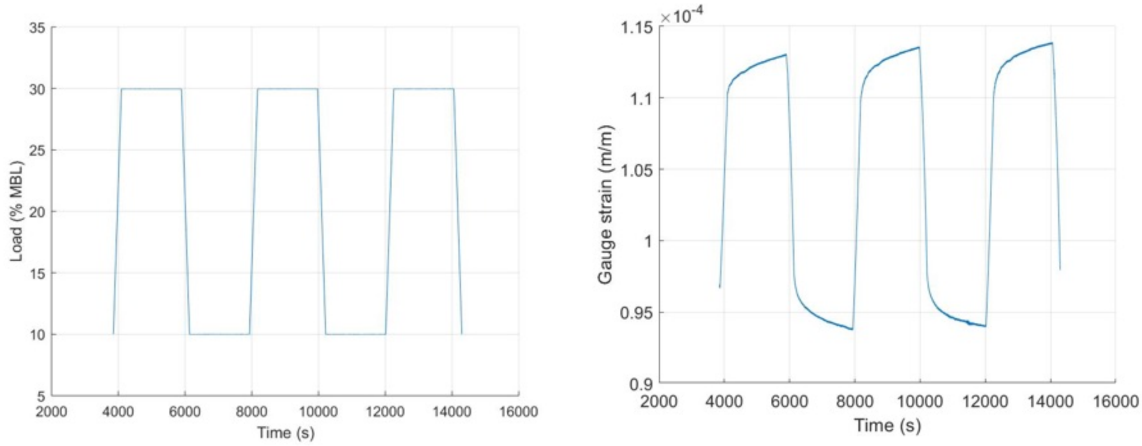

Figure 51 Load and gauge strain time series for Test 01 at DMaC.

5.1.5.2 Stiffness calculations

For the conducted tests, stiffness is calculated as a relationship between the applied load and resulting elongation (measured by changes in gauge length, L_G) based on the below equation.

$$K = \frac{\Delta F}{\%\ \text{Strain}}$$

5.1.5.2.1 Bedding in

The values of stiffness at the end of bedding-in can be determined, as the slope determined from a linear regression of the force-strain data points measured during the last five 10-30% cycles. Figure 52 shows this regression plot for Test 01 at DMaC

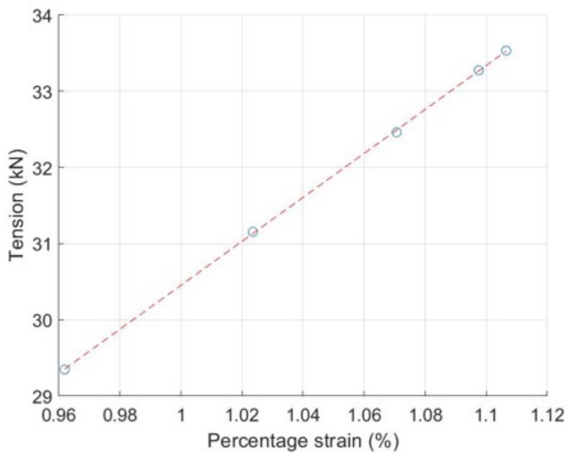

Figure 52 Regression plot for calculating stiffness at the end of dynamic bedding-in for Test 01 at DMaC.

Table 15 shows the stiffness values at the end of bedding-in. For Test 05, two values are shown, one for the first loading (Test 05a) and a second for the reloading cycles after being left unloaded overnight (Test 05b).

Table 15 Stiffness at the end of the dynamic bedding-in for all tests at both facilities.

Test	**End of bedding in stiffness (kN/%)**	
	DMaC	IFREMER
01	30.05	28.6 (10-20 %)
02	28.42	28.3
03	29.84	27.0
04	30.64	26.6
05a	32.49	26.8
05b	26.28	27.2

5.1.5.2.2 Quasi-static stiffness for all load cycles

Stiffness values are calculated for the first, second and third quasi-static loading cycles of the samples. These are defined as the change in load divided by the change in strain between the initial strain at 10% MBL just before loading and the maximum final strain after 30 minutes at the higher 30% load just before unloading. Values are shown in Table 16 below for DMaC.

Table 16 Quasi-static stiffness for all tests at DMaC.

	Quasi-static stiffness (kN/%)		
Test	Cycle 1	Cycle 2	Cycle 3
01	20.84	17.02	16.92
02	20.37	16.57	16.53
03	20.54	16.82	16.71
04	21.63	17.52	17.22
05a	21.94	18.22	17.86
05b	21.73	18.41	17.97

Results for the quasi-static stiffness of Test 02, Test 03, Test 04 and the two sets of Test 05 are shown in Table 17. The strain values for the first specimen were not reliable and are not included.

Table 17 Quasi-static stiffness for all tests at IFREMER.

	Quasi-static stiffness (kN/%)	
Test	Cycle 2	Cycle 3
01	18.1	18.1
02	17.7	17.7
03	17.7	17.7
04	17.5	17.4
05a	18.1	18.2
05b	18.1	18.1

5.1.5.2.3 Dynamic stiffness

The final set of stiffness values measured was the dynamic stiffness, measured at three load levels for cycles with a period of 15 seconds. These values are defined as the slope of all the force-strain pairs recorded during the last five loading cycles at each level, as shown for Test 01 at DMaC in Figure 53.

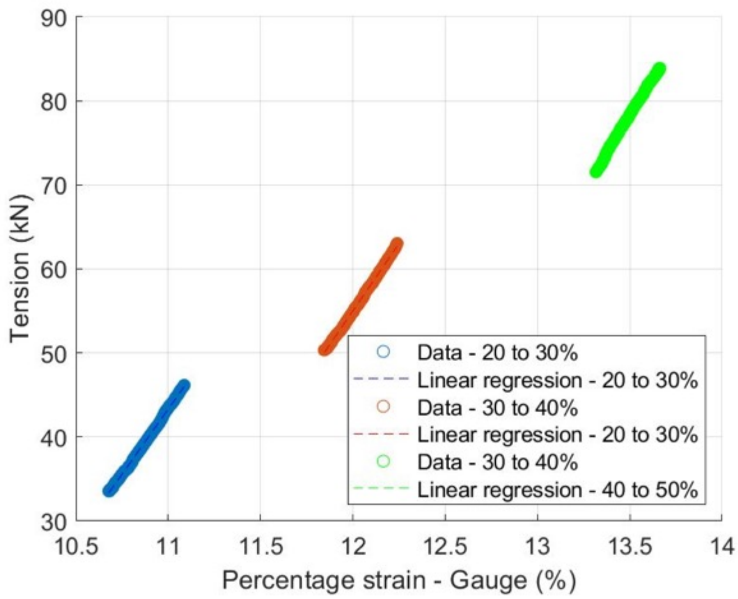

Figure 53 Regression plots for calculating dynamic stiffness at three load ranges for Test 01 at DMaC.

Table 18 shows the measured values for dynamic stiffness of each specimen at DMaC.

Table 18 Dynamic stiffness for all tests at DMaC.

Test	20-30%	30-40%	40-50%
01	31.00	32.12	35.42
02	28.89	32.61	35.53
03	29.22	31.80	35.56
04	30.53	32.05	36.03
05a	29.56	31.85	34.75
05b	29.95	32.34	35.93

Table 19 shows the measured values for each specimen at IFREMER.

Table 19 Dynamic stiffness for all tests at IFREMER.

Test	20-30%	30-40%	40-50%
01	32.8	37.0	37.6
02	35.5	38.5	31.1
03	33.2	35.7	39.7
04	32.8	36.8	42.0
05a	30.5	37.0	37.8
05b	32.5	36.5	37.4

5.1.5.3 Break tests

Table 20 displays the specified vs achieved break load and corresponding sample elongation for all tests at each test facility.

Table 20 Specified vs achieved break load and corresponding sample elongation at each test facility.

Test	Nominal break load, kN	Achieved break load (kN)	
		DMaC	IFREMER
01	168	213.91	218
02		194.49	220
03		182.71	195
04		200.79	176
05		212.82	227

There is some variability in the test results but these values are all higher than the nominal minimum break load (168 kN) provided by the rope supplier, with some up to 35% higher.

The failure modes for individual break tests are tabulated in Table 21 for DMaC.

Table 21 Failure mode for each test at DMaC.

Test	Failure mode
Test 01	One strand broke near end of splice
Test 02	One strand broke near end of splice 
Test 03	One strand broke near end of splice
Test 04	One strand broke near end of splice
Test 05	One strand broke at end of splice 

5.1.6 Comparison of rope materials

The mean dynamic stiffness values of the PP+PE rope specimens can be compared to those commonly used to characterise 100% polyester and 100% Polyamide 6 (nylon) ropes for mooring lines. Such values can be expressed in normalized form by dividing the stiffness by the MBL and converting to strain rather than % strain. Some typical values are given in Table 22 below, and the comparison with values for the PP+PE rope tested here clearly show that the dynamic stiffness of this hybrid PP+PE rope is lower than that of 100% PET but higher than that of polyamide 6.

Table 22 Comparison of dynamic stiffness of sample with pure polyester and nylon ropes.

Material	20 – 30%	30 – 40%	40 – 50%
Polyester	27	30	33
PP+PE (IFREMER)	19.6	22	23.9
PP+PE (DMaC)	17.77	19.12	21.15
Nylon 6	-	10	13

5.1.7 Comparison of round robin test facilities

5.1.7.1 Static bedding in

Figure 54 and Figure compares the initial load-strain plots recorded for each test during the first loading up to 50% break load for DMaC and IFREMER, respectively.

This plot shows that the responses of the five samples during first loading are similar, with a maximum strain at 50% MBL of around 11%. The second loading after a 24 hour unload, Test 05b, shows a higher stiffness.

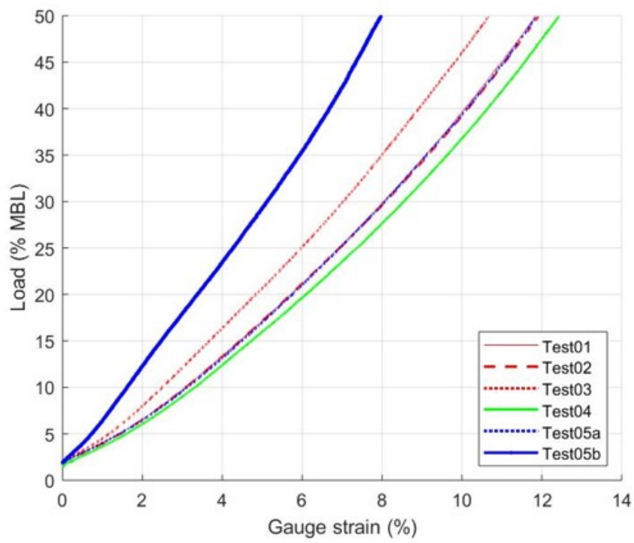

Figure 54 First loading of samples at DMaC and IFREMER.

5.1.7.2 Dynamic bedding in

Figure 55 shows the stiffness of the various test specimens after the dynamic bedding-in. The mean value for the bedding-in stiffness, 28.9 kN/%, is calculated from Test 01 to Test 05a (Test 05b is not included).

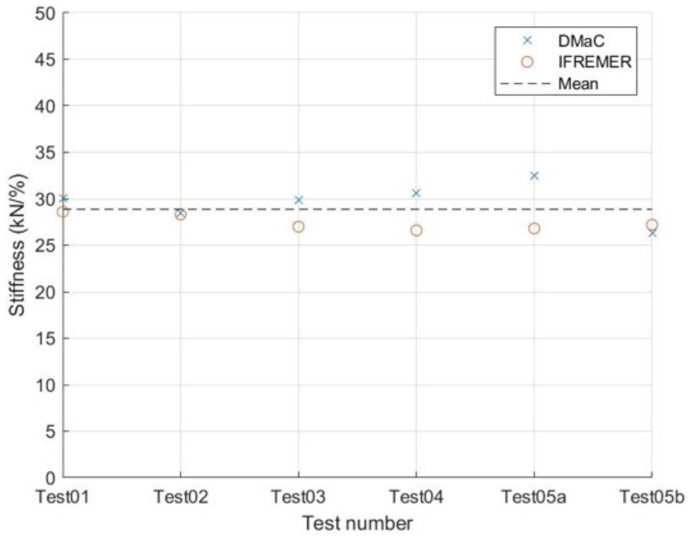

Figure 55 Mean and sample stiffness at the end of dynamic bedding-in.

The percentage difference of bedding-in stiffness from the mean value is displayed in Table 23.

Table 23 Percentage difference from mean stiffness at the end of dynamic bedding-in.

	Percentage difference from mean (%)	
Test number	DMaC	IFREMER
Test 01	4.1	-0.9
Test 02	-1.6	-2.0
Test 03	3.3	-6.5
Test 04	6.1	-7.9
Test 05a	12.5	-7.2
Test 05b	-9.0	-5.8

Two observations can be made:

- Stiffness at both facilities is within 12.5% of the mean, including the measurement in Test 05b.
- Variance of the measurements at IFREMER is lower than at DMaC

5.1.7.2.1 QS loading

Figure 56 shows the average stiffness of the various test specimens for the last two quasi-static cycles. The mean value for the quasi-static stiffness, 17.4 kN/%, is calculated from Test 01 to Test 05a for DMaC and Test 02 to Test 05a for IFREMER. Test 05b is not included for both facilities, whereas, Test 01 is not included for IFREMER.

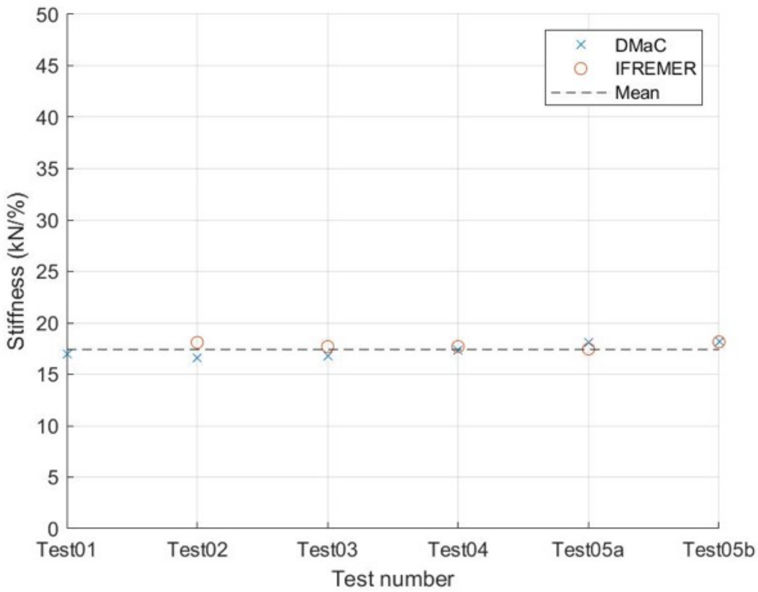

Figure 56 Mean and sample quasi-static stiffness.

The percentage difference of quasi-static stiffness of each specimen from the mean value is displayed in Table 24.

Table 24 Percentage difference from mean quasi-static stiffness.

	Percentage difference from mean (%)	
Test number	DMaC	IFREMER
Test 01	-2.5	-
Test 02	-4.9	4.0
Test 03	-3.7	1.7
Test 04	-0.2	1.7
Test 05a	3.6	0.3
Test 05b	4.5	4.3

Two observation can be made:

- Stiffness at both facilities is within 5% of the mean, therefore, a higher agreement is seen than the bedding-in stiffness.
- Variance in quasi-static stiffness is lower at IFREMER relative to DMaC samples

5.1.7.2.2 Dynamic stiffness

Figure 57 shows the stiffness of the various test specimens for the three dynamic load ranges, that is, for 20 – 30% MBL, 30 – 40% MBL and 40 – 50% MBL, applied to each sample. The mean values for the dynamic stiffness, 31.4 kN/%, 34.5 kN/% and 37.5 kN/% are calculated from Test 01 to Test 05a for DMaC and IFREMER (Test 05b is not included).

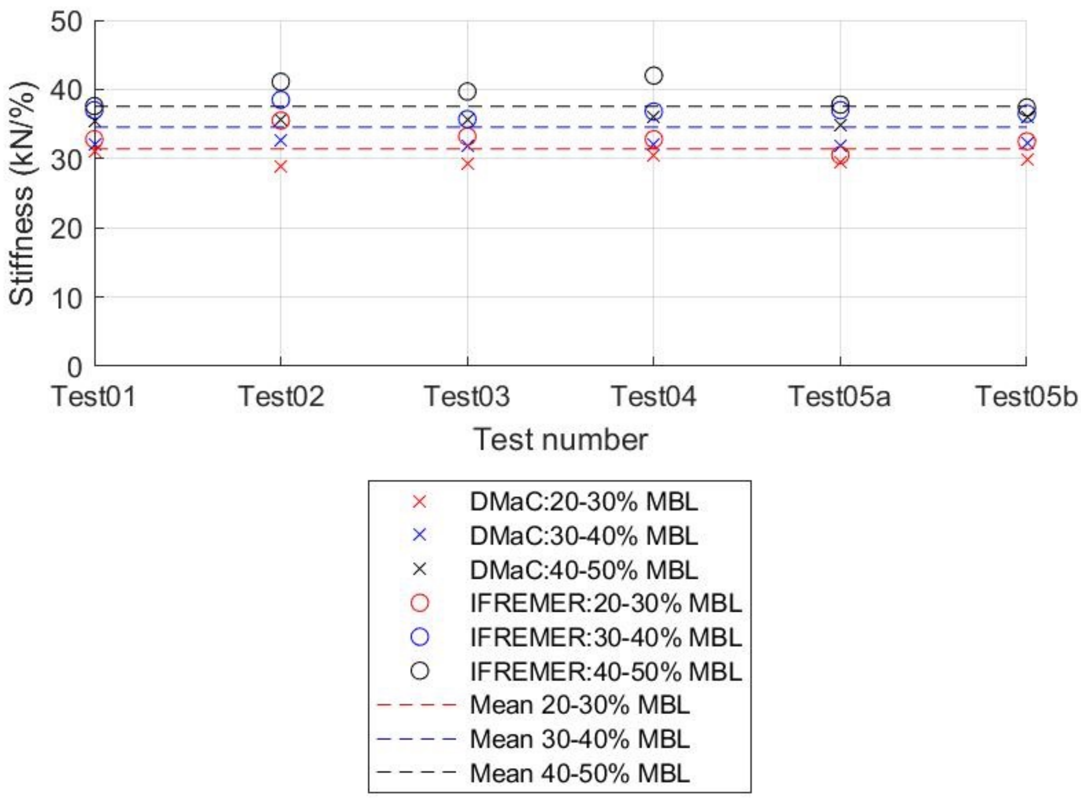

Figure 57 Mean and sample dynamic stiffness for cyclic loading of 20-30%, 30-40% and 40-50% MBL.

The percentage difference of dynamic stiffness of all three load ranges of each sample from the mean values is displayed in Table 25.

Table 25 Percentage difference from mean dynamic stiffness.

Percentage difference from mean (%)						
	20 – 30 % MBL		30 – 40 % MBL		40 – 50 % MBL	
Test number	DMaC	IFREMER	DMaC	IFREMER	DMaC	IFREMER
Test 01	-1.3	4.4	-7.0	7.1	-5.7	0.1
Test 02	-8.0	13.1	-5.6	11.5	-5.4	9.5
Test 03	-6.9	5.7	7.9	3.3	-5.3	5.7
Test 04	-2.8	4.5	-7.2	6.5	-4.0	11.9
Test 05a	-5.9	-2.9	-7.8	7.1	-7.5	0.7
Test 05b	-4.6	3.5	-6.4	5.7	-4.3	-0.4

Two observations can be made:

- Stiffness at IFREMER is within 15% of the mean relative to 10% for DMaC at all applied cyclic load ranges
- Variance for the measurements at DMaC is lower than at IFREMER

5.1.7.3 Break test

Figure 58 shows the break load of the various test specimens at each test facility. The mean value for the break load, 204 kN (121 % MBL), is calculated from Test 01 to Test 03 for DMaC and IFREMER (Test 04 and Test 05 are not included).

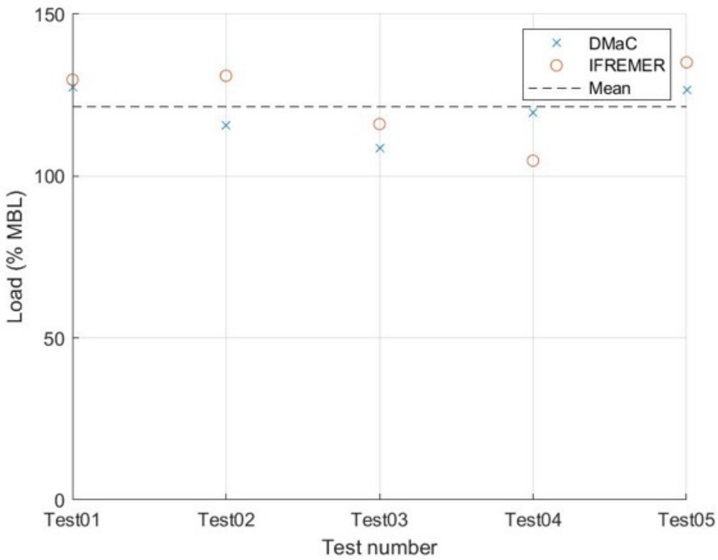

Figure 58 Mean and sample break loads.

The percentage difference of the break load of each specimen from the mean value, 204 kN, is displayed in Table 26.

Table 26 Percentage difference of sample break loads from mean break break load.

	Percentage difference from mean (%)	
Test number	DMaC	IFREMER
Test 01	4.8	6.9
Test 02	-4.7	7.8
Test 03	-10.4	-4.4
Test 04	-1.6	-13.7
Test 05	4.3	11.2

Two observations can be made:

- All samples exceeded the break load specified by the manufacturer, some by up to 35%
- Variance for break test measurements is lower at DMaC than IFREMER

5.1.8 Comparison of cyclic test plans

Three test plans were implemented as part of this RRT at each facility. All specimens were bedded in and loaded (quasi-statically and dynamically) similarly. However, while samples for Test 01 to Test 03 were loaded to failure immediately after the cyclic loading, Test 04 and

Test 05 were treated differently. Based on the similarity of implementing Phase A on all five samples, statistical parameters for Phase A (dynamic bedding-in, quasi-static loading and dynamic loading) are calculated based on measurements from all five samples. Please note, measurements from the second implementation of Phase A on sample 05 are not included. Additionally, the quasi-static bedding-in of Specimen 01 from IFREMER is not included due to the programming error that occurred whilst performing the test.

As the break test, Phase B, is conducted in similar fashion for Test 01, Test 02 and Test 03 only, therefore, only three tests are used to calculate the mean break load of the samples at each facility. Also, it must be noted that the results for the break test of Specimen 04 are not comparable between test facilities as the rest period and conditions were not comparable (refer to Section 5.1.4).

Figure 59 shows the mean stiffness properties and error bars for the PE+PP blend rope for various stages in the implemented load regime.

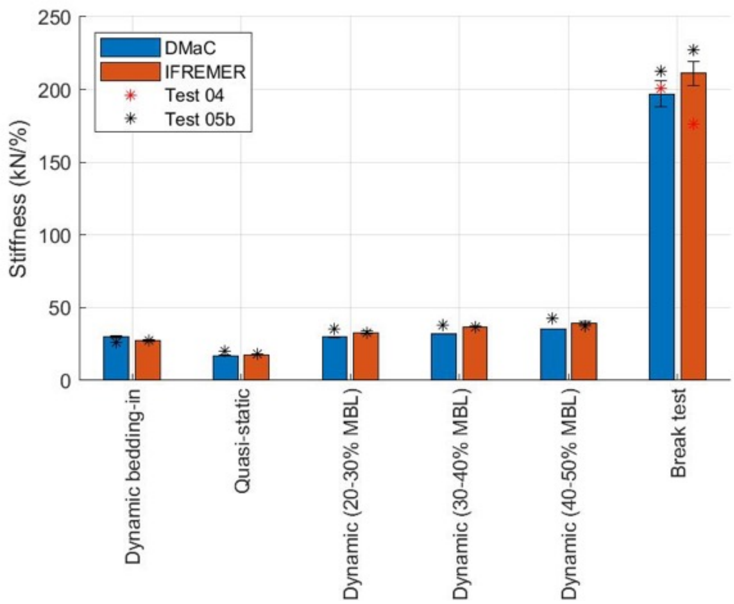

Figure 59 Comparison of break stiffness of Test 04 and all stiffness values for Test 05b with mean stiffness at each facility.

The mean stiffness and standard deviation for all test stages are tabulated in Table 27 for both test facilities.

Table 27 Mean stiffness and standard deviation for all stages of the test plan at each facility.

Stage	Mean stiffness (kN/%)		Standard deviation (kN/%)	
	DMaC	IFREMER	DMaC	IFREMER
Dynamic bedding-in	30.3	27.5	1.47	0.92
Quasi-static loading	17.1	17.7	0.59	0.27

Dynamic loading (20 – 30% MBL)	29.8	33.0	0.89	1.78
Dynamic loading (30 – 40% MBL)	32.1	37.0	0.32	1.00
Dynamic loading (40 – 50% MBL)	35.5	39.6	0.46	1.95
Break test	197.0	211.0	15.76	13.89

It can be observed that the highest variability in stiffness values occurs for the break test at both facilities. Mean stiffness values at IFREMER are higher than at DMaC except for that at the end of dynamic bedding in. Also, the standard deviation between samples is higher at DMaC for all stages except the three dynamic loading ranges.

The figure shows that the second implementation of Phase A in Test 05 (referred to as Test 05b) leads to higher stiffness values for quasi-static and dynamic loading at DMaC. At IFREMER, it is observed that while the quasi-static stiffness of the sample is higher than the mean, dynamic stiffness values are lower than the mean of five samples undergoing Phase A once.

5.1.9 Recommendations

- Tests performed independently in two test facilities will provide similar results, provided that a strict protocol is followed. The inter-facility comparison shows that precision of results varies between facilities, however, it is difficult to attribute this variance to the difference in the facilities or variation in sample quality without further investigations. Three or more facilities must be included in an RRT for an improved understanding.
- The ISO protocol for offshore polyester moorings is suitable for MRE applications; however, it is recommended that the guidance should be extended to incorporate higher loading frequencies, in order to improve rope dynamic response assessment.
- The tensile properties of the hybrid ropes are intermediate between those of 100% pure constituents, and also depend on rope construction parameters.

5.2 Tidal blade testing

5.2.1 Campaign objectives

The overall aim of the cross-cutting round robin campaign is to investigate the essential parameters for developing the accurate numerical models for composite wind turbine blades that are critical in blade design. In this study, 3 separate numerical models were developed, and experimental testing was performed on the wind turbine blade, in parallel. In order to achieve the aim of the study, a number of objectives must be achieved:

- To determine the relevant input parameters for modelling a composite wind turbine blade,

- To develop three separate full-scale numerical models of a composite wind turbine blade,
- To perform experimental physical testing of a composite wind turbine blade, and
- To validate the three numerical models by comparing their output to the results from the experimental testing.

5.2.2 Model choice

The full-scale wind turbine blade tested in this study is a 13 m commercial turbine blade from a 225 kW upwind wind turbine. The blade is 13 m long and its external geometry is constructed with modified NACA 63 series air-foils. A photograph of the blade is shown in Figure 5.1. The blade is manufactured from glass-fibre reinforced powder epoxy composite material using a novel "one-shot" manufacturing process, which cures the different parts of a wind turbine blade (i.e., skin sections, spar caps web, and root) in one single process to avoid the need for adhesive bonding. Steel inserts in the root of the blade provide a connection to the turbine hub when in operation and to a steel test fixture for the testing campaigns.

Figure 5.1: 13 m wind turbine blade after being manufactured and finished.

5.2.3 Test campaign description

Initially, the relevant input parameters for a full-scale wind turbine blade, which are the blade geometry, composite design, material properties, and loading, were compiled. In parallel, the full-scale wind turbine blade underwent structural mechanical (static and dynamic) testing and the 3 independent numerical models were developed. These numerical models have exactly the same input parameters but use different FE software packages—ABAQUS, ANSYS, and CalculiX. Numerical predictions on the deflected shape of the blade and strains along the length of the blade were compared to the results from the structural testing in order to validate and contrast the model outputs. A graphical summary of the process methodology used in this study for fairly comparing the 3 numerical models is presented in Figure 60.

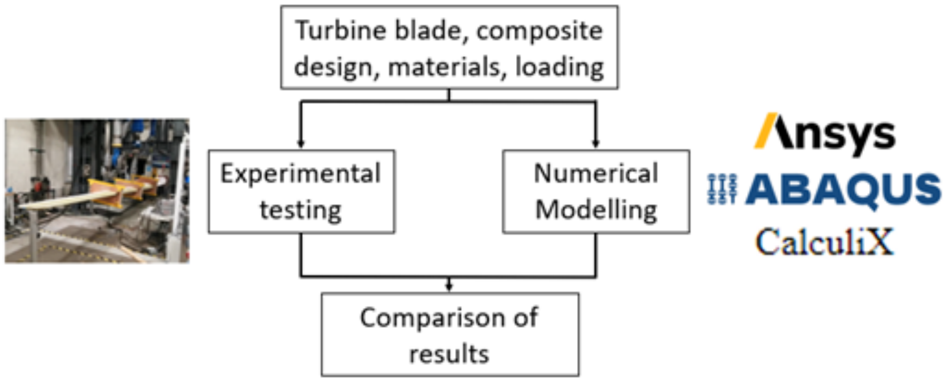

Figure 60 Methodology for fairly comparing the 3 numerical models that are developed in this study.

5.2.4 Cross-cutting round robin results

In order to investigate the accuracy of the three numerical models, the outputs from the models are compared to the results from the structural testing. Initially, the blade mass and natural frequencies are compared using the results of the dynamic test. Following this, the deflection of the blade and the strains along the length of the blade are compared using the results of the static test in both the flapwise and edgewise directions.

The full results from the testing are included in [26]. However, the comparison of the blade deflection based on the results from the flapwise static testing are compared to the output from the numerical models is presented in Figure 61, as an example of the findings from the campaign. The measurements were taken at 4 locations (at 4 m, 7.5 m, 8 m, and 13 m (blade tip) from the root) during the physical testing. However, it should be noted that only tip deflection data is available for the 25% and 50% load case in the flapwise direction due to issues with stringpot displacement sensors at the other locations. In general, the estimations from the 3 numerical models agree well with the measured values. The ANSYS and CalculiX models are in very good agreement with a difference of 1.1% and −3.3%, respectively, in the deflection at the tip for the 100% load case, compared to the measured value of 0.41 m. The estimate for the tip deflection from the ABAQUS model is 0.363 m, which is a difference of −11.5% compared to the measured value. However, this is still a reasonable agreement with the results from the structural testing.

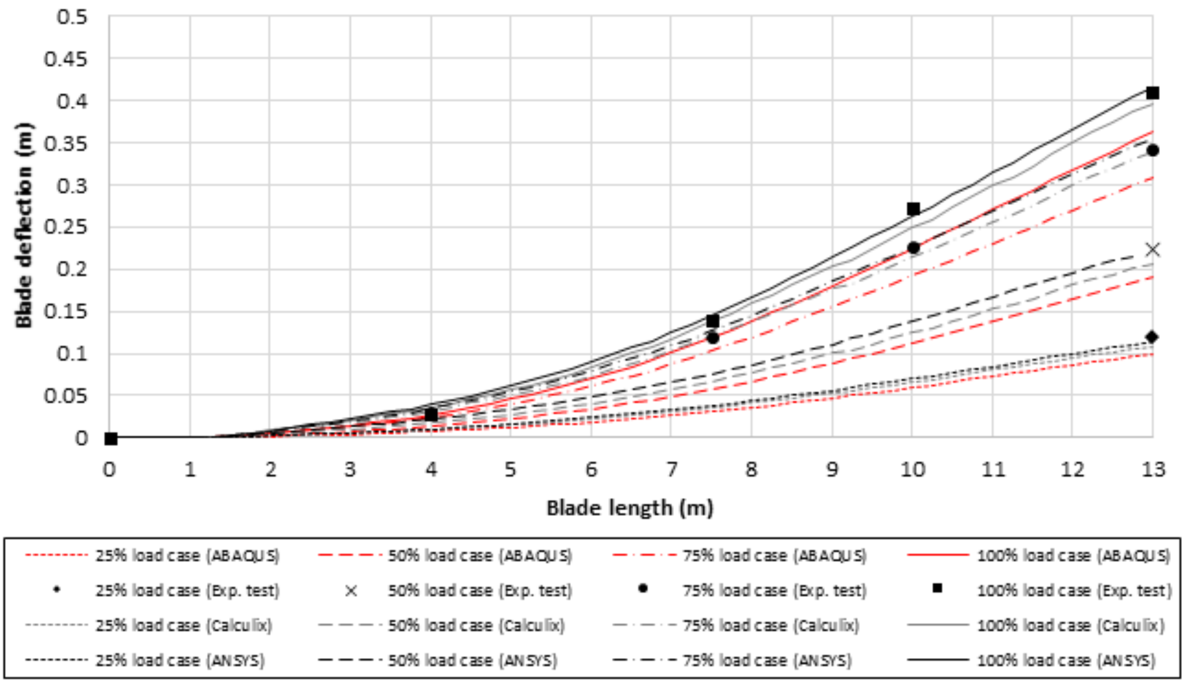

Figure 61 Comparison between the results from the 3 numerical models (ABAQUS, ANSYS, and CalculiX) and the results from the experimental static test showing the deflection along the blade (in m) for each of the load cases in the flapwise direction.

5.2.5 Recommendations for standardised testing

Overall, there was reasonable agreement between the three numerical models and the results from the experimental testing programme but there are some differences, which are in part due to the differing methodologies used to develop each of the numerical models; a summary of these differences of the three FE models are presented in Table 28. Although each of the numerical models uses the same set of input parameters, the selection of FE modelling methodology, including FE software, element types, and loading introduction mechanism, can cause differences in the numerical results.

Table 28 Comparison of the modelling methodologies

	ANSYS	ABAQUS	CalculiX
Element type:	Shell element SHELL281	Shell element S4	Solid element C3D20R, C3D15
Element stress/strain components:	3	3	6
Load introduction mechanism:	Rigid link	Rigid link	Uniform distributed loads
Solver:	ANSYS APDL	ABAQUS	CalculiX

The blade mass given by the 3 numerical models ranges from 615 kg to 653 kg, with a standard deviation of 16.7 kg, which is less than the actual blade mass of 674 kg. One possible reason for the models underestimating the mass is that the steel inserts have not been included. Regarding the natural frequencies, the ANSYS model has the highest accuracy of the three, with an average difference of 9.7%. From this study, the CalculiX model is found to be more accurate in predicting the blade tip deflections in both flapwise and edgewise testing scenarios, while the ABAQUS and ANSYS models underestimate the blade edgewise stiffness. Considering that the CalculiX model employs layered solid elements and the other two models utilise the shell element models, it can be concluded that the layered solid element is suitable for analysing the blade response under both flapwise and edgewise loading while the shell element-based blade model may not be recommended for predicting the edgewise deflection. When examining the strain values overall, the three numerical models underestimate the strain in both flapwise and edgewise configurations, compared to the results from the experimental testing programme. The ABAQUS and ANSYS models estimate very similar strain results under the flapwise loading. However, in the edgewise direction, the strain values given by each of the two models are rather different. Unlike with the deflection results, the CalculiX model is consistently giving lower strain values compared to the other two numerical models. The comparisons between the strain values under different testing scenarios indicate that the stress values predicted by the three numerical models may be underestimated. Considering that the composite laminate failure prediction under extreme loads and the wind turbine blade service life calculation rely on the stress and strain values given by the FE analysis, it appears that the selection of modelling methodology can be a source of uncertainties in the wind turbine design.

5.2.6 Recommendations for future round robin activities

For composite wind and tidal turbine blades, the thick sections, in particular around the root and along the spar caps, are critical and the greatest unknown. Therefore, future activities would focus on thick section composites, where R&D activities would focus on:

- Performance of immersed thick section composites
- Manufacturing of thick section composites and ensuring thorough wet out through the section
- Structural testing of root and spar cap components for composite wind and tidal turbine blades

The greatest challenge during the cross-cutting round robin campaign was managing the small budget, which resulted in 3 numerical models and 1 validation testing campaign. Therefore, if this campaign was repeated, the researchers would seek a larger budget to carry out testing at, at least, 3 testing facilities. In order to aid with this, a smaller composite demonstrator would be used, which would undergo static and dynamic testing at the 3 testing facilities, followed by full-fatigue testing at the final facility. This would yield greater insight into the testing procedures of the 3 testing facilities and give greater confidence in the results from the physical testing.

5.2.7 Published papers – cross-cutting

Published paper documenting the cross-cutting round robin activities:

Finnegan, W.; Jiang, Y.; Dumergue, N.; Davies, P.; Goggins, J. Investigation and Validation of Numerical Models for Composite Wind Turbine Blades. J. Mar. Sci. Eng. 2021, 9, 525. https://doi.org/10.3390/jmse9050525

5.2.8 Description of open access dataset

The open access dataset from the cross-cutting round robin campaign contains the results from the structural testing and finite element analysis (FEA) of a 13m turbine blade, which has been manufactured from glass fibre reinforced powder epoxy. The dataset includes the results from dynamic and static testing of the blade. The results from the dynamic testing includes the natural frequencies and mass of the blade. The results from the static testing display the deflection, and associated strains, in both the flapwise and edgewise directions, where the load was applied in increments of 25% of the maximum design load.

The open access dataset from the cross-cutting round robin campaign is available at [27]:

Finnegan William, Jiang Yadong, Dumergue Nicolas, Davies Peter, Goggins Jamie (2021). Structural testing and FEA dataset for a composite turbine blade. SEANOE. https://doi.org/10.17882/80564

5.3 Subsea umbilical cable

Table 29 below lists all tests included in the RRT plan together with the main objectives of each test. The table also specifies which test method is based on an industry standard or recommendation.

Table 29 Overview of conducted cable test types and objectives, chosen approach, used facility and standard.

Test type	Approach	Reference Standard	Objectives
Mechanical properties			
Tensile test	Static	ISO 13628-5 [28]	Axial stiffness; Axial structural damping
"Quasi-static" bend test	Static	ISO 13628-5	Bend stiffness
	Fatigue life testing		
Cyclic bend test	Dynamic	DNV-RP-F401 [29]	Dynamic bend stiffness

The results in this report are based on testing conducted at the Dynamic Marine Component (DMaC) test facility based in Falmouth Docks and owned by the University of Exeter.

For each test, a uniform test signal is defined, specifying displacement or force parameters for both axes. However, the choice of the sampling rate, interpolation method for the time series, control parameters, data logging channels and time steps is defined by the test facility manager. Finally, the input test data is sent to the rig controller and written to the input file of the controller to start the test.

Test measurements recorded through real time data streaming of the output signal include:

- Axial tension
- Axial displacement
- Bending moment
- Bending angle

The logged data file is then downloaded and archived to analyse the outputs at DMaC.

5.3.1 Test facility

Constructed during 2010, the Dynamic Marine Component (DMaC) has been designed to replicate the dynamic operational and fatigue loads that offshore components typically experience in-service. The facility, as shown in Figure 62, includes a hydraulically powered tailstock for the application of user-defined loads (harmonic and irregular time-series).

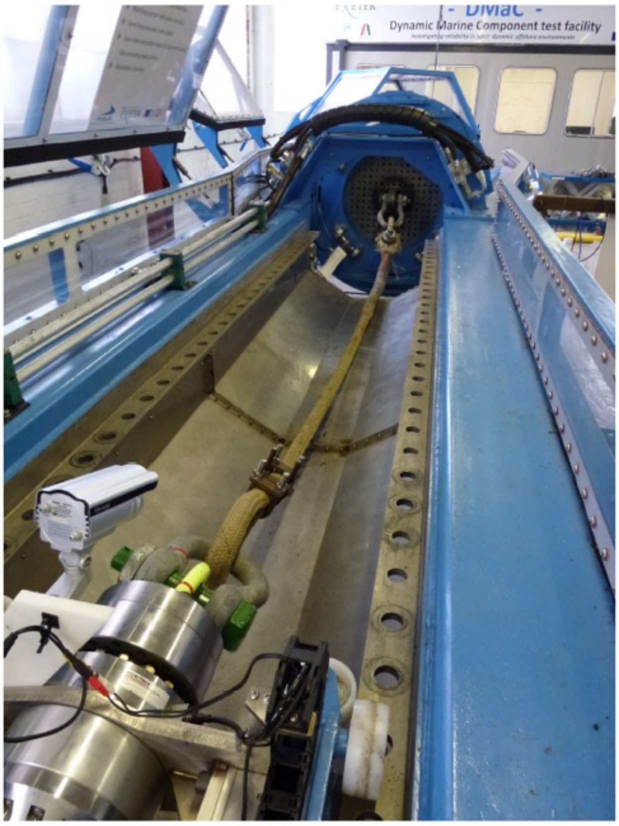

Figure 62 DMaC test facility at the University of Exeter.

It differs from existing tension test machines in that it also possesses a hydraulically powered headstock, providing an additional three degrees-of-freedom (roll, pitch and yaw). This feature is particularly useful for the testing of subsea components which are subjected to bending or torsion at one end (for example cables, umbilicals and risers). Additionally, the DMaC has been designed so that the components being tested can be fully submerged in fresh water.

5.3.2 Test layout

5.3.2.1 Sample

The test specimen is a HVAC 3.3 kV marine power umbilical cable with a length of 3.5 m and cross-sectional area of 60 mm^2. It was provided courtesy by JDR cable systems and is a typical subsea umbilical.

The several layers of a typical umbilical cable can be seen in Figure 63 [30]. Although the actual components of the umbilical will vary for offshore renewable energy converters, the construction, armouring and general properties are comparable.

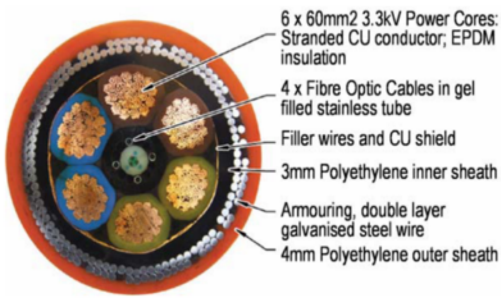

Figure 63 Cross-section of a typical marine power umbilical [30].

5.3.2.2 Cable terminations

There are fixtures available for testing the specimen at DMaC test rig due to prior tests conducted on the cable.

The cable was connected to DMaC at both the moving headstock and the tensile forcing end of the rig. At the headstock, the cable had been secured into a steel socket using resin fabricated by JDR. In order to connect the socket to the bottom plate of the test rig, a circular steel plate had been welded onto the socket. The socket was bolted to the bottom plate of the headstock to make a rigid connection as seen in Figure 64.

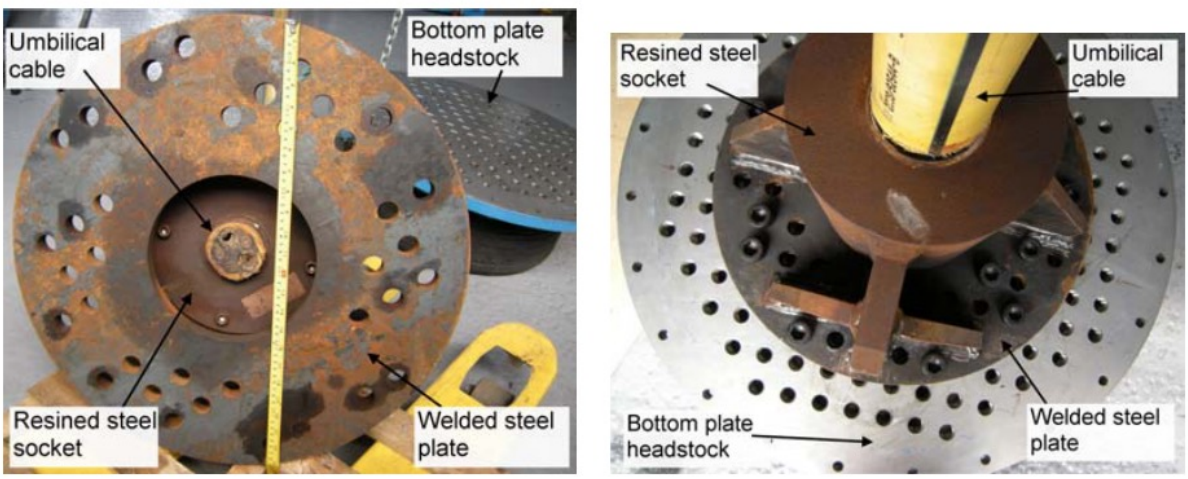

Figure 64 Rear (left) and top (right) view of the end termination of the cable sample at the headstock end.

At the other end, where the tensile force is exerted, the cable is clamped by two cylindrical steel sections which are fitted with internal rips that grip the cable. The clamp is tightened with bolts at either side of the armoured cable and will be connected to the load cell on the hydraulic linear cylinder, using a pin joint connection as seen in Figure 65.

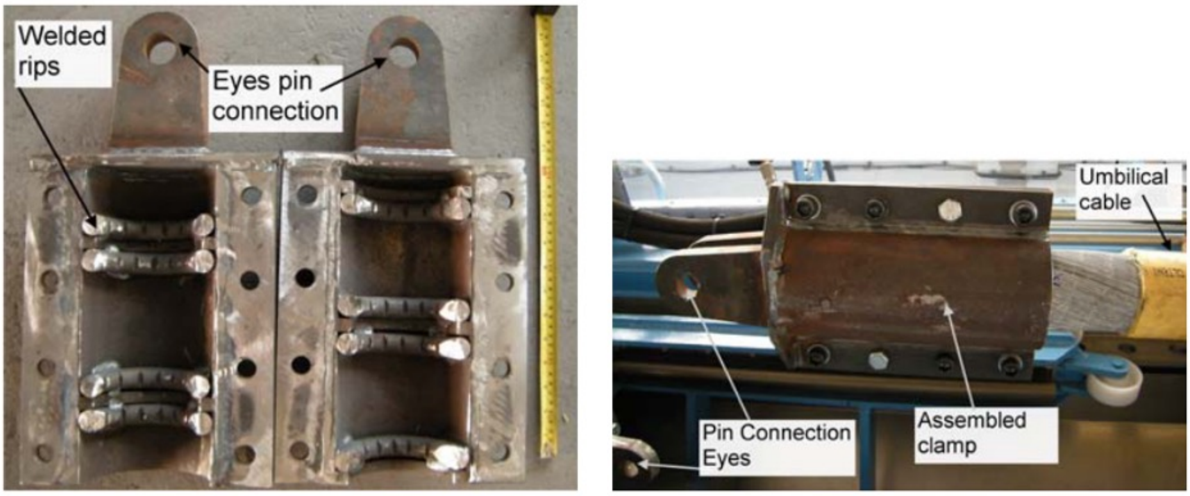

(a) Inside view (b) Clamp assembled

Figure 65 Umbilical cable termination (a) inside view and (b) assembled clamp at the linear cylinder tailstock end.

5.3.2.3 Test configurations

Two test configurations can been applied by the DMAC test rig as shown in Figure 66, respectively:

- Test configuration 1: End A) no-rotation on cantilever support and End B) induced rotation on cantilever support.
- Test configuration 2: End A) no-rotation on pin support and End B) induced rotation on cantilever support

It must be noted that the pin support allows rotation with fixed translation, whereas, the cantilever support allows no rotation or translation.

Test configuration 2 will generate a constant curvature so it is adopted for the testing at DMaC.

Figure 66 Configuration 1(left) and Configuration 2 (right) at DMaC.

Figure 67 displays the experimental set-up with the cable fitted to the test rig and the fixtures can be seen.

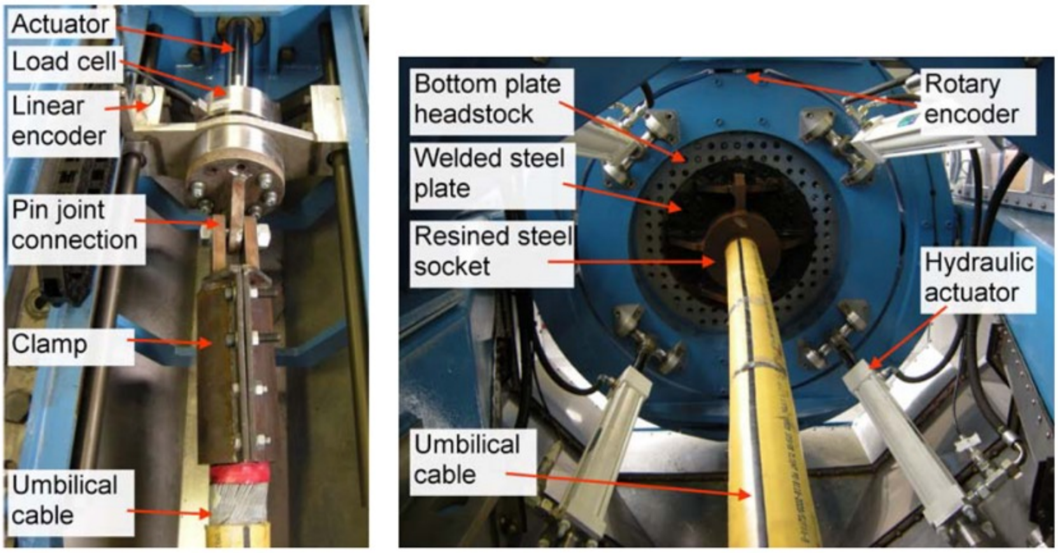

Figure 67 Experimental set-up with umbilical cable fitted to test rig at the (a) linear actuator and (b) moving headstock end.

5.3.3 Test methodology

The load response of a marine umbilical can be determined by its stiffness properties; therefore, effective evaluation of these properties is crucial for robust reliability estimation of the cable properties. To compare the basic capabilities of the test rigs using the stiffness behaviour of the cable specimen, the following three parameters are significant:

- Tensile stiffness
- Quasi-static bending stiffness
- Dynamic bending stiffness

This section outlines the test plan for determining tensile stiffness in Section 5.3.3.1, quasi-static bend stiffness and dynamic stiffness in in Section 5.3.3.2.

5.3.3.1 Tensile test

The primary test objective is the measurement of cable elongation to calculate axial stiffness of the cable specimen.

The measurement of elongation ϵ_i under tensile load T_i for sample *i*, allows the calculation of the axial stiffness, K_A as:

$$K_A = \frac{T_i}{\epsilon_i}$$

Using Test Configuration 2, a simple tension test is performed where the angle of the induced rotation is fixed at 0 degree.

A minimum load, T_0, is applied to ensure that the cable sample is approximately straight between End A and End B. The cable sample initial length L_0 is measured.

Axial tensile load is applied in 4 increments from T_0 up to a maximum of T_{MAX}. Each load increment applied in 30 seconds to be followed by a 50 second hold at constant load. When T_{MAX} is reached, the load is maintained for 300 seconds.

While T_0 was set as 1 kN, T_{MAX} was determined at 25 kN based on investigations in [30] which lead to continuous cable slip from the clamp at loads of over 65 kN.

The load is then reduced from T_{MAX} to T_0 reversing the procedure above. The full tensile loading sequence applied to the test cable samples is shown in Figure 68 below.

Throughout the cycle, load and elongation are recorded and logged.

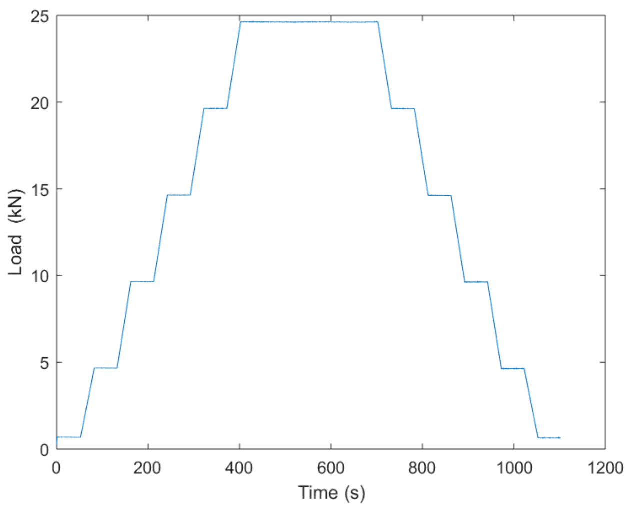

Figure 68 Input signal of the applied tensile load for axial stiffness testing.

5.3.3.2 Dynamic bend moment and stiffness

Cable bend stiffness is a measure of the resistance of a cable to applied bending. Following the Euler-Bernoulli beam theory, bend stiffness is a function of elastic modulus E and the second moment of area I of the cable cross-section. When the applied bending moment M_i and the resulting curvature κ_i are known for sample i, bend stiffness, K_B is given by the slope of the curve produced by plotting M vs κ.

While it is generally accepted that cable bend stiffness varies as a function of the applied loads, relatively little data from experimental work in this area has been published and often a constant K_B value is provided by the cable manufacturers. In this case, the M_i vs κ_i plot results in a straight line defined by the relation:

$$K_B = \frac{M_i}{\kappa_i}$$

This approach is justified by the fact that in static or lightly dynamic applications bend stiffness would essentially impact cable handling and deployment activities and the assessment of the cable stability in operations. In those cases, only the bend stiffness magnitude at specific curvatures is required, while *EI* variations under varied combined loads are less relevant.

Under bend stiffness testing, induced rotation is applied about the horizontal axis to vary the bending moment. The curvature is derived from the geometric relationship between the horizontal rotation angle and the measured bending moment under the idealised condition that the cable describes a circular arc.

In order to compare the dynamic behaviour of the test rigs, cyclic bending is applied to the cable specimen at three different rotation angle groups. The cable is set up, held at a specified pre-tension and bent at an angle of 15 degrees. This is followed by cyclic bending as illustrated by the time series in Figure 69.

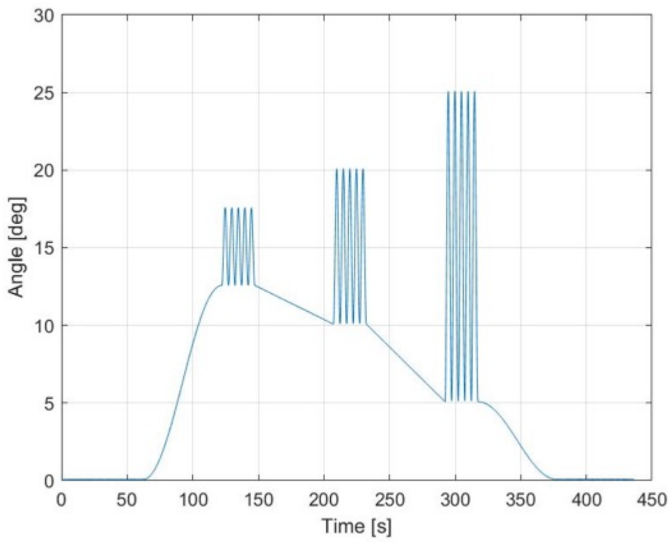

Figure 69 Input signal of bending angle for measurement of dynamic stiffness at a defined pre-tension.

As it can be seen, three rotation groups with increasing cyclic rotation angle are applied. Five cycles are applied at a frequency of 0.2 Hz for each rotation angle group and the hold between the applications of the cyclic rotation groups is 60 s.

The above method is repeated for pre-tensions of 2.5 kN, 3.5 kN and 5 kN to investigate the influence of varying tensile loads on dynamic bending stiffness. The combined tensile load and rotation angle ranges for the investigations are summarised in Table 30.

Table 30 Tensile load and rotation angle range for the dynamic bend stiffness tests.

		Rotation angle group [degrees]		
		15±2.5	15±5	15±10
Tensile load [kN]	2.5	5 cycles	5 cycles	5 cycles
	3.5	5 cycles	5 cycles	5 cycles
	5	5 cycles	5 cycles	5 cycles

5.3.4 Results

This section summarises the results of the umbilical cable test campaign undertaken at DMaC.

As a result of the tensile testing of the umbilical cable described in Section 5.3.3.1, the displacement of the sample was recorded and is presented in Figure 70.

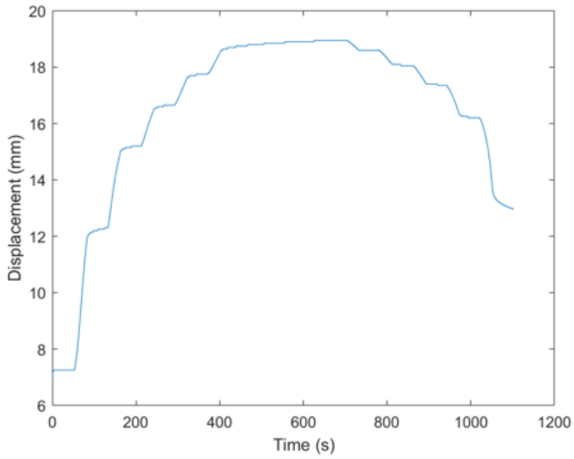

Figure 70 Displacement time series of the tensile test conducted at DMaC.

As it can be observed, 50% hysteresis is observed in the sample. The possibility of slippage is discounted as only a 0.4 mm increase in the elongation is observed when the load is held constant at 25 kN.

The displacement for the three rotation groups described in the previous section can be seen in Figure 71.

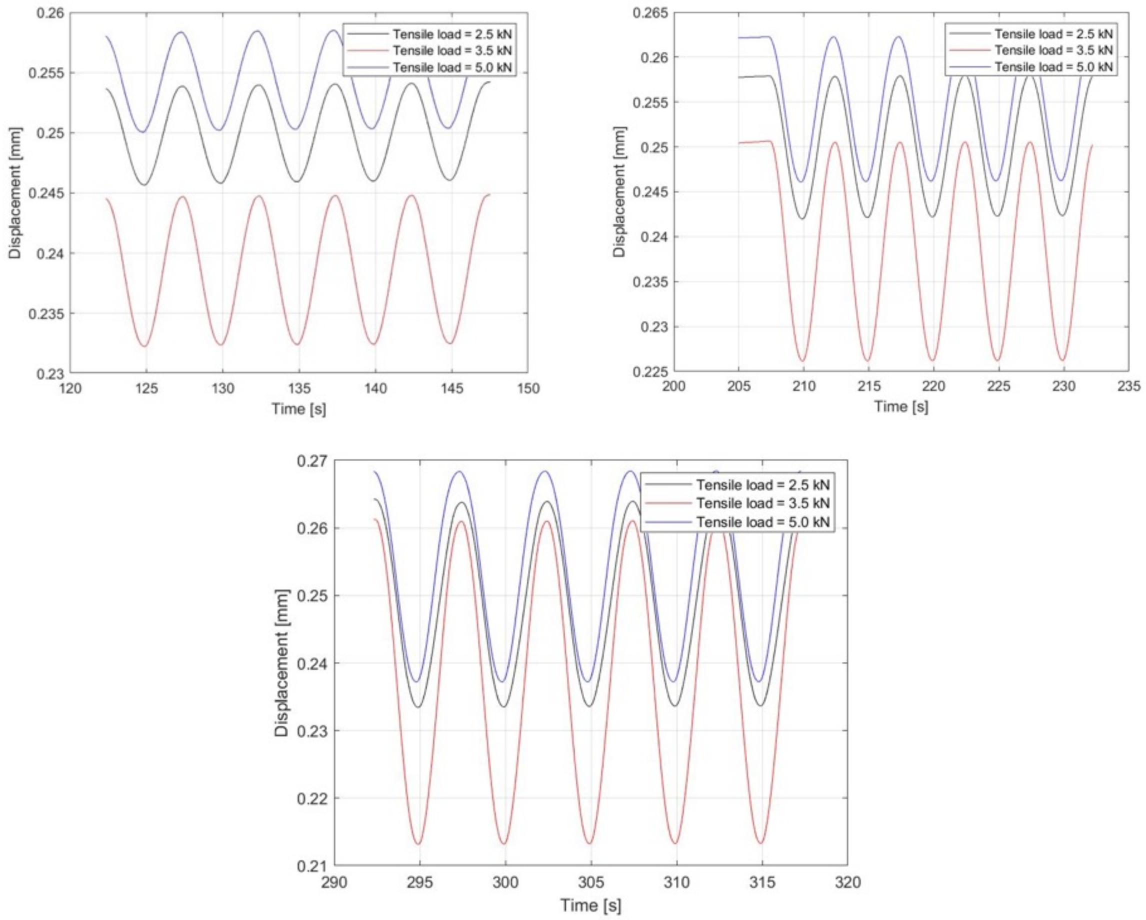

Figure 71 Displacement of the three rotation groups ±2.5 deg (top left), ±5 deg (top right) and ±10 deg (bottom) for all three tensile ranges compared.

The loads for the three rotation groups are summarised in Figure 72.

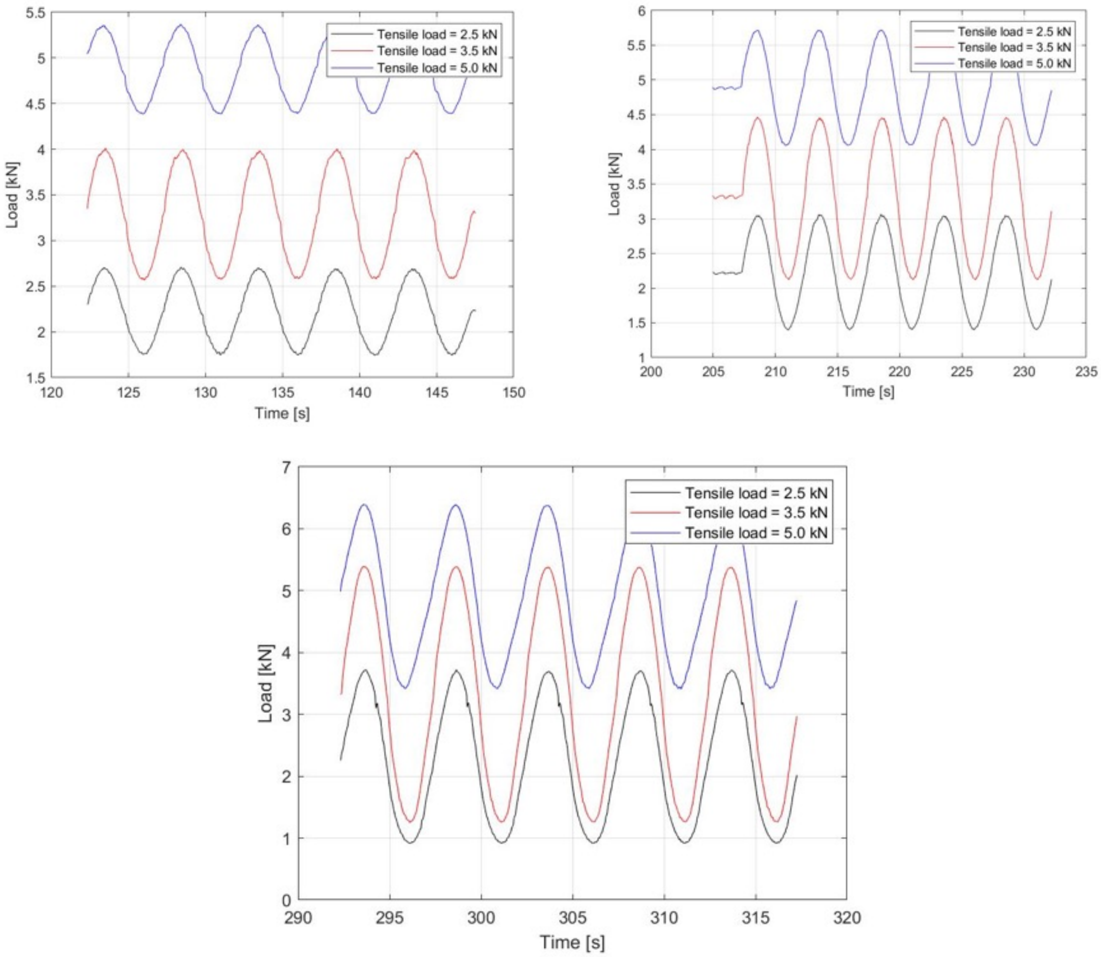

Figure 72 Load of the three rotation groups ±2.5 deg (top left), ±5 deg (top right) and ±10 deg (bottom) for all three tensile ranges compared.

The bending moment for the three rotation groups can be seen below in Figure 73.

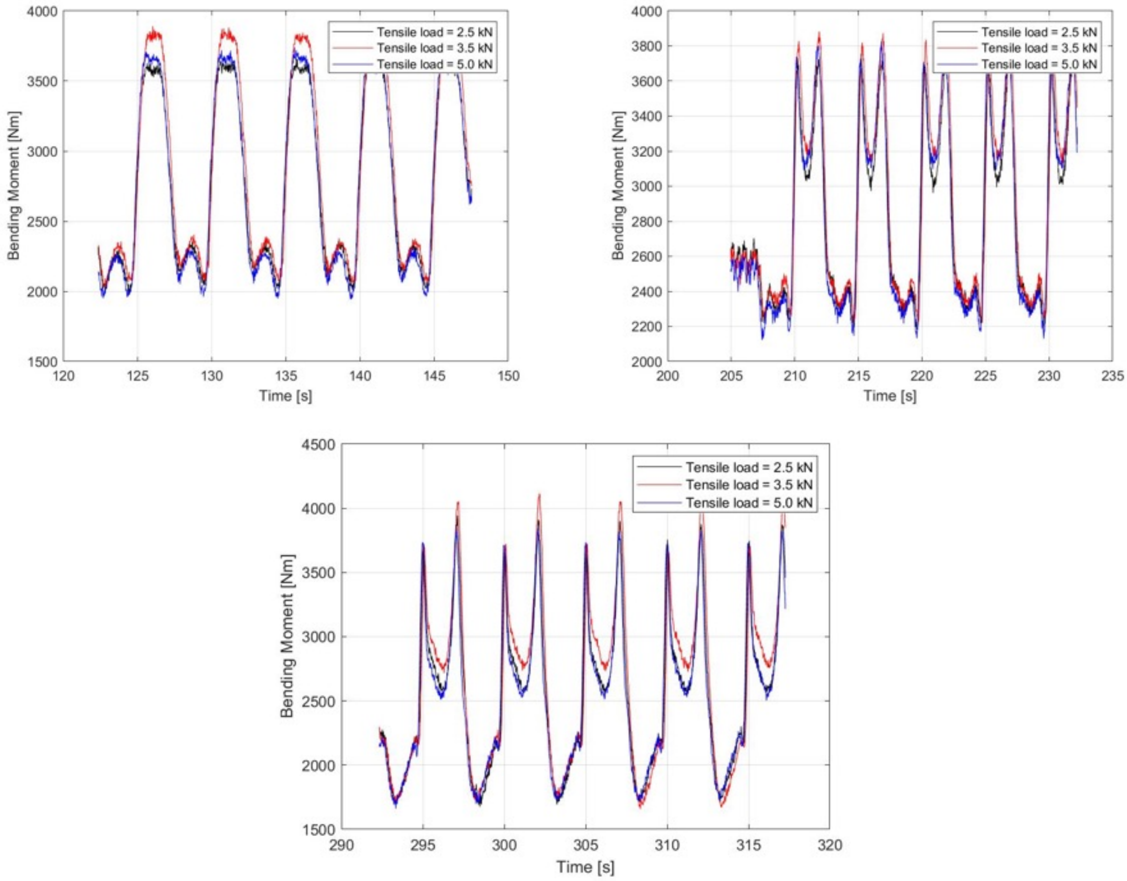

Figure 73 Bending moment of the three rotation groups ±2.5 deg (top left), ±5 deg (top right) and ±10 deg (bottom) for all three tensile ranges compared.

5.3.5 Recommendation for future testing

- Drafting the test plan for an RRT campaign provided an opportunity to understand the similarities and differences between different cable test facilities. Therefore, technology developers must thoroughly enquire about the capabilities of available facilities when choosing the facility that is best suited to their needs.
- The cable RRT at DMaC has provided an opportunity to conduct a calibration campaign to ensure the reproducibility of the results. Regular calibration must be conducted at component test facilities to ensure that the tests at the facilities are representative of actual physical parameters.

6 Summary

This report has presented the findings of the round robin test programme in MaRINET2. This programme involved testing generic tidal, wave and floating wind devices in several research facilities around Europe. Cross-cutting activities were also conducted as part of this research programme.

The purpose of the round-robin tests was to determine the impact that the facility has on the results of laboratory testing, evaluate and improve laboratory testing methodologies and make recommendations for future areas of research. One of the most important outcomes of the round robin testing campaign was the production of open-access datasets that can be used by the offshore renewable energy sector. These datasets arem available through the MaRINET2 e-infrastructure, which indexes all the research outcomes from MaRINET2 including published reports and journal papers. The e-infrastructure is accessible through the MaRINET2 website (www.marinet2.eu) and the OpenAIRE Explore website: https://explore.openaire.eu

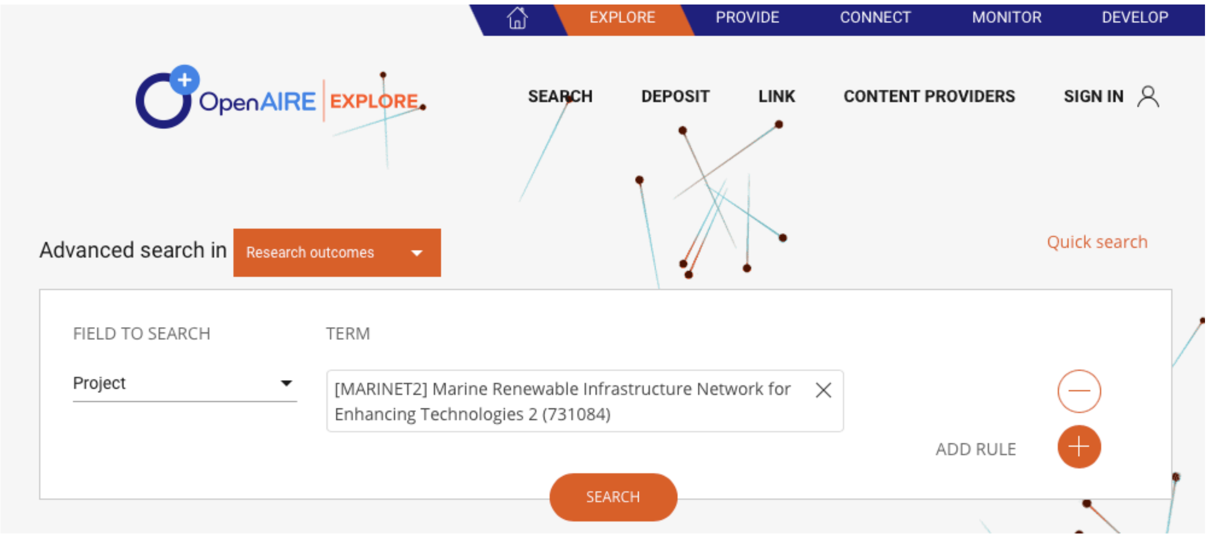

7 References

[1] B. Gaurier *et al.*, "Tidal energy 'Round Robin' tests comparisons between towing tank and circulating tank results," *Int. J. Mar. Energy*, vol. 12, no. December, pp. 87–109, 2015, doi: 10.1016/j.ijome.2015.05.005.

[2] B. Gaurier *et al.*, "Tidal energy 'Round Robin' tests comparisons between towing tank and circulating tank results," *Int. J. Mar. Energy*, vol. 12, pp. 87–109, Dec. 2015, doi: 10.1016/J.IJOME.2015.05.005.

[3] B. Gaurier *et al.*, "MaRINET2 Tidal Energy Round Robin Tests—Performance Comparison of a Horizontal Axis Turbine Subjected to Combined Wave and Current Conditions," *Journal of Marine Science and Engineering* , vol. 8, no. 6. 2020, doi: 10.3390/jmse8060463.

[4] EquiMar, *Protocols for the Equitable Assessment of Marine Energy Converters*. Edinburgh: Institute for Energy Systems, School of Engineering, The University of Edinburgh, 2011.

[5] ITTC, "ITTC-Recommended Procedures and Guidelines: Model Tests for Current Turbines 7.5-02-07-03.9," 7.5-02-07–03.9, 2017.

[6] A. S. Bahaj, A. F. Molland, J. R. Chaplin, and W. M. J. Batten, "Power and thrust measurements of marine current turbines under various hydrodynamic flow conditions in a cavitation tunnel and a towing tank," *Renew. Energy*, vol. 32, no. 3, pp. 407–426, 2007, doi: 10.1016/j.renene.2006.01.012.

[7] S. Fu, S. Ordonez-Sanchez, R. Martinez, C. Johnstone, M. Allmark, and T. O'Doherty, "Using Blade Element Momentum Theory to Predict the Effect of Wave-Current Interactions on the Performance of Tidal Stream Turbines," *Int. Mar. Energy J.*, vol. 4, no. 1, pp. 25–36, 2021.

[8] R. Martinez *et al.*, "Tidal Energy Round Robin Tests: A Comparison of Flow Measurements and Turbine Loading," *Journal of Marine Science and Engineering* , vol. 9, no. 4. 2021, doi: 10.3390/jmse9040425.

[9] A. H. Day *et al.*, "Hydrodynamic modelling of marine renewable energy devices: A state of the art review," *Ocean Eng.*, vol. 108, pp. 46–69, 2015.

[10] M. Badger *et al.*, "MaRINET2 D6.3 E-Infrastructure use cases and guidelines," 2020. [Online]. Available: https://www.marinet2.eu/wp-content/uploads/2021/06/D6.3-E-Infrastructure-Use-Cases.pdf.

[11] J. Ohana *et al.*, "Round robin tests of a hinged raft wave energy converter," 2021.

[12] T. Davey *et al.*, "Round Robin Testing: Exploring Experimental Uncertainties through a Multifacility Comparison of a Hinged Raft Wave Energy Converter," *J. Mar. Sci. Eng.*, vol. 9, no. 9, 2021, doi: 10.3390/jmse9090946.

[13] F. M. Judge, E. Lyden, M. O'Shea, B. Flannery, and J. Murphy, "Uncertainty in Wave Basin Testing of a Fixed Oscillating Water Column Wave Energy Converter," *ASCE-ASME J Risk Uncert Engrg Sys Part B Mech Engrg*, vol. 7, no. 4, p. 040902, 2021.

[14] D. R. Noble, S. Draycott, T. A. D. Davey, and T. Bruce, "Design diagrams for wavelength discrepancy in tank testing with inconsistently scaled intermediate water depth," *Int. J. Mar. Energy*, vol. 18, pp. 109–113, 2017, doi: https://doi.org/10.1016/j.ijome.2017.04.001.

[15] IEC, "TS 62600-103:2018 Guidelines for the early stage development of wave energy converters - Best practices and recommended procedures for the testing of pre-prototype devices." IEC, 2018.

[16] A. N. Robertson, E. E. Bachynski, S. Gueydon, F. Wendt, P. Schünemann, and J. Jonkman, "Assessment of Experimental Uncertainty for a Floating Wind Semisubmersible Under Hydrodynamic Loading," in *Volume 10: Ocean Renewable Energy*, Jun. 2018, p. V010T09A076, doi: 10.1115/OMAE2018-77703.

[17] S. Draycott and D. R. Noble, "Test recommendations and gap analysis report, MaRINET2 Deliverable 2.1," 2018. doi: 10.13140/RG.2.2.22509.90081.

[18] D. R. Noble *et al.*, "Standardising Marine Renewable Energy Testing: Gap Analysis and Recommendations for Development of Standards," *Journal of Marine Science and Engineering* , vol. 9, no. 9. 2021, doi: 10.3390/jmse9090971.

[19] S. Gueydon *et al.*, "Round Robin Laboratory Testing of a Scaled 10 MW Floating Horizontal Axis Wind Turbine," *J. Mar. Sci. Eng.*, vol. 9, no. 9, 2021, doi: 10.3390/jmse9090988.

[20] S. Gueydon *et al.*, "A heuristic approach for inter-facility comparison of results from round robin testing of a floating wind turbine in irregular waves," *J. Mar. Sci. Eng.*, vol. 9, no. 9, p. 1030, 2021.

[21] F. Sandner *et al.*, "INNWIND.EU Deliverable 4.3.3 - Innovative Concepts for Floating Structures," 2014. [Online]. Available: http://www.innwind.eu/publications/deliverable-reports.

[22] J. Ohana, M. Le Boulluec, E. Peron, C. Klinghammer, A. Tancray, and E. Mansuy, "Open jet blower type wind generator with variable wind speed capability for physical model testing of offshore structures," in *Proceedings of the 5th International Conference on Application of Physical Modelling to Port and Coastal Protection*, 2014, pp. 375–384.

[23] H. Bredmose *et al.*, "The Triple Spar campaign: Model tests of a 10MW floating wind turbine with waves, wind and pitch control," *Energy procedia*, vol. 137, pp. 58–76, 2017.

[24] B. J. Jonkman, "TurbSim user's guide: Version 1.50," National Renewable Energy Lab.(NREL), Golden, CO (United States), 2009.

[25] International Organization for Standardization, "Fibre ropes for offshore stationkeeping — Polyester ISO 18692," 2007.

[26] W. Finnegan, Y. Jiang, N. Dumergue, P. Davies, and J. Goggins, "Investigation and Validation of Numerical Models for Composite Wind Turbine Blades," *J. Mar. Sci. Eng.*, vol. 9, no. 5, p. 525, 2021.

[27] W. Finnegan, Y. Jiang, N. Dumergue, P. Davies, and J. Goggins, "Structural testing and FEA dataset for a composite turbine blade." SEANOE, Civil Engineering, School of Engineering, National University of Ireland Galway, H91 HX31, Ireland, May 11, 2021, doi: 10.17882/80564.

[28] International Organization for Standardization, "ISO 13628-5: Petroleum and natural gas industries - Design and operation of subsea production systems -- Subsea umbilicals," 2009.

[29] DNV GL, "DNVGL-RP-F401: Electrical power cables in subsea applications," 2017.

[30] P. Thies, "Advancing reliability information for Wave Energy Converters," 2012.

Appendix

Wind round robin interfacility comparison: numerical results

For an explanation of all terms, refer to [20].

Table 31 Mean values and standard deviations of surge and pitch stiffness coefficients for every experimental set-up

Set-up	Result	Mean	STD
A	K_{11} (N/m)	22.36	0.58
B	K_{11} (N/m)	23.37	0.71
C	K_{11} (N/m)	23.54	0.48
D	K_{11} (N/m)	34.32	0.71
E	K_{11} (N/m)	22.50	0.40
A	K_{55} (N.m/deg)	3.87	0.07
B	K_{55} (N.m/deg)	4.01	0.07
C	K_{55} (N.m/deg)	4.11	0.07
D	K_{55} (N.m/deg)	3.95	0.07
E	K_{55} (N.m/deg)	3.93	0.08

Table 32 Mean values and standard deviations of surge and pitch stiffness coefficients over all static thrust tests

Set-ups	Result	Mean	STD/Mean (%)
A, B, C, D, E	K_{11} (N/m)	25.22	18.7
A, B, C, D, E	K_{55} (N.m/deg)	3.97	2.7

Table 33 Mean values and standard deviations of surge and pitch stiffness coefficients across all setups with identical mooring line azimuth angles of 120 deg

Set-ups	Result	Mean	STD/Mean (%)
A, B, C, E	K_{11} (N/m)	22.86	3.0
A, B, C, E	K_{55} (N.m/deg)	3.97	2.7

Table 34 Mean values and standard deviations of surge-decay results for every experimental setup

Set-up	Result	Mean	STD
A	T_{surge} (s)	19.60	0.24
B_0	T_{surge} (s)	19.88	0.01
B	T_{surge} (s)	19.55	0.16
C_0	T_{surge} (s)	19.67	0.16
C	T_{surge} (s)	18.99	0.10
D_0	T_{surge} (s)	16.40	0.05
D	T_{surge} (s)	15.92	0.06
E	T_{surge} (s)	18.61	0.97
A	P_{surge} (-)	0.06	0.03
B_0	P_{surge} (-)	0.04	0.02
B	P_{surge} (-)	0.02	0.05
C_0	P_{surge} (-)	0.06	0.06
C	P_{surge} (-)	0.11	0.03
D_0	P_{surge} (-)	0.00	-
D	P_{surge} (-)	0.04	0.04
E	P_{surge} (-)	0.13	0.02
A	Q_{surge} (1/m)	3.13	1.08
B_0	Q_{surge} (1/m)	3.36	0.16
B	Q_{surge} (1/m)	3.71	0.62
C_0	Q_{surge} (1/m)	3.63	0.30
C	Q_{surge} (1/m)	3.09	0.75
D_0	Q_{surge} (1/m)	4.25	0.75
D	Q_{surge} (1/m)	3.44	0.53
E	Q_{surge} (1/m)	3.97	1.49

Table 35 Mean values and standard deviations of surge-decay results over all decays of setups with the power cable

Set-ups	Result	Mean	STD/Mean (%)
A, B, C, D, E	T_{surge} (s)	18.18	8.6
A, B, C, D, E	P_{surge} (-)	0.07	78.7
A, B, C, D, E	Q_{surge} (1/m)	3.62	26.4

Table 36 Mean values and standard deviations of surge-decay results over all decays of setups with similar surge mooring stiffness (all set-ups include the power cable)

Set-ups	Result	Mean	STD/Mean (%)
A, B, C, E	T_{surge} (s)	18.47	7.5
A, B, C, E	P_{surge} (-)	0.07	72.7
A, B, C, E	Q_{surge} (1/m)	3.68	28.5

Table 37 Mean values and standard deviations of heave-decay results for every experimental set-up.

Set-up	Result	Mean	STD
A	T_{heave} (s)	2.67	0.01
B	T_{heave} (s)	2.66	0.00
C_0	T_{heave} (s)	2.69	0.01
C	T_{heave} (s)	2.69	0.00
D_0	T_{heave} (s)	2.66	0.01
D	T_{heave} (s)	2.66	0.00
E	T_{heave} (s)	2.67	0.01
A	P_{heave} (-)	0.00	-
B	P_{heave} (-)	0.00	-
C_0	P_{heave} (-)	0.00	-
C	P_{heave} (-)	0.00	-
D_0	P_{heave} (-)	0.00	-
D	P_{heave} (-)	0.00	-
E	P_{heave} (-)	0.00	-
A	Q_{heave} (1/m)	13.56	1.04
B	Q_{heave} (1/m)	14.23	1.29
C_0	Q_{heave} (1/m)	16.40	1.12
C	Q_{heave} (1/m)	15.20	1.03
D_0	Q_{heave} (1/m)	12.40	0.80
D	Q_{heave} (1/m)	12.89	1.48
E	Q_{heave} (1/m)	13.01	1.50

Table 38 Mean values and standard deviations of heave-decay results over all decays of set-ups with the power cable.

Set-ups	Result	Mean	STD/Mean (%)
A, B, C, D, E	T_{heave} (s)	2.67	0.5
A, B, C, D, E	P_{heave} (-)	0.00	-
A, B, C, D, E	Q_{heave} (1/m)	13.94	12.1

Table 39 Mean values and standard deviations of pitch-decay results for every experimental set-up.

Set-up	Result	Mean	STD
A	T_{pitch} (s)	3.39	0.00
B_0	T_{pitch} (s)	3.39	0.00
B	T_{pitch} (s)	3.40	0.00
C_0	T_{pitch} (s)	3.42	0.01
C	T_{pitch} (s)	3.42	0.00
D_0	T_{pitch} (s)	3.38	0.00
D	T_{pitch} (s)	3.39	0.01
E	T_{pitch} (s)	3.40	0.00
A	P_{pitch} (-)	0.00	-
B_0	P_{pitch} (-)	0.00	-
B	P_{pitch} (-)	0.00	-
C_0	P_{pitch} (-)	0.00	-
C	P_{pitch} (-)	0.00	-
D_0	P_{pitch} (-)	0.00	-
D	P_{pitch} (-)	0.00	-
E	P_{pitch} (-)	0.00	-
A	Q_{pitch} (1/m)	2.89	0.36
B_0	Q_{pitch} (1/m)	2.86	0.21
B	Q_{pitch} (1/m)	2.97	0.21
C_0	Q_{pitch} (1/m)	4.01	0.47
C	Q_{pitch} (1/m)	3.16	0.18
D_0	Q_{pitch} (1/m)	4.69	0.71
D	Q_{pitch} (1/m)	4.15	0.70
E	Q_{pitch} (1/m)	3.11	0.90

Table 40 Mean values and standard deviations of pitch-decay results over all decays of set-ups with the power cable.

Set-ups	Result	Mean	STD/Mean (%)
A, B, C, D, E	T_{pitch} (s)	3.40	0.3
A, B, C, D, E	P_{pitch} (-)	0.00	-
A, B, C, D, E	Q_{pitch} (1/m)	3.21	21.8

Table 41 List of irregular wave tests selected for the comparison. All parameters are given at model scale.

Spectral shape	T_p (s)	H_s (m)	Wind thrust (N)	Facilities
JONSWAP ($\gamma = 3.3$)	1.29	0.05	0	A, B, C, D
JONSWAP ($\gamma = 3.3$)	1.29	0.75	0	A, B, C, D
JONSWAP ($\gamma = 3.3$)	1.81	0.10	0	A, B, C, D
JONSWAP ($\gamma = 3.3$)	1.81	0.15	0	A, B, C, D
JONSWAP ($\gamma = 3.3$)	2.58	0.10	0	A, B, C, D
JONSWAP ($\gamma = 3.3$)	2.58	0.15	0	A, B, C, D
JONSWAP ($\gamma = 3.3$)	2.58	0.20	0	A, B, C, D

Table 42 Values of wave parameters and metrics across all facilities for JONSWAP Tp= 1.29s, Hs=5.0 cm.

Metrics	A	B	C	D
$T_{P_{real}}$ / $T_{P_{theo}}$ (-)	1.00	0.98	1.00	1.02
Hs_{real} / Hs_{theo} (-)	1.1	0.9	0.9	1.1
Ss_{real} / Ss_{theo} (-)	1.0	0.9	0.9	1.1
Surge: T_r *(s)*	19.9	19.5	16.6	16.6
Heave: T_r *(s)*	2.69	2.66	2.68	2.65
Pitch: T_r *(s)*	3.39	3.44	3.40	3.39
Surge: M_{WF} *(-)*	0.31	0.36	0.31	0.28
Heave: M_{WF} *(-)*	0.24	0.27	0.23	0.22
Pitch: M_{WF} *(deg/m)*	12	13	12	10
Tension PS line: M_{WF} *(N/m)*	1.8	1.9	2.4	2.3
Tension SB line: M_{WF} *(N/m)*	1.5	1.6	2.4	2.3
Tension St line: M_{WF} *(N/m)*	3.2	3.7	3.5	2.3

Table 43 Deviations of wave parameters and metrics across all facilities for JONSWAP Tp=1.29s, Hs=5.0cm.

Metrics	STD/Mean (%)
$T_{P_{real}}$	1.4
Hs_{real}	9.3
Ss_{real}	9.6
Surge: T_r	9.8
Heave: T_r	0.7
Pitch: T_r	0.7
Surge: M_{WF}	10.4
Heave: M_{WF}	9.0
Pitch: M_{WF}	10.0
Tension PS line: M_{WF}	13.9
Tension SB line: M_{WF}	25.1
Tension St line: M_{WF}	18.9

Table 44 Values of wave parameters and metrics across all facilities for JONSWAP Tp= 1.29s, Hs=7.5cm.

Metrics	A	B	C	D
$T_{p_{real}} / T_{p_{theo}}$ (-)	1.00	0.98	1.00	1.02
Hs_{real} / Hs_{theo} (-)	1.1	1.0	0.9	1.1
Ss_{real} / Ss_{theo} (-)	1.0	0.9	0.9	1.1
Surge: T_r *(s)*	20.0	19.4	17.2	16.7
Heave: T_r *(s)*	2.69	2.66	2.69	2.68
Pitch: T_r *(s)*	3.39	3.40	3.39	3.39
Surge: M_{WF} *(-)*	0.32	0.35	0.32	0.28
Heave: M_{WF} *(-)*	0.24	0.26	0.24	0.22
Pitch: M_{WF} *(deg/m)*	11	13	12	10
Tension PS line: M_{WF} *(N/m)*	1.9	1.7	2	2.4
Tension SB line: M_{WF} *(N/m)*	1.5	1.5	2	2.4
Tension St line: M_{WF} *(N/m)*	3.3	3.6	3.6	2.4

Table 45 Deviations of wave parameters and metrics across all facilities for JONSWAP Tp=1.29s, Hs=7.5cm.

Metrics	STD/Mean (%)
$T_{p_{real}}$	1.7
Hs_{real}	8.5
Ss_{real}	8.3
Surge: T_r	8.9
Heave: T_r	0.5
Pitch: T_r	0.2
Surge: M_{WF}	8.7
Heave: M_{WF}	6.8
Pitch: M_{WF}	8.6
Tension PS line: M_{WF}	14.2
Tension SB line: M_{WF}	23.3
Tension St line: M_{WF}	17.9

Table 46 Values of wave parameters and metrics across all facilities for JONSWAP Tp= 1.81s, Hs=10.0cm.

Metrics	A	B	C	D
T_{Preal} / T_{Ptheo} (-)	1.00	1.00	0.99	1.00
Hs_{real} / Hs_{theo} (-)	1.0	1.0	0.9	1.0
Ss_{real} / Ss_{theo} (-)	1.0	1.0	0.9	1.1
Surge: T_r *(s)*	19.9	20.0	18.4	16.6
Heave: T_r *(s)*	2.70	2.64	2.67	2.68
Pitch: T_r *(s)*	3.40	3.45	3.40	3.37
Surge: M_{WF} *(-)*	0.57	0.58	0.57	0.56
Heave: M_{WF} *(-)*	0.41	0.42	0.43	0.4
Pitch: M_{WF} *(deg/m)*	8.1	8.7	8.7	8.2
Tension PS line: M_{WF} *(N/m)*	3.3	3.2	3.7	5.4
Tension SB line: M_{WF} *(N/m)*	3.2	3	3.5	5.7
Tension St line: M_{WF} *(N/m)*	6.9	7	7	6.6

Table 47 Deviations of wave parameters and metrics across all facilities for JONSWAP Tp=1.81s, Hs=10.0cm.

Metrics	STD/Mean (%)
T_{Preal}	0.4
Hs_{real}	5.2
Ss_{real}	4.9
Surge: T_r	8.4
Heave: T_r	0.9
Pitch: T_r	0.9
Surge: M_{WF}	1.5
Heave: M_{WF}	3.3
Pitch: M_{WF}	4.2
Tension PS line: M_{WF}	26.9
Tension SB line: M_{WF}	32.4
Tension St line: M_{WF}	2.2

Table 48 Values of wave parameters and metrics across all facilities for JONSWAP Tp= 1.81s, Hs=15.0 cm.

Metrics	A	B	C	D
$T_{P_{real}}$ / $T_{P_{theo}}$ (-)	1.00	1.01	1.00	1.00
Hs_{real} / Hs_{theo} (-)	1.0	1.0	0.9	1.0
Ss_{real} / Ss_{theo} (-)	1.0	1.0	0.9	1.0
Surge: T_r *(s)*	20.0	20.9	19.3	16.7
Heave: T_r *(s)*	2.70	2.67	2.66	2.67
Pitch: T_r *(s)*	3.44	3.45	3.39	3.37
Surge: M_{WF} *(-)*	0.57	0.59	0.58	0.56
Heave: M_{WF} *(-)*	0.42	0.42	0.43	0.39
Pitch: M_{WF} *(deg/m)*	8.4	8.6	8.2	8
Tension PS line: M_{WF} *(N/m)*	3.7	3.3	3.7	5.5
Tension SB line: M_{WF} *(N/m)*	3.2	3	3.5	5.7
Tension St line: M_{WF} *(N/m)*	6.9	7.1	7.1	6.7

Table 49 Deviations of wave parameters and metrics across all facilities for JONSWAP Tp=1.81s, Hs=15.0cm.

Metrics	STD/Mean (%)
$T_{P_{real}}$	0.5
Hs_{real}	5.2
Ss_{real}	5.4
Surge: T_r	9.4
Heave: T_r	0.7
Pitch: T_r	1.1
Surge: M_{WF}	1.7
Heave: M_{WF}	3.6
Pitch: M_{WF}	3.1
Tension PS line: M_{WF}	24.2
Tension SB line: M_{WF}	32.1
Tension St line: M_{WF}	2.3

Table 50 Values of wave parameters and metrics across all facilities for JONSWAP Tp= 2.58s, Hs=10.0cm.

Metrics	A	B	C	D
$T_{p_{real}} / T_{p_{theo}}$ (-)	0.99	0.99	1.00	1.00
Hs_{real} / Hs_{theo} (-)	1.0	1.0	1.0	1.0
Ss_{real} / Ss_{theo} (-)	1.0	1.0	1.0	1.0
Surge: T_r *(s)*	14.9	19.9	19.4	19.9
Heave: T_r *(s)*	2.71	2.71	2.68	2.69
Pitch: T_r *(s)*	3.39	3.43	3.42	3.43
Surge: M_{WF} *(-)*	0.79	0.8	0.78	0.91
Heave: M_{WF} *(-)*	0.93	0.94	0.96	1
Pitch: M_{WF} *(deg/m)*	31	34	41	44
Tension PS line: M_{WF} *(N/m)*	4.7	4.8	6	10
Tension SB line: M_{WF} *(N/m)*	4.9	4.5	5.6	11
Tension St line: M_{WF} *(N/m)*	11	11	11	13

Table 51 Deviations of wave parameters and metrics across all facilities for JONSWAP Tp=2.58s, Hs=10.0cm.

Metrics	STD/Mean (%)
$T_{p_{real}}$	0.4
Hs_{real}	3.2
Ss_{real}	3.0
Surge: T_r	12.9
Heave: T_r	0.6
Pitch: T_r	0.6
Surge: M_{WF}	7.1
Heave: M_{WF}	3.5
Pitch: M_{WF}	16.6
Tension PS line: M_{WF}	39.0
Tension SB line: M_{WF}	44.6
Tension St line: M_{WF}	5.8

Table 52 Values of wave parameters and metrics across all facilities for JONSWAP Tp= 2.58s, Hs=15.0cm.

Metrics	A	B	C	D
$T_{p_{real}}$ / $T_{p_{theo}}$ (-)	0.99	0.99	1.00	1.00
Hs_{real} / Hs_{theo} (-)	1.0	1.0	1.0	1.0
Ss_{real} / Ss_{theo} (-)	1.0	1.0	1.0	1.0
Surge: T_r (s)	14.9	21.5	21.1	28.6
Heave: T_r (s)	2.71	2.72	2.67	2.69
Pitch: T_r (s)	3.38	3.40	3.42	3.42
Surge: M_{WF} (-)	0.79	0.8	0.79	0.92
Heave: M_{WF} (-)	0.84	0.86	0.87	0.9
Pitch: M_{WF} (deg/m)	28	30	34	41
Tension PS line: M_{WF} (N/m)	4.8	4.9	5.8	10
Tension SB line: M_{WF} (N/m)	4.9	4.6	5.5	10
Tension St line: M_{WF} (N/m)	11	11	11	13

Table 53 Deviations of wave parameters and metrics across all facilities for JONSWAP Tp=2.58s, Hs=15.0cm.

Metrics	STD/Mean (%)
$T_{p_{real}}$	0.4
Hs_{real}	3.1
Ss_{real}	2.7
Surge: T_r	26.1
Heave: T_r	0.8
Pitch: T_r	0.6
Surge: M_{WF}	7.6
Heave: M_{WF}	2.8
Pitch: M_{WF}	18.1
Tension PS line: M_{WF}	38.8
Tension SB line: M_{WF}	43.0
Tension St line: M_{WF}	6.3

Table 54 Values of wave parameters and metrics across all facilities for JONSWAP Tp= 2.58s, Hs=20.0cm.

Metrics	A	B	C	D
$T_{p_{real}}$ / $T_{p_{theo}}$ (-)	0.99	0.99	1.00	1.00
Hs_{real} / Hs_{theo} (-)	1.0	1.0	1.0	1.0
Ss_{real} / Ss_{theo} (-)	1.0	1.0	1.0	1.0
Surge: T_r (s)	14.9	22.3	21.3	30.3
Heave: T_r (s)	2.70	2.72	2.66	2.70
Pitch: T_r (s)	3.38	3.39	3.43	3.40
Surge: M_{WF} (-)	0.8	0.8	0.8	0.92
Heave: M_{WF} (-)	0.81	0.84	0.84	0.83
Pitch: M_{WF} (deg/m)	26	28	30	36
Tension PS line: M_{WF} (N/m)	4.8	5	5.8	9.9
Tension SB line: M_{WF} (N/m)	5	4.7	5.4	9.9
Tension St line: M_{WF} (N/m)	11	11	11	9.9

Table 55 Deviations of wave parameters and metrics across all facilities for JONSWAP Tp=2.58s, Hs=20.0cm.

Metrics	STD/Mean (%)
$T_{p_{real}}$	0.4
Hs_{real}	3.1
Ss_{real}	3.7
Surge: T_r	28.5
Heave: T_r	0.9
Pitch: T_r	0.7
Surge: M_{WF}	7.1
Heave: M_{WF}	1.9
Pitch: M_{WF}	14.8
Tension PS line: M_{WF}	37.2
Tension SB line: M_{WF}	39.2
Tension St line: M_{WF}	6.0

Table 56 List of irregular wave tests selected for the comparison with thrust. All parameters are given at model scale.

Spectral shape	T_p (s)	H_s (m)	Wind thrust (N)	Facilities
JONSWAP ($\gamma = 3.3$)	1.29	0.05	7	A, B, C, D
JONSWAP ($\gamma = 3.3$)	1.29	0.075	7	A, B, C, D
JONSWAP ($\gamma = 3.3$)	1.81	0.10	7	A, B, C, D
JONSWAP ($\gamma = 3.3$)	1.81	0.15	7	A, B, C, D

Table 57 Values of wave parameters and metrics across all facilities for JONSWAP Tp=1.29s, Hs=5.0cm, T=7N.

Metrics	A	B	C	D
T_{Preal} / T_{Ptheo} (-)	1.00	0.99	1.00	1.02
Hs_{real} / Hs_{theo} (-)	1.1	0.9	0.9	1.1
Ss_{real} / Ss_{theo} (-)	1.0	0.9	0.9	1.1
Surge: T_r (s)	19.9	19.5	16.6	16.6
Heave: T_r (s)	2.69	2.66	2.68	2.65
Pitch: T_r (s)	3.39	3.44	3.40	3.39
Surge: M_{WF} (-)	0.31	0.36	0.31	0.28
Heave: M_{WF} (-)	0.24	0.28	0.23	0.22
Pitch: M_{WF} (deg/m)	12	14	12	10
Tension PS line: M_{WF} (N/m)	1.8	1.9	2.4	2.3
Tension SB line: M_{WF} (N/m)	1.5	1.6	2.4	2.5
Tension St line: M_{WF} (N/m)	3.2	3.8	3.5	3

Table 58 Deviations of wave parameters and metrics across all facilities for JONSWAP Tp=1.29s, Hs=5.0cm, T=7N.

Metrics	STD/Mean (%)
T_{Preal}	1.4
Hs_{real}	9.7
Ss_{real}	10.5
Surge: T_r	9.8
Heave: T_r	0.7
Pitch: T_r	0.7
Surge: M_{WF}	11.3
Heave: M_{WF}	10.0
Pitch: M_{WF}	10.9
Tension PS line: M_{WF}	13.4
Tension SB line: M_{WF}	26.8
Tension St line: M_{WF}	10.8

Table 59 Values of wave parameters and metrics across all facilities for JONSWAP Tp=1.29s, Hs=7.5cm, T=7N.

Metrics	A	B	C	D
T_{Preal} / T_{Ptheo} (-)	1.00	0.98	1.00	1.02
Hs_{real} / Hs_{theo} (-)	1.1	1.0	0.9	1.1
Ss_{real} / Ss_{theo} (-)	1.0	0.9	0.9	1.1
Surge: T_r (s)	20.0	19.4	17.2	16.7
Heave: T_r (s)	2.69	2.66	2.69	2.68
Pitch: T_r (s)	3.39	3.40	3.39	3.39
Surge: M_{WF} (-)	0.32	0.35	0.32	0.28
Heave: M_{WF} (-)	0.24	0.26	0.24	0.22
Pitch: M_{WF} (deg/m)	11	13	12	10
Tension PS line: M_{WF} (N/m)	1.9	1.7	2	2.4
Tension SB line: M_{WF} (N/m)	1.5	1.5	2	2.5
Tension St line: M_{WF} (N/m)	3.3	3.6	3.6	3

Table 60 Deviations of wave parameters and metrics across all facilities for JONSWAP Tp=1.29s, Hs=7.5cm, T=7N.

Metrics	STD/Mean (%)
$T_{p_{real}}$	1.6
Hs_{real}	8.5
Ss_{real}	8.4
Surge: T_r	8.9
Heave: T_r	0.5
Pitch: T_r	0.2
Surge: M_{WF}	8.6
Heave: M_{WF}	6.7
Pitch: M_{WF}	8.5
Tension PS line: M_{WF}	14.3
Tension SB line: M_{WF}	26.1
Tension St line: M_{WF}	8.8

Table 61 Values of wave parameters and metrics across all facilities for JONSWAP Tp=1.81s, Hs=10.0cm, T=7N.

Metrics	A	B	C	D
$T_{p_{real}}$ / $T_{p_{theo}}$ (-)	1.00	1.00	0.99	1.00
Hs_{real} / Hs_{theo} (-)	1.0	1.0	0.9	1.0
Ss_{real} / Ss_{theo} (-)	1.0	1.0	0.9	1.1
Surge: T_r *(s)*	20.0	20.0	18.4	16.6
Heave: T_r *(s)*	2.69	2.64	2.67	2.68
Pitch: T_r *(s)*	3.41	3.45	3.40	3.37
Surge: M_{WF} (-)	0.57	0.58	0.57	0.56
Heave: M_{WF} (-)	0.41	0.43	0.43	0.4
Pitch: M_{WF} *(deg/m)*	8.1	8.8	8.7	8.2
Tension PS line: M_{WF} *(N/m)*	3.2	3.2	3.7	5.4
Tension SB line: M_{WF} *(N/m)*	3.2	3	3.5	5.7
Tension St line: M_{WF} *(N/m)*	6.8	7	7	6.6

Table 62 Deviations of wave parameters and metrics across all facilities for JONSWAP Tp=1.81s, Hs=10.0cm, T=

Metrics	STD/Mean (%)
T_{Preal}	0.5
Hs_{real}	5.4
Ss_{real}	5.4
Surge: T_r	8.6
Heave: T_r	0.8
Pitch: T_r	0.9
Surge: M_{WF}	1.8
Heave: M_{WF}	3.5
Pitch: M_{WF}	4.2
Tension PS line: M_{WF}	26.9
Tension SB line: M_{WF}	32.4
Tension St line: M_{WF}	2.4

Table 63 Values of wave parameters and metrics across all facilities for JONSWAP Tp=1.81s, Hs=15.0cm, T=7N.

Metrics	A	B	C	D
T_{Preal} / T_{Ptheo} (-)	1.00	0.99	1.00	1.00
Hs_{real} / Hs_{theo} (-)	1.0	1.0	0.9	1.0
Ss_{real} / Ss_{theo} (-)	1.0	1.0	0.9	1.0
Surge: T_r *(s)*	19.7	21.6	19.3	16.7
Heave: T_r *(s)*	2.71	2.68	2.66	2.67
Pitch: T_r *(s)*	3.43	3.44	3.39	3.37
Surge: M_{WF} *(-)*	0.57	0.57	0.58	0.56
Heave: M_{WF} *(-)*	0.42	0.42	0.43	0.39
Pitch: M_{WF} *(deg/m)*	8.3	8.2	8.2	8
Tension PS line: M_{WF} *(N/m)*	3.7	3.2	3.7	5.5
Tension SB line: M_{WF} *(N/m)*	3.2	3	3.5	5.7
Tension St line: M_{WF} *(N/m)*	6.9	6.9	7.1	6.7

Table 64 Deviations of wave parameters and metrics across all facilities for JONSWAP Tp=1.81s, Hs=15.0cm, T=7N.

Metrics	STD/Mean (%)
T_{Preal}	0.3
Hs_{real}	5.4
Ss_{real}	5.4
Surge: T_r	10.4
Heave: T_r	0.8
Pitch: T_r	1.0
Surge: M_{WF}	1.2
Heave: M_{WF}	3.4
Pitch: M_{WF}	1.5
Tension PS line: M_{WF}	24.9
Tension SB line: M_{WF}	32.7
Tension St line: M_{WF}	2.0